Atomic Layer Deposition onto Fibers

von der Fakultät für Naturwissenschaften der Technischen Universität Chemnitz genehmigte Dissertation zur Erangung des akademischen Grades

doctor rerum naturalium
(Dr. rer. nat.)

Vorgelegt von (akademischen Grad, Vorname, Name): Dr. Amit Kumar, Roy
Geboren am 06.01.1981 in Orgram (Indien)
eingereicht am 23.05.2011

Gutachter: (Titel, akademischen Grad, Vorname, Name):
Prof. Dr. Werner A. Goedel
Prof. Dr. Michael Hietschold

Tag der Verteidigung: 14.03.12
http://archiv.tu-chemnitz.de/pub/

Bibliographische Beschreibung und Referat

Atomlagenabscheidung auf Fasern

Amit Kumar Roy

Schlagwörter: Atomlagenabscheidung, Kohlefaser, Oxidationsbeständigkeit, Aluminiumoxid, Titanoxid, Aluminiumphosphat, Doppelschichten, gepulste chemische Gasphasenabscheidung, Oxid-Mikroröhren, dünne Schichten, ALD-Reaktor

Das Hauptziel dieser Dissertation bestand darin nachzuweisen, dass die Atomlagenabscheidung (engl. atomic layer deposition (ALD)) auf „endlose“ Fasern angewendet werden kann. Es wurde ein Reaktor zur Atomlagenabscheidung gestaltet, der speziell für die Beschichtung meterlanger Faserbündel geeignet ist. Aluminiumoxid, Titanoxid, Doppelschichten aus Aluminiumoxid und Titanoxid sowie Aluminiumphosphat wurden mit Hilfe des selbstgebauten Reaktors auf Kohlefaserbündel abgeschieden. Rasterelektronenmikroskopische (REM) und transmissionselektronenmikroskopische (TEM) Aufnahmen zeigten, dass die Beschichtung auf den Fasern einheitlich und oberflächentreu war. Des Weiteren wurde eine gute Adhäsion zwischen Beschichtung und Fasern beobachtet.

Das Prinzip der Beschichtung mit Titanoxid und Aluminiumoxid mit Hilfe der ALD war bereits vorher bekannt und im Rahmen dieser Dissertation jedoch erstmals auf "endlose" Fasern angewendet. Des Weiteren wird in dieser Dissertation erstmals gezeigt, dass es möglich ist, Aluminiumphosphat mittels ALD abzuscheiden (sowohl auf planaren Oberflächen als auch auf Fasern). Aluminiumphosphat könnte von besonderem Interesse in der Faserbeschichtung sein, da es ein relativ weiches Material ist und könnte daher als eine Art „schwacher“ Verbindung zwischen Faser und Matrix in Kompositen dienen.

Die Oxidationsbeständigkeit von beschichten Kohlefasern wurde im Vergleich zu unbeschichteten Fasern bis zu einem gewissen Grad erhöht. Monoschichten von Aluminiumoxid und Titanoxid waren dafür wenig effektiv. Aluminiumphosphat-beschichtete Fasern waren deutlich besser geeignet als die beiden anderen. Eine

Doppelschicht aus Titanoxid gefolgt von Aluminiumoxid verbesserte die Oxidationsbeständigkeit nochmals deutlich gegenüber allen anderen Beschichtungen, die in dieser Dissertation verwendet wurden.

Mikroröhren aus Aluminiumoxid, Titanoxid und Doppelschichten wurden durch die selektive Entfernung der zugrunde liegenden Kohlefasern erhalten. Einzelne Mikroröhren waren von benachbarten Röhren getrennt und sie weisen eine nahezu einheitliche Wanddicke auf.

Abstract

Atomic Layer Deposition onto Fibers

Amit Kumar Roy

Chemnitz University of Technology, Faculty of Natural Science

The main goal of this dissertation was to show that the principle of atomic layer deposition (ALD) can be applied to “endless” fibers. A reactor of atomic layer deposition has been designed, especially for coating depositions onto meter long bundles of fibers. Aluminum oxide (alumina), titanium oxide (titania), double layers of alumina and titania, as well as aluminium phosphate have been deposited onto bundles of carbon fibers using the home-built reactor. Scanning electron microscopic (SEM) and transmission electron microscopic (TEM) images indicate that the coatings were uniform and conformal onto fiber surface. There was a good adhesion of the coatings to the fibers.

Alumina has been deposited using two separate aluminum sources (aluminum trichloride and trimethylaluminum), and water as a source of oxygen. In case of alumina deposition using aluminum trichloride and water, initial deposition temperature was 500 °C. In these conditions, a part of the fiber bundle has been damaged. Thus, the deposition temperature was decreased to 300 °C and the fibers were unaffected. In addition, during this process hydrochloric acid is formed as a byproduct which is a corrosive substance and affects the reactor and there was a chloride impurity in the coatings. Thus, aluminum trichloride precursor was replaced by trimethylalumium.

Alumina deposition onto carbon fibers using trimethylaluminum and water was carried out at a temperature of 77 °C. SEM images revealed that the fibers were unaffected and the coatings were uniform and conformal. Oxidation resistance of the carbon fibers was improved slightly after alumina deposition. Oxidation onset temperature of the uncoated fibers was about 630 °C. The resistance was linearly increased with the coating thickness (up to 660 °C) and getting saturated over a thickness of 120 nm.

Titania coatings have been deposited using titanium tetrachloride and water. The physical appearances of the titania coatings were similar to the alumina coatings. The

oxidation onset temperature of the titania coated carbon fibers was similar to the uncoated fibers but the rate of oxidation was decreased than the uncoated fibers.

Two double layer coatings were deposited, alumina followed by titania (alumina/titania), and titania followed by alumina (titania/alumina). If the fibers were coated with the double layer of alumina/titania, they had almost same oxidation onset as alumina coated fibers but the rate of oxidation was decreased significantly compared to alumina coated fibers. This feature is independent of the thickness of the titania layers, at least in the regime investigated (50 nm alumina followed by 13 nm and 40 nm titania). On the other hand, the oxidation onset temperature of fibers coated with titania/alumina (20 nm titania /30 nm alumina) was approximately 750 °C. The fibers were burned completely when temperature was further increased to 900 °C and held another 60 minutes at 900 °C. This is significantly better than any other coating used in this dissertation.

ALD of titania and alumina in principle was known beforehand, this dissertation here applies this knowledge for the first time to “endless” fibers. Furthermore, this dissertation shows for the first time that one can deposit aluminum phosphate via ALD (planar surface as well as fibers). Aluminum phosphate might be special interest in the fiber coating because it is a rather soft material and thus might be used to obtain a “weak” coupling between fiber and matrix in composites.

Aluminum phosphate was deposited using trimethylaluminum and triethylphosphate as precursors. Energy dispersive X-ray spectroscopy and solid state nuclear magnetic resonance spectra confirmed that the coating comprises aluminum phosphate (orthophosphate as well as other stoichiometries). Scanning electron microscopic images revealed that coatings are uniform and conformal. In cases of alumina and titania, it was observed that the coatings were delaminated from the ends of cut fibers and thus formed of clear steps. On the other hand, for aluminum phosphate coating it was observed that the border between coating and underlying fiber often being smeared out and thus formed an irregular line. It seems in case aluminum phosphate cohesion is weaker than adhesion, thus it might be act a “weak” interface between fiber and matrix.

Alumina, titania, and double layer microtubes have been obtained after selective removal of the underlying carbon fibers. The carbon fibers were selectively removed via thermal oxidation in air at temperatures exceeding 550 °C. SEM and TEM images indicate

that the inner side of the tube wall has the same morphology like the fibers. In addition, it was observed that the individual microtubes were separated from their neighbors and they had almost uniform wall thicknesses. The longest tubes had a length of 30 cm.

Table of contents

Bibliographische Beschreibung und Referat 2

Abstract 4

List of abbreviations 10

1. General introduction and outline of this dissertation 12

1.1 References 20

2. Atomic layer deposition: Process and reactor 25

2.1 Introduction 25

2.2 Principle of atomic layer deposition 26

2.3 Materials and methods 29

2.3.1 Precursors 29

2.3.2 Precursors transportation 31

2.3.3 Carrier and purge gas 32

2.3.4 ALD reactors 32

2.4 Flow-Type ALD reactor for fiber coating 33

2.5 Conclusion 35

2.6 References 35

3. Single layer oxide coatings 38

3.1 State of the art 38

3.2 Alumina coating using non-flammable precursors 39

3.2.1 Introduction 39

3.2.Result and discussion 39

3.3 Alumina coating using organometallic precursor 46

3.2.1 Introduction 46

3.2.2 Results and discussion 46
3.4 Titania coating using titanium tetrachloride and water 59
3.4.1 Introduction 59
3.4.2 Results and discussion 59
3.5 Experimental Part 67
3.5.1 General experiments 67
3.5.2 Alumina coating using aluminum chloride and water 69
3.5.3 Alumina coating using trimethylalumium and water 69
3.5.4 Titania coating 72
3.6 Conclusions 72
3.7 References 74

4. Coating thickness and morphology 78
4.1 Introduction 78
4.2 Results and discussion 80
4.2.1 Purge time 15 s 81
4.2.2 Purge time 30 s 85
4.2.3 Purge time 45 s to 100 s 85
4.3 Experimental part 88
4.4 Conclusions 89
4.5 References 89

5. Alumina and titania double layer coatings 91
5.1 Introduction 91
5.2 Results and discussion 92
5.3 Experimental part 102
5.4 Conclusions 103
5.5 References 103

6. Atomic layer deposition of aluminum phosphate 105

6.1 Introduction 105

6.2 Results and discussion 106

6.3 Experimental part 113

6.4 Conclusions 114

6.5 References 115

7. Alumina microtubes 117

7.1 Introduction 117

7.2 Results and discussion 118

7.2.1 Fibers before coating deposition 118

7.2.2 Coatings on the carbon fibers 118

7.2.3 Microtubes 121

7.3 Experimental part 127

7.4 Conclusions 128

7.5 References 128

8. Conclusions 131

Acknowledgements 136

Curriculum Vitae 138

Selbständigkeitserklärung 142

List of abbreviations

AAS	Atomic absorption spectroscopy
$AlCl_3$	Aluminum chloride
ALD	Atomic layer deposition
ALE	Atomic layer epitaxy
$AlMe_3$	Trimethylalumium
$AlPO_4$	Aluminum phosphate
Alumina	Aluminum oxide
α_m	Coefficient of thermal expansion of the matrix
α_f	Coefficient of thermal expansion of the fiber
BN	Boron nitride
$CaPO_4$	Calcium phosphate
$CePO_4$	Cerium phosphate
CMC	Ceramic matrix composites
CTE	Coefficient of thermal expansion
CVD	Chemical vapor deposition
CVI	Chemical vapor infiltration
d	Represent thickness of the coating
DNA	Deoxyribonucleic acid
DRAM	Dynamic random access memory
EDXS	Energy dispersive X-ray spectroscopy
F-CVI	Force flow chemical vapor infiltration
HBO_2	Meta boric acid
H_3BO_3	Ortho boric acid
HOOH	Hydrogen peroxide
I-CVI	Isothermal/isobaric chemical vapor infiltration
$LaPO_4$	Lanthanum phosphate
m_f	Total mass of alumina a single fiber with a certain length
m_t	Total mass of the alumina coated fiber with a certain length

ML	Monolayer
MMC	Metal matrix composite
NMR	Nuclear magnetic resonance
PAN	Polyacrylonitrile
P-CVI	Pressure gradient chemical vapor infiltration
PEALD	Plasma enhance atomic layer deposition
PECVD	Plasma enhance chemical vapor deposition
PMC	Polymer matrix composite
PVD	Physical vapor deposition
ρ_c	Density of the carbon fiber
ρ_m	Density of the alumina coating
SEM	Scanning electron microscopy
Silica	Silicon oxide
TEM	Transmission electron microscopy
TEFL	Thin film electroluminescence
$TiCl_4$	Titanium tetrachloride
Titania	Titanium oxide
TGA	Thermogravimetric analyzer
$T_{process}$	Process temperature of fiber reinforced composites
T_{room}	Room temperature
V_c	Volume of the carbon fiber
V_a	Volume of the alumina coating

Chapter 1

1. General introduction and outline of this dissertation

Fibers are often embedded into various matrices to improve their toughness through a distributed damage mechanism[1]. The predominant reason for this effect is that cracks propagating through the matrices do not crack the fibers. Thus, finally the mechanical load that otherwise would give rise to a large stress in a small volume at the tip of the crack is distributed over a large number of fibers, therefore, yielding a reduced stress that is spread out over a large volume. In addition, they can retain good tensile strength even in the presence of holes and notches because reinforcing fiber can transfer mechanical load (either monotonic or cyclic) in other parts and also hold various parts of the matrix. This particular property increases the life-time of the composites to a certain extent which is useful to design various structures and components with higher reliability compare to monolithic matrix. The entire mechanical characteristic and the life-time of the composite depend on the chemical compositions of the constituents (fiber and matrix), architecture of fibers, processing conditions, chemical compatibility of the constituents, coefficient of thermal expansion (CTE) of the constituents etc.. Thus, it is necessary to select appropriate fiber for a certain matrix, for example, polymers are often reinforced by carbon, glass, and aramid fibers because of mutual compatibility.

Fiber reinforced composites are used in almost every field of science and technology starting from aerospace to medical science because of their wide variation in properties. Fiber reinforced composites are already well established for the applications at room temperature and moderate temperatures. However, there is a lack of materials for high temperatures (>1200 °C) applications. There are mainly three different types of composites such as polymer matrix composite (PMC), metal matrix composite (MMC), and ceramic matrix composites (CMC). PMC and MMC are known for several decades; and, they are used for various purposes at room temperature and moderate temperatures. On the other hand, CMC is quite young but promising, especially for high temperature applications because ceramic materials have high melting points[2]. However, one of the

problems is the thermal stability of the reinforcing fibers. Most polycrystalline ceramic fibers (e.g., SiC and oxide fibers) which are the most commonly used ceramic fibers in CMCs, start to creep beyond 1200 °C because of change in the polycrystalline microstructures[3]. Tensile strength of these fibers decreases with the increase of temperature and duration of exposure. On the other hand, carbon fibers can keep high strength almost intact at high temperatures. In addition, carbon fibers have very good life-time at oxygen-free environment. However, in presence of oxygen and/or moisture, carbon fibers degrade via oxidation, comparatively at low temperatures. Thus, carbon fibers might use for the reinforcement of CMC, if the thermal oxidations are prevented. Thermal oxidations might be prevented by covering the fibers with an oxidation barrier coating before embedding into matrices[4].

An elongated substance having a uniform diameter or thickness of 250 µm and an aspect ratio of more than 100 can be defined as fiber[1]. The material can be various types such as polymers, metals, nonmetals, and ceramics. Fibers have some unique features that mainly because of their small cross section and large aspect ratio, such as a) high degree of flexibility b) high strength compare to bulk material made out of same chemical compositions. High degree of flexibility can be explained mainly because of their small diameter, which permits a variety of techniques to be employed for making fiber reinforced composites. The large aspect ratio and high strength make fibers a suitable candidate for reinforcing material because in one hand it provides high strength to the composite and on the other hand it does not alter the overall mass of the composites. Another important aspect of the fibers is the long length which makes it imperative to incorporate them in some continuous medium, e.g., various kinds of matrices to hold them together to make a fiber reinforced composites. There are various architectures possible for fiber such as a) An untwisted bundle of fibers aligned in a single direction b) woven fiber, in plane weave pattern c) knitted fiber. As mentioned above, these architectures are also important for the fiber reinforced composites. In this thesis, coatings have been deposited onto commercially available Polyacrylonitrile (PAN) based graphitic carbon fiber. They are bundle of fibers aligned in a single direction. Carbon fiber has immense importance in the field of fiber reinforced composites because it has excellent properties: a) very high tensile strength b) light

weight (theoretical density 2.27 g cm^{-3}) c) chemical inertness, i.e., chemical compatibility with almost all kinds of matrices at least at room temperature and moderates temperatures (up to 300 °C), in addition they are quite inexpensive. Although, elemental carbon itself present in nature in various forms, it has hexagonal graphite structure in carbon fibers.

Commercially available carbon fibers are synthesized in industry by paralyzing polymeric precursors like polyacrylonitrile (PAN)[1, 5]. Depending on the precursors and processing route, one can obtain a variety of carbon fibers with various strengths and moduli. They are classified as high strength, high modulus, intermediate modulus, super high modulus etc. Polyacrylonitrile (PAN) and Pitch are two very commonly used precursors for carbon fibers. The common steps for manufacturing carbon fibers as follows: a) Extrusions of polymer melt or solution into a precursor fiber. b) Precursor fibers are oxidized in presence of air at temperatures of 200 °C to 400 °C. c) This is followed by a step called carbonization, where these oxidized fibers are heated at high temperatures of 1000 °C to 2000 °C in pure inert gas atmosphere; normally at the end of this step the fibers have 85% to 99% carbon content. d) Next step is optional, called graphitization, where the fibers are heated to very high temperatures around 2500 °C in inert gas atmosphere. This step increases the carbon content to more than 99% and also increases the graphite content to a large extent.

Continuous fiber reinforced composites are made either gas phase or liquid phase processing route. Out of liquid phase processing, liquid infiltration is one of the very common ways to prepare continuous fiber reinforce composite. Liquid melt of the matrix material infiltrates performs of carbon fibers at high temperatures and is forced into voids by external pressure, either by piston (squeeze casting infiltration)[6] or by an inert gas pressure (gas pressure infiltration)[7]. Afterwards, the composites are slowly cooled down to room temperature. The composites which form by this method often have thermal stress inside. This constraint comes from the fact that it is made of dissimilar materials. Thus, the thermal stress is a result of the mismatch in the coefficients of thermal expansion (CTE) between the reinforcing fibers and matrix materials.

If the CTE of the fiber and matrix are α_f and α_m, respectively. Composite processing temperature and room temperature are $T_{process}$, T_{room}, respectively. Difference in CTE of fiber and matrix is $\Delta\alpha = (\alpha_f - \alpha_m)$. Difference in temperature of process temperature and room temperature is $\Delta T = (T_{process} - T_{room})$.

One can say that the thermal strain = $\Delta T \cdot \Delta\alpha$ Eq. (1)

As mentioned, liquid infiltration is performed at high temperatures (≥1000 °C) and the final products are cooled down to room temperature which can cause a large magnitude of thermal stress inside the composites (see equation 1). Thermal stress generated will depend on the fiber volume fraction in composite, fiber architecture and diameter, thermal mismatch, thermal difference ($T_{process} - T_{room}$), and modulus ratio of fiber and matrix material. Thermal stress often converts into cracks mainly in the matrix which propagate through whole composite upon monotonic and cyclic loading (see Figure 1)[8]. Realizing these problems, fiber-matrix interface modification was started for improving the life-time of the composites.

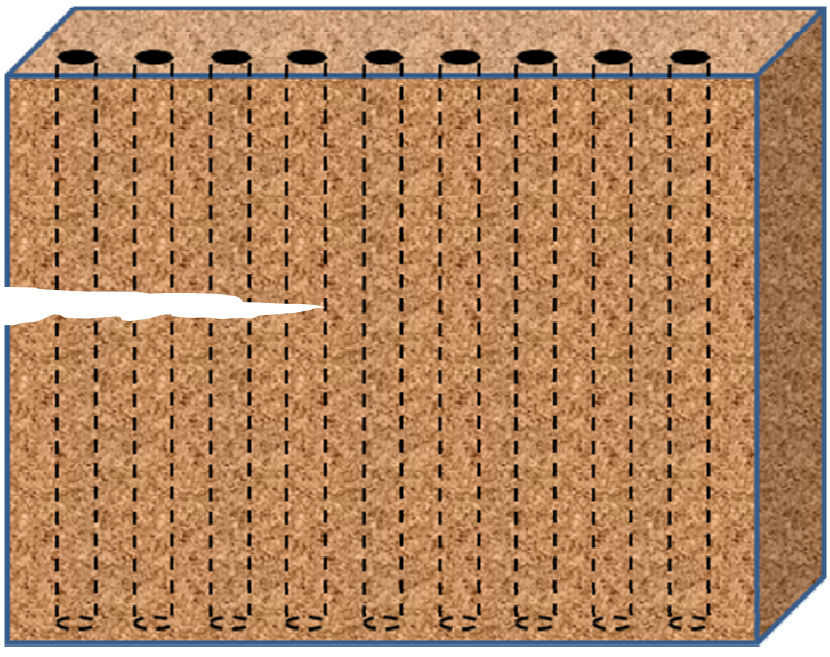


Figure 1: Schematic diagram of fiber reinforced composite, crack forms in the matrix part and propagated through the composite.

(These Schematic diagram are drown using the concept published in Figure 1 and 2 of reference 8)

There are various approaches to improve the life-time of fiber reinforced ceramic matrix composites by designing fiber-matrix interface which are as follows (schematically shown in Figure 2.)[9]. a) Coating of fibers with a solid lubricant material with gliding planes at molecular level like graphitic carbon and turbostratic boron nitride (BN)[10]. b) Porous interface design, either the matrix or the coating at the interface is made porous[11]. c) Fugitive coating; a fiber coating is removed after matrix densification to leave a gap between fiber and matrix[12]. d) Interfaces are also designed by double layer coating of fiber with two ceramic materials.[13] e) Multilayer coating by using two materials alternatively.

Fiber-matrix interfaces are designed in such a way that cracks formed in the matrix and propagating toward fiber can either be deflected into the interface or arrested within it. Out of all the approaches, fiber coating by solid lubricant materials (graphitic carbon, and boron nitride) as shown in Figure 2a is very common to improve the composites. It is known that the coating thickness should be in the range of nanometers for optimum performance. There are mainly five different criteria of a good coating material[6, 14] a) thermal expansion coefficient should be in between that of the matrix and the fiber b) absence of chemical reaction either with the matrix or fiber at the time of fabrication and also during applications c) high oxidation resistant in dry and moist conditions d) stable at high temperature e) cracks deflection/gliding ability. In general, coating should be thick enough to protect the fibers from cracks and environmental oxidations but if it is too thick than it may reduce the tensile strength significantly[15]. In addition, a single layer coating material could not fulfill all the criteria at a time; for example, materials with layer structures, (graphitic carbon and boron nitride) are able to glide or deflect cracks at the interface but they are susceptible to oxidation, especially at high temperatures in presence of oxygen and moisture. Due to the lack of an ideal coating material which can fulfill all criteria at a time, double layer or multiple layer coatings made out of two or three materials are applied to the fiber. In this double or multiple layer coating by two materials, one of the materials is chemically and thermally compatible with the matrix and another one with the fiber and they are compatible each other. In the last two approaches, double layer and multilayer coatings on fiber can deflect the cracks

at the interface and also improve oxidation resistance of the fiber. The main strategy behind this double, especially multiple layer coatings is if a single or a pair of the layers damaged during applications, other layers can protect the fiber and matrix. Coatings are applied onto the fibers by various techniques before embedding into matrices[16]. Coatings on fibers are prepared either from gas phase route or liquid phase route. a) Liquid phase route- sol-gel method for coating preparation. b) Gas phase route- chemical vapor deposition, chemical vapor infiltration (CVI).

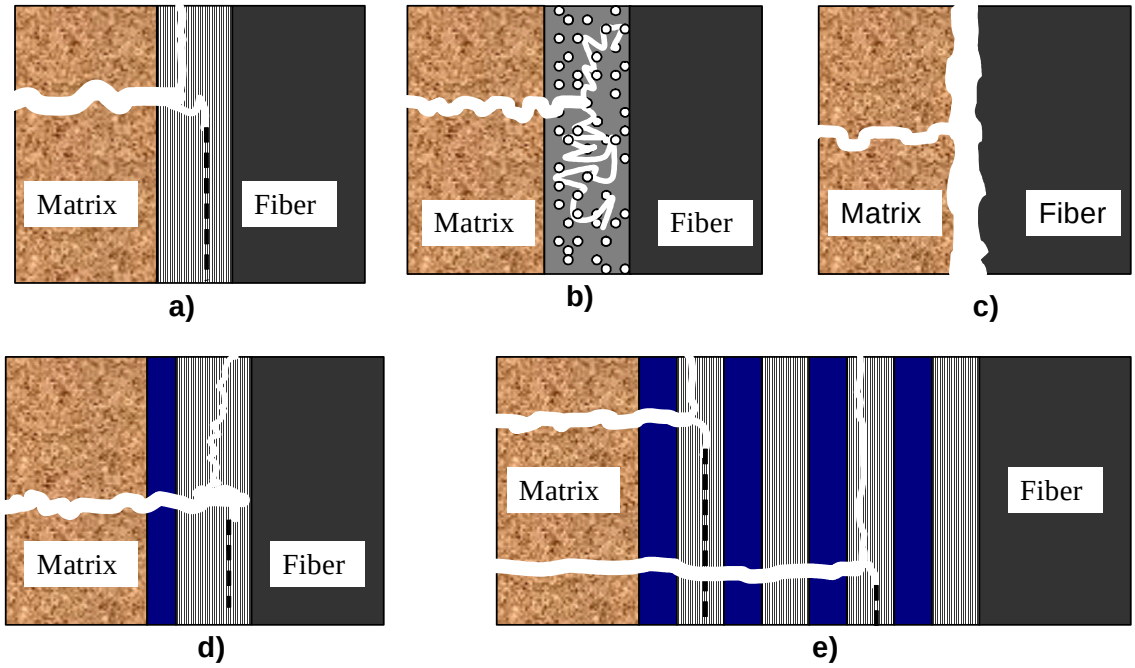


Figure 2: Schematic diagram of various types of interface: a) Layered structure interface, crack deflected in various layers b) Porous interface, cracks are deflected at pores c) Small vacant interface, created by fugitive coating, crack cannot propagate to fiber, i.e., fiber-matrix debonding d) Double layer interface, first ceramic coating layer adjacent to fiber are weakly bonded and having layered structure, second one hard in nature, protecting fiber from oxidation e) represents alternate multilayer coating by two ceramics, first one from the fiber side is weakly bonded to fiber and another one hard in nature to protect the fiber from oxidation.

(These Schematic diagram are drown using the concept published in Figure 3 of reference 9)

Sol-gel method for fiber coating is simple and economical. In this method sol of the desired ceramics are prepared and the fibers are guided through the sol for coating. Normally, sol of oxides is prepared by aqueous solution of corresponding materials. But there are some interesting results of oxide preparation by nonhydrolytic sol-gel method[17]. Characteristic of the coating depends on several factors, such as, concentration of coating liquid, particle surface charge, density, viscosity, wetting relationship between the liquid and fiber. Liquid–phase precursors often form bridge between fibers in a bundle. In the case, where bridges are extensively linked, they can impede infiltration of matrix and increase the matrix porosity at the time of ceramic matrix composite preparation. As a result strength of the ceramic matrix composite decreases extensively.

CVD is an extensively used gas phase technique for fiber coating[16]. Graphitic carbon and BN coatings on fiber bundles have been accomplished almost exclusively by CVD. It can also be used for oxide coating but deposition of multicomponent oxide is often difficult. Normally, coatings of high thickness uniformity can be achieved by this method. Bridging of fibers by this method of coating is not common but can happen when fibers are close to each other. Stoichiometry of the coating can vary from fiber to fiber between the centre and surface of the fiber bundle because of differences in the deposition kinetics of the individual gaseous reactants.

By CVI-process interface and the matrix are successfully deposited[2c, d]. In general, deposition temperature is between 900 °C to1100 °C. According to the various conditions applied, this process has several names: like isothermal/isobaric CVI (I-CVI), and force flow CVI (F-CVI) pressure gradient CVI (P-CVI). This method is very much useful for preparing nanometer thick multilayer coatings on fiber.

Other deposition techniques such as physical vapor deposition (PVD) and laser ablation that use sputtering of the coating material from a solid target by an electron beam or laser to fibers are of limited value for coating fiber bundles. These are line of sight techniques that are unsuitable for deposition of coatings onto the inner fibers in a bundle unless they are spread out so that they do not shadow each other.

In principle all these processing technique may be suitable for graphitic carbon fiber. However, in oxygen and moist conditions none of them is effective because the fibers are susceptible to oxidizing conditions, e.g., carbon fiber rapidly decreases wait

above 400 °C in oxidizing environment. Thus, all the conventional methods discussed here having merits and demerits but they are effective for the deposition of restricted material composition, such as oxide & non-oxide materials deposition on oxide fiber and non-oxide coating on non-oxide fiber (such as graphitic carbon fibers) etc.. But unfortunately, these deposition techniques are not suitable for oxide coating on non-oxide fiber. Thus, there is a demand of a smart coating technique that can deposit uniform coatings in each individual fiber at low temperatures, which can control the thickness in the range of nanometers. There might be one possibility to use controlled chemical vapor deposition which avoid direct oxygen sources (such as O_3, H_2O, HOOH) and use instead oxygen containing chemicals (such as alkoxides or esters) as precursors[18]. Another technique to reduce oxidative damage is to guide oxygen or oxygen containing precursors into the deposition chamber at some delay after the other precursors[19].

One technique to obtain conformal coating of well controlled thickness, penetrating deep into trenches is atomic layer deposition (ALD)[20]. ALD is a sequential cyclic vapor deposition process in which substrates are exposed to two (or more) precursors in a sequential manner. In between precursor pulses, there is step called purge step in which reaction chamber is either purged an inert gas and/or evacuated to reduced pressure. Each of the precursors reacts with the surface, ideally forming a chemisorbed monolayer that exposes functional groups that can react with the subsequent precursor. ALD is one of the most promising deposition tools for advanced thin film technology. ALD process and their applications in thin film technology have been discussed in various publications[20]. Microelectronic industry is reducing integrated circuits features while increasing aspect ratio and complexity. This requires the deposition of thin, highly conformal insulating oxide layers in the range of nanometers. In microelectronic industry, ALD is used to develop dynamic random access memory (DRAM), decoupling filter, transistor gate etc[21].. Thus, ALD is one of the major deposition tools in the microelectronic industry. In addition, nowadays ALD becomes more and more used for the coating and modification of organic, even delicate, materials at rather mild conditions, e.g. synthetic polymers such as polyethylene and polyvinylalcohol[22] biopolymers such as celluloses[23] spider silk[24] and carbon nanotubes[25]. To the best of my knowledge there was no report of atomic layer deposition onto bundle of ‘endless’ reinforcing fibers.

The main goal of this dissertation was to show that the principle of atomic layer deposition can be applied to 'endless' reinforcing fiber. This goal has been achieved by successive completion of the following sub-projects:

(I) Atomic layer deposition (ALD) reactor was designed, especially for coating deposition onto bundle of fibers.

Using this reactor following coatings have been deposited onto carbon fibers:

(II) Aluminum oxide (alumina).

(III) Titanium oxide (titania).

(IV) Double layers of alumina and titania, i.e., alumina followed by titania, titania followed by alumina.

(V) Aluminum phosphate, to the best of my knowledge aluminum phosphate is a new ALD coating.

All these materials were characterized by using several techniques, such as scanning electron microscopy, transmission electron microscopy, thermogravimetric analysis, atomic absorption spectroscopy etc.. In general, coatings were uniform and conformal on the fiber surface. Nanometers thick oxides and aluminum phosphate coating improved oxidation resistance to a little extent. Improvement of oxidation resistance varied from coating to coating and to a certain extent on the coating thickness. In case of double layer coatings, oxidation resistance depended on the sequence of coatings, for example, titania followed by alumina coating can improve oxidation resistance significantly of the fibers compared to alumina followed by titania. Alumina, titania and double layers microtubes have been prepared by using respective coated fibers as templates. Thus, atomic layer depositions have been used successfully for the preparation of various coatings onto carbon fibers.

1.1 References

1. Chawla, N.; Chawla, K. K. Metal matrix composites. **2006**, New York, Springer, ISBN 9789387233062.

2. a) Lamouroux, F.; Bertrand, S.; Pailler, R.; Naslain, R.; Cataldi, M., Oxidation-resistant carbon-fiber-reinforced ceramic-matrix composites. *Composite Science and*

Technology **1999,** *59* (7), 1073-1085. b) Wunder, V.; Popovska, N.; Wegner, A.; Emig, G.; Arnold, W., Multilayer coatings on CFC composites for high-temperature applications. *Surface and Coatings Technology* **1998,** *101* (1-3), 329-332. c) Naslain R., Design, preparation and properties of non-oxide CMCs for application in engines and nuclear reactors: an overview. *Composite Science and Technology* **2004**, *64 (2),* 155-170. d) Naslain R. R., SiC-Matrix Composites: Nonbrittle Ceramics for Thermo-Structural Application. *Applied Ceramic Technology* **2005**, *2* (2), 75-84.

3. Lesniewski, C.; Aubin, C.; Bunsell, A. R., Property Structure Characterization of a Continuous Fine Alumina Silica Fiber. *Composite Science and Technology* **1990,** *37* (1-3), 63-78.

4. a) Wang, Y. Q.; Zhou, B. L.; Wang, Z. M., Oxidation Protection of Carbon-Fibers by Coatings. *Carbon* **1995,** *33* (4), 427-433. b) Liu, Y.; Cheng, L.; Zhang, L.; Wu, S.; Li, D.; Xu, Y., Oxidation protection of multilayer CVD SiC/B/SiC composites for 3D C/Sic composite. *Materials Science and Engineering A*, **2007**, *466* (1-2), 172-177.

5. a) Goodhew, P. J.; Clarke, A. J.; Bailey, J. E., Review of Fabrication and Properties of Carbon-Fibers, *Materials Science and Engineering* **1975,** *17* (1), 3-30. b) Johnson, D. J.; Tyson, C. N., Fine Structure of Graphitized Fibres. *Journal of Physics D: Applied Physics* **1969,** *2* (6), 787-795. c) Diefendorf, R. J.; Tokarsky, E., High-Performance Carbon-Fibers. *Polymer Engineering and Science* **1975,** *15* (3), 150-159.

6. a) Seong, H. G.; Lopez, H. F.; Rohatgi, P. K., Microsegregation during solidification of graphitic fiber-reinforced aluminum alloys under external heat sinks. *Metallurgical and Materials Transactions A* **2007,** *38A* (1), 138-149. b) Rohatgi, P. K.; Tiwari, V.; Gupta, N., Squeeze infiltration processing of nickel coated carbon fiber reinforced Al-2014 composite. *Journal of Materials Science* **2006,** *41* (21), 7232-7239. c) Seong, H. G.; Lopez, H. F.; Gajdardziska-Josifovska, M.; Rohatgi, P. K., Nucleation effects in thermally managed graphite fiber-reinforced Al-Cu and Al-Si composites. *Metallurgical and Materials Transactions A* **2007,** *38A* (11), 2796-2804.

7. Degischer, H. P.; Schulz, P.; Lacom, W., Properties of continuous fibre reinforced Al- and Mg-matrix composites produced by gas pressure infiltration," *Cmmc 96* -

Proceedings of the First International Conference on Ceramic and Metal Matrix Composites, Parts 1 and 2 **1997,** *127-131*, 99-110.

8. Evans, A. G.; Zok, F. W. The physics and mechanics of fibre-reinforced brittle matrix composite. *Journal of Materials Science*, **1994**, *29*(15), 3857-3896.

9. Naslain, R. R., The design of the fibre-matrix interfacial zone in ceramic matrix composites, *Composites Part A* **1998,** *29* (9-10), 1145-1155.

10. a) Hackl, G.; Gerhard, H.; Popovska, N., Coating of carbon short fibers with thin ceramic layers by chemical vapor deposition. *Thin Solid Films* **2006,** *513* (1-2), 217-222. b) Shimoda, K.; Park, J. S.; Hinoki, T.; Kohyama, A., Influence of pyrolytic carbon interface thickness on microstructure and mechanical properties of SiC/SiC composites by NITE process. *Composite Science and Technology* **2008,** *68* (1), 98-105.

11. Lange, F. F.; Tu, W. C.; Evans, A. G., Processing of Damage-Tolerant, Oxidation-Resistant Ceramic-Matrix Composites by a Precursor Infiltration and Pyrolysis Method. *Materials Science and Engineering A* **1995,** *195* (1-2), 145-150.

12. Saruhan, B.; Schmucker, M.; Bartsch, M.; Schneider, H.; Nubian, K.; Wahl, G., "Effect of interphase characteristics on long-term durability of oxide-based fibre-reinforced composites" *Composites Part A* **2001,** *32* (8), 1095-1103.

13. a) N. P. Bansal, Y. L. Chen, Chemical, mechanical and microstructural characterization of low-oxygen containing silicon carbide fibers with ceramic coatings. *Journal of Materials Science* **1998, 33** (22), 5277-5289. b) P. Bertrand, M-H Vidal-setif, R. Valle, R. Mevrel, On the Effects of Surface Treatments on the Mechanical Strength of Carbon Fibres. *Journal of Materials Science*, **1998**, 33 (20), 5029. c) Sun, E. Y.; Nutt, S. R.; Brennan, J. J., High-temperature tensile behavior of a boron nitride-coated silicon carbide-fiber glass-ceramic composite. *Journal of the American Ceramic Society* **1996,** *79* (6), 1521-1529. d) Bertrand, P.; Vidal-Setif, M. H.; Mevrel, R., The CVD of pyrolytic carbon and titanium diboride coatings on carbon fibre yarns for use in aluminium-based composites. *Surface and Coatings Technology* **1997,** *96* (2-3), 283-292.

14. Friedrich, C.; Gadow, R.; Speicher, M., Protective multilayer coatings for carbon-carbon composites. *Surface and Coatings Technology* **2002,** *151*, 405-411.

15. Bertrand, P.; Vidal-Setif, M. H.; Valle, R.; Mevrel, R., On the effects of surface treatments on the mechanical strength of carbon fibres. *Journal of Materials Science* **1998,** *33* (20), 5029-5036.

16. Kerans, R. J.; Hay, R. S.; Parthasarathy, T. A.; Cinibulk, M. K., Interface design for oxidation-resistant ceramic composites. *Journal of the American Ceramic Society* **2002,** *85* (11), 2599-2632.

17. a) Lafond, V.; Mutin, P. H.; Vioux, A., Control of the texture of titania-silica mixed oxides prepared by nonhydrolytic sol-gel. *Chemistry of Materials* **2004,** *16* (25), 5380-5386. b) Bourget, L.; Corriu, R. J. P.; Leclercq, D.; Mutin, P. H.; Vioux, A., Non-hydrolytic sol-gel routes to silica. *Journal of Non-Crystalline Solids* **1998,** *242* (2-3), 81-91. c) Vioux, A., Nonhydrolytic sol-gel routes to oxides. *Chemistry of Materials* **1997,** *9* (11), 2292-2299.

18. a) Nigro, R. L.; Malandrino, G.; Fragala, I. L., Metal-organic chemical vapor deposition of CeO_2 < 100 > oriented films on no-rolled Hastelloy C276. *Chemistry of Materials* **2001,** *13* (12), 4402-4404. b) Giolando, D. M.; Kirchhoff, J. R.; Mueller, H.; Nguyen, P. Q.; Odeh, I. N., CVD of alumina on carbon and silicon carbide microfiber substrates for microelectrode development. *Chemical Vapor Deposition* **2002,** *8* (3), 93-98. c) Jones, A. C.; Aspinall, H. C.; Chalker, P. R.; Potter, R. J.; Manning, T. D.; Loo, Y. F.; O'Kane, R.; Gaskell, J. M.; Smith, L. M., MOCVD and ALD of high-kappa dielectric oxides using alkoxide precursors. *Chemical Vapor Deposition* **2006,** *12* (2-3), 83-98.

19. Zhao, G.; Giolando, D. M.; Kirchhoff, J. R., Chemical-Vapor-Deposition Fabrication and Characterization of Silica-Coated Carbon-Fiber Ultramicroelectrodes. *Analytical Chemistry* **1995,** *67* (15), 2592-2598.

20. a) Suntola, T.; Antson, J., Method for producing compound thin film. *U.S. Patent* **1977**, No: 4058430. b) Suntola, T., Atomic Layer Epitaxy. *Thin Solid Films* **1992,** *216* (1), 84-89.c) Puurunen, R. L. Surface chemistry of atomic layer deposition: A case study for the trimethylaluminum/water process. *Journal of Applied Physics* **2005,** *97* (12), 121301-1213052. d) Niinisto, L.; Paivasaari, J.; Niinisto, J.; Putkonen, M.; Nieminen, M., Advanced electronic and optoelectronic materials by Atomic Layer Deposition: An overview with special emphasis on recent progress in processing of high-k dielectrics and

other oxide materials. *Phiycas Status Solidi A* **2004,** *201* (7), 1443-1452. d) Knez, M.; Niesch, K.; Niinisto, L., Synthesis and surface engineering of complex nanostructures by atomic layer deposition. *Advanced Materials* **2007,** *19* (21), 3425-3438.

21. a) Nafis, S.; Owyang, J.; Chatterji, S., The thin-film landscape for ALD processing. *Solid State Technol* **2006,** *49* (5), 37-42. b) Musgrave, C. B.; Gordon, R. G., Precursors for atomic layer deposition of high-k dielectrics. *Future Fab International* **2005**, *18* (18), Section 7: Process Gases, Chemicals and Materials. c) Schumacher, M.; Baumann, P. K.; Seidel, T. AVD and ALD as two complementary technology solutions for next generation dielectric and conductive thin-film processing. *Chemical Vapor Deposition* **2006,** *12* (2-3), 99-108.

22. Groner, M. D.; Fabreguette, F. H.; Elam, J. W.; George, S. M., Low-temperature Al_2O_3 atomic layer deposition. *Chemistry of Materials* **2004,** *16* (4), 639-645.

23. a) Kemell, M.; Pore, V.; Ritala, M.; Leskela, M.; Linden, M., Atomic layer deposition in nanometer-level replication of cellulosic substances and preparation of photocatalytic TiO_2/cellulose composites. *Journal of the American Ceramic Society* **2005,** *127* (41), 14178-14179. b) Hyde, G. K.; Park, K. J.; Stewart, S. M.; Hinestroza, J. P.; Parsons, G. N., Atomic layer deposition of Conformal inorganic nanoscale coatings on three-dimensional natural fiber systems: Effect of surface topology on film growth characteristics. *Langmuir* **2007,** *23* (19), 9844-9849.

24. Lee, S. M.; Pippel, E.; Gosele, U.; Dresbach, C.; Qin, Y.; Chandran, C. V.; Brauniger, T.; Hause, G.; Knez, M., Greatly Increased Toughness of Infiltrated Spider Silk. *Science* **2009,** *324* (5926), 488-492.

25. a) Farmer, D. B.; Gordon, R. G., Atomic layer deposition on suspended single-walled carbon nanotubes via gas-phase noncovalent functionalization. *Nano Letters* **2006,** *6* (4), 699-703. b) Zhan G.-D; Du X.; King D. M.; Hakim L. F.; Liang X., McCormick J. A., Weimer A. W., Atomic Layer Deposition of Bulk Quantities of Surfactant – modified Single-walled Carbon Nanotubes, *Journal of the American Ceramic Society* **2008**, *91*(3), 831-835.

2. Atomic layer deposition: Process and reactor

2.1 Introduction

A brief review of atomic layer deposition (ALD) is presented here. One can find the detail of ALD processes and their application in various references[1-6]. The microelectronic industries are reducing the feature size of integrated circuits while increasing their aspect ratio and complexity. This requires the deposition of very thin, highly conformal layers of thickness in the range of nanometers. ALD is one of the most promising deposition tools for advanced thin film technology. Furthermore, materials e. g., oxides with high dielectric constant or high refractive index are not easily deposited by conventional method rather than ALD[7, 8]. Example of device that are produced via ALD are dynamic random access memory (DRAM), decoupling filter, transistor gate etc..

ALD, also known as atomic layer epitaxy (ALE), was first developed in 1970 by T. Suntola and J. Antson to fulfill the requirement of producing high-quality; large-area flat panel displays based on thin film electroluminescence (TFEL)[9]. Their first patent describes the deposition of ZnS, SiO_2 and GaP materials9. On the other hand, there was also report about ALD by Professor Aleskovskii and coworkers from Soviet Union in 1960s. These are exclusively in Russian language and thus, less commonly known in the international community. Professor Aleskovskii and coworkers describe the deposition of titanium oxide (titania) by using titanium tetrachloride ($TiCl_4$) and water (H_2O), and the deposition of germanium oxide by using tetrachloride and water respectively[6]. Nowadays, ALD was used almost exclusively for the production of inorganic devices, becomes more and more used for the coating and modification of organic, even delicate material at rather mild conditions, e.g., synthetic polymers[10], polyethylene powder[11],and carbon nanotubes[12], and for the coating of fibers, e.g., cotton[13] and spider silk[14]. In addition, ALD is not only useful to deposit oxides, sulphides, nitrides compounds but also can deposit metals[15].

2.2 Principle of atomic layer deposition

ALD is a sequential chemical vapor deposition method. Various precursors are delivered to the reactor through separate pulses. There are at least two different precursors needed. These precursors are delivered in a sequential manner. In between two precursors, an excess of precursor and byproducts of the chemical reactions are purge out of the reactor by an inert gas (such as nitrogen, argon). One complete cycle, schematically shown in Figure 1, involved four steps which are as follows:

(I) The surface of the substrate is exposed to precursor1 and occurred an adsorption or reaction of the precursor1 with the substrate surface.

(II) Any excess of precursor1 and byproducts are purged from the reaction chamber.

(III) Precursor2 is delivered to the reaction chamber, and gives rise to a chemical reaction on the surface to produce one layer of the desired films.

(IV) Any excess precursor2 and the other byproducts are purged out.

The steps (II) and (IV) are called purge steps; in which, either the reaction chamber is purged by an inert gas and/or evacuated to a reduced pressure. These steps are repeated multiple times to obtain a desire film thickness.

Purge steps not only secures that there is no mixing of precursors in the gas phase but as well removes the possibility of undesired reactions with byproducts on the deposited films. As a result in ideal conditions, homogeneous and uniform thin films are formed on the substrate[16]. In step 1 and step 3 the exposure of substrate surface of the precursors not only deposit neutral but as well surface active species which carry on the deposition process at the next step. Exposure of presursor1 followed by one purge step (e.g., step 1 and step 2) is called the first ALD half-cycle. The following two steps are the second half-cycle. If the precursor doses reach the surface saturation limit in both half-cycles, the thickness of the deposited film will be constant in each cycle and will not increase further with increasing precursor concentration or exposure time. Ideally one expect the formation of one monolayer in each cycle, but in practice, only a distinct fraction of a monolayer (e.g., half of a monolayer) forms due to steric hindrance between precursors which limits the number of molecules capable to adsorb onto the surface. Only using small molecules and elements as the precursors, a full monolayer growth per cycle might be possible. In addition, the number of adsorption sites at the surface also

affects the amount of molecules adsorbed. Depending on the process and reactor being used, one complete cycle takes 0.5 to a few seconds and deposits a film with of a thickness between 0.01 to 0.3 nm. In general, the reaction of a precursor with a given surface depends on temperatures, at two low temperature the precursor might adsorbed physically even in an amount exceeding a monolayer, on the other hand, the reaction rate or necessary rearrangement of sterically hindered groups might be too slow to reach full saturation at reasonable times.

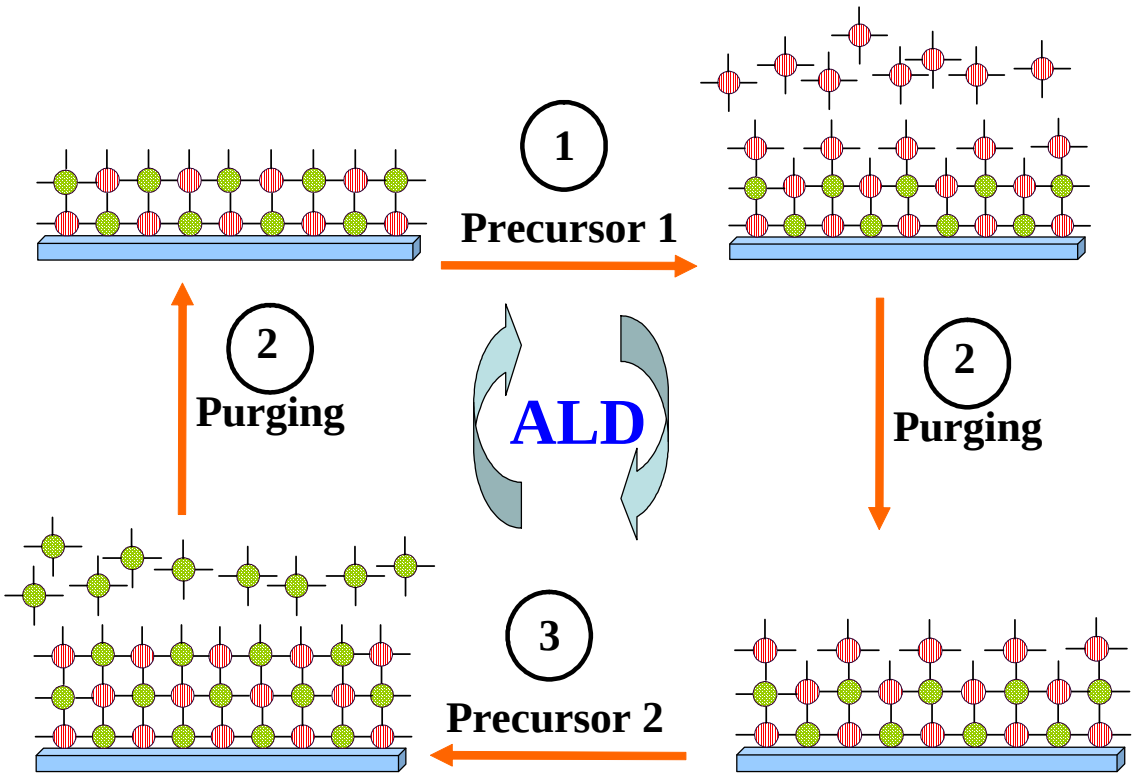


Figure 1: Scheme of atomic layer deposition (ALD) after few cycles of deposition: In step 1, a substrate is exposed to precursor 1, activate surface species react to precursor 1. Similarly in step 3, other types of surface active species react with precursors 2. Step 2 and step 4 are purge steps, before exposure to precursors; In these step the reactor is purged with an inert gas and/or evacuated to a reduce pressure. These four steps comprise one complete cycle, which repeated several times to obtain a desired film thickness. (There will be reaction byproducts in step 1 and step 3, for shake of clarity; they are excluded).

Even at high temperatures, in the reaction equilibrium there might still unfavorable degree of conversion left. Furthermore, at too high a temperature, precursors might decompose to form undesirable deposits exceeding a monolayer even in the absence of a second precursor. Regarding this particular effect, a very useful concept was introduced by T. S. Suntola and coworkers, is the so-called `ALD-window`[17]. At temperature outside the window, one observes deviation from the ALD mechanism. The deposition rate is constant inside the ALD-window region provided that the precursor concentrations and exposure times are over the saturation limit.

In general, ALD has several advantages which are as follows:
(I) One can obtain precise thickness of the deposited film in the rage of nanometers due to constant growth rate in each cycle.
(II) Uniform film formation throughout whole substrate surfaces.
(III) Very efficient in step coverage and coating of porous material, i.e., conformal coatings.
(IV) Easy preparation of multi component layers.
(V) Low temperature deposition process which might avoid unnecessary side reactions.
(VI) Useful for interface modifications.
(VII) Easy to control precursor dose because only a precursor concentration above surface saturation limit is needed.
(VIII) In ideal conditions, uniformly dense, pinhole free film forms (elimination of undesired side reaction with byproducts).

ALD has disadvantages too, which are as follows:
(I) A specially constructed reactor is needed.
(II) Very slow deposition rate (0.01 to 0.3 nm per cycle).
(III) Limited number of precursor available.
(IV) A significant amount of precursors are wasted during processing.

The major disadvantage is the slow deposition rate because only a fraction of a single monolayer can be deposited in one cycle[18]. As a result deposition rates of 100 nm h^{-1}

to 300 nm h^{-1} are obtained. In its extreme can be 1 µm h^{-1}. However, the low growth rate does not indicate low productivity: It is possible to increase the productivity either by increasing the batch volume of the substrates (in our case by coating "endless" fibers) or by coating in parallel batches. It is possible because of the limited highly conformal growth.

2.3. Materials and method

2.3.1 Precursors

The availability of appropriate precursor is one of the limitations in ALD process. In principle, the ALD precursors may be gasious, or volatile liquids or volatile solids. Appropriate precursors should have following properties[8, 18].

(I) The vapor pressure must be high enough at the deposition temperatures (at least about 0.1 Torr equilibrium vapor pressure) for mass transportation.

(II) It should have enough thermal stability to sustained decomposition temperatures.

(III) It should react or adsorb to the active sites created by other precursors.

(IV) Precursors or reaction byproducts should not be destructive to the deposited films.

(V) Reaction byproducts should be volatile enough in the deposition conditions to obtained thin films free from impurities.

Furthermore, it is desirable that precursors should be economical in addition, non-toxic and should be safe to handle. However, there is an open question of how much benefit one can obtained by using such precursors.

Because of all these criteria it is very difficult to find an ideal ALD precursor. Often, it needs to to compromise with the precursors properties for successful atomic layer depositions.

There are various materials (such as carbides, nitrides, oxides, sulfide, metal, metalloids, etc.) have been deposited from various types of precursors. There is a very well written review article regarding all types of atomic layer deposition by using various precursors[6]. All the precursors can be classified mainly two groups, I) inorganic precursors (such as hydride, halide, and oxyhalide etc) and II) organometallics precursors (true organometallics, alkoxides, β-diketonate, alkyl amides).

In metal or metalloid halides, metal or metalloid atom are directly bonded to halogen atom (such as fluorine, chlorine, bromine, and iodine), for example, zinc dichloride, titanium tetrachloride, silicon tetrachloride, hafnium tetrachloride. However, these halides are usually solids with low volatilities. There are few expectations, such as titanium tetrachloride, and silicon tetrachloride etc., which are liquids in room temperature and relatively successful ALD precursor for titanium oxide (titania) and silicon oxide (silica), respectively titanium nitride and silicon nitride deposition. On the other hand, cleavage of metal-chlorine bonds has a high activation barrier, and one needs high temperatures to dissociate these bonds. Hence, ALD processing temperatures are relatively higher when various chlorides are used as precursors. In these high temperatures substrates can be affected, especially soft materials, like carbon fibers[19], and organic polymeric materials. Additionally, metal halides release acidic byproducts like hydrofluoric acid (HF), hydrochloric acid (HCl), hydrobromic acid (HBr), hydroiodiic acid (HI) etc., which may etch the deposited films, leading to non-uniform film thicknesses, and may also cause corrosion in reactor. There are few hydrides precursors for material deposition, such as silicon hydride often used for silicon and silicon carbide depositions.

Mostly organometallics precursors are used for ALD. True organometallic precursors, where metal or metalloid atom directly bonded to carbon, $M(C_xH_y)_n$, for example, trimethylalumium ($Al(CH_3)_3$). These types of precursors are quite good for depositing oxides, for example alumina is often deposited using trimethylalumium, and H_2O as precursors. Metal and metalloid alkoxides are another type of precursors used for various oxide depositions. In metal alkoxides, metal atoms are bounded to alkoxides ($M-(O-C-R)_n$) ligand through an oxygen atom, such as titanium isopropoxides, and silicon ethoxyde, which are successful precursor for titania and silica depositions. β-diketonates ($M=(O_2C_3R_3)_n$, such as $Cr(acetylacetonate)_3$, $Fe(acetylacetonate)_3$ where each diketonato ligand is bound to the metal through two metal-oxygen bonds (the ligand "chelates" the metal center). $Cr(acetylacetonate)_4$ and $Fe(acetylacetonate)_3$ are often used for the depositions of chromium oxide and iron oxide respectively. In metal alkyl amides, the metal atom is bounded to alkyl amides ligand through a nitrogen atom, such as titanium dimethylamide, $Ti(N(CH_3)_2)_4$, often use for titanium nitride deposition.

To conclude, a particular class of compound is not suitable for all kind of depositions but it depends on the physical and chemical properties of the individual elements and the processing conditions. Furthermore, ALD of new materials are usually takes additional effort because of suitable precursors. Suitable precursors either needs to synthesised or identified.

2.3.2 Precursor transportation

As mentioned, the physical state of the precursors can be solid, liquid and gas at room temperature[18]. As they are in various states, transportations into the reaction chamber of these precursors will also vary. For transportation purpose, all these precursors can be divided into two groups: a) precursors with a vapor pressure at room temperature in the range of the operating pressure (1 to 10 mbar) b) precursors with a vapor pressure at room temperature lower than the operating pressure (1 to 10 mbar). The precursors with high vapor pressure, i.e., either gaseous or highly volatile liquids are led into the reactor from their external cylinders or vessels by pulsing with fast valves. Bubblers and transport gas are not needed to transport them into the reaction chamber since the source vapors are enter the reactor as a consequence of the pressure difference. Once this gaseous precursor enters into the reactor, the vapor is transport further by the carrier gas flow inside the reactor.

Precursors with low vapor pressures at room temperature such as low volatile liquids and solids need heating and transport systems to deliver them into the reaction chamber. Precursors are heated to an appropriate temperature for sufficient vapor pressure. In research reactors, for instance, a vapor pressure around 0.1 mbar at room temperature has been found out to be a good starting point for a new precursor. There are mainly two ways for transportation, one is to have them in external vessels and heated at an optimum temperature for and transport into the reactor through metal tube. The whole external supply vessel and the metal tubes up to the reactor should be heated at a constant temperature; otherwise, precursor will condense or solidified inside the tubes and the deposition process will be interrupted. Another possibility is to place the precursors in a part of the reactor separated by a valve or a slit from the main deposition chamber, where

they are heated to obtain appropriate vapor pressures and transported to the deposition chamber via a carrier gas.

2.3.3. Carrier and purge gases

A gas which is inert for the chemical process, used to carry the precursors and to purge out the reaction chambers[18]. Normally, either nitrogen or argon is used as carrier gas as well as purge gas. Often reactor is designed in such a way that the same steam of flow is acting as carrier as well as purge gas. Inert gas flow is regulated by mass flow controllers and the flow rate is maintained according the reactor geometry, pumping speed, operating pressure etc.. In case of reactors used for small scale research, the flow rate is maintained between 20 to 50 sccm (standard cubic centimetre per minute), whereas the largest production reactors require between 20,000 to 50,000 sccm. One of the major aspects of carrier gas is the purity because it is one of the main sources of impurities for an ALD process. The minimum purity should be 99.999%.

2.3.4. ALD reactors

ALD processes can be performed in various kinds of reactors and also in various pressure ranges from atmospheric to ultrahigh vacuum ($<10^{-9}$ mbar)[18]. ALD reactors are mainly divided into two types: (II) inert gas flow reactor, operating under viscous or transition flow conditions at a pressure around 0.1 to 10 mbar, and (II) ultrahigh vacuum reactor, operating under molecular flow conditions at a pressure of $< 10^{-9}$ mbar. Inert gas flow type reactors are more advantageous over the ultrahigh vacuum reactors. There are several reasons: (I) Both the precursor exposure and purge steps are rapid for flow type reactor. (II) Flow type reactors have more precursor utilization efficiency compare to ultrahigh vacuum reactors because in ultrahigh vacuum reactors precursors molecule make only few collision with the substrate surface before being pumped out and thus have a limited probability to react. On the other hand, in the flow type reactors, a particular precursor molecule can make multiple hits while being transported through the reactor. As a result, reaction probability and thereby precursor utilization efficiency are increased, and saturation of the chemisorptions layer is accelerated which makes the process faster. (III) Ultrahigh vacuum reactors are much more expensive compare to flow

type reactors. (IV) It is easier to design a flow type reactor for large batch processing compare to ultrahigh vacuum reactors. (V) Flow type reactor can also be constructed for laboratory scale research more easily than ultrahigh vacuum reactor.

The major parts of the ALD reactors are:

(I) Reaction chamber and separate precursor container.

(II) Flow control system (such as, automated valves either pneumatic or solenoid vales) for each of the individual precursor.

(III) Carrier gas and purge gas flow control systems, for example, mass flow controllers.

(IV) Heating devices for precursor chambers, reaction chamber, and tubing, efficient heating device which can maintain homogenous temperatures.

(V) Special vacuum pumps and exhaust equipment which can sustain corrosive chemical environments.

(VI) Pressure monitoring devices, for example, pressure gauges.

As mentioned in ALD, one of the advantage is that no need to maintain homogenous precursor flux in each cycle, however, important thing is that precursor flux should be always over the saturation dose, i.e., there is no upper limit for precursor flux. This gives lot of flexibility in ALD reactor design.

2.3 Flow-Type ALD reactor for fiber coating

Commercially available ALD reactors mostly used in industry are flow type reactors. These reactors are carefully designed to minimize the pulse and purge times and to maximize the precursor utilization efficiency. These kinds of reactors are available in both small size and large size production. To the best of my knowledge, there was no commercially available ALD reactor which can be used for coating deposition onto bundle of fibers. There might have been one possibility to use commercially available ALD reactor with open tubular chamber by manipulating various parts, however, commercially available reactors are expensive (reactor for small scale only for research purpose cost 150 – 220 thousand euro). Thus, in this thesis, a reactor was designed, especially, for atomic layer deposition onto bundle of reinforcing fibers. The detail description of this reactor is as follows (see Figure 2 published in papers[19, 20]): A reaction tube, 1 m long and 4 cm in diameter, made out of stainless steel is placed inside a 70 cm

long tube furnace. The fiber holder is 30 cm long with 12 channels made out of stainless steel.

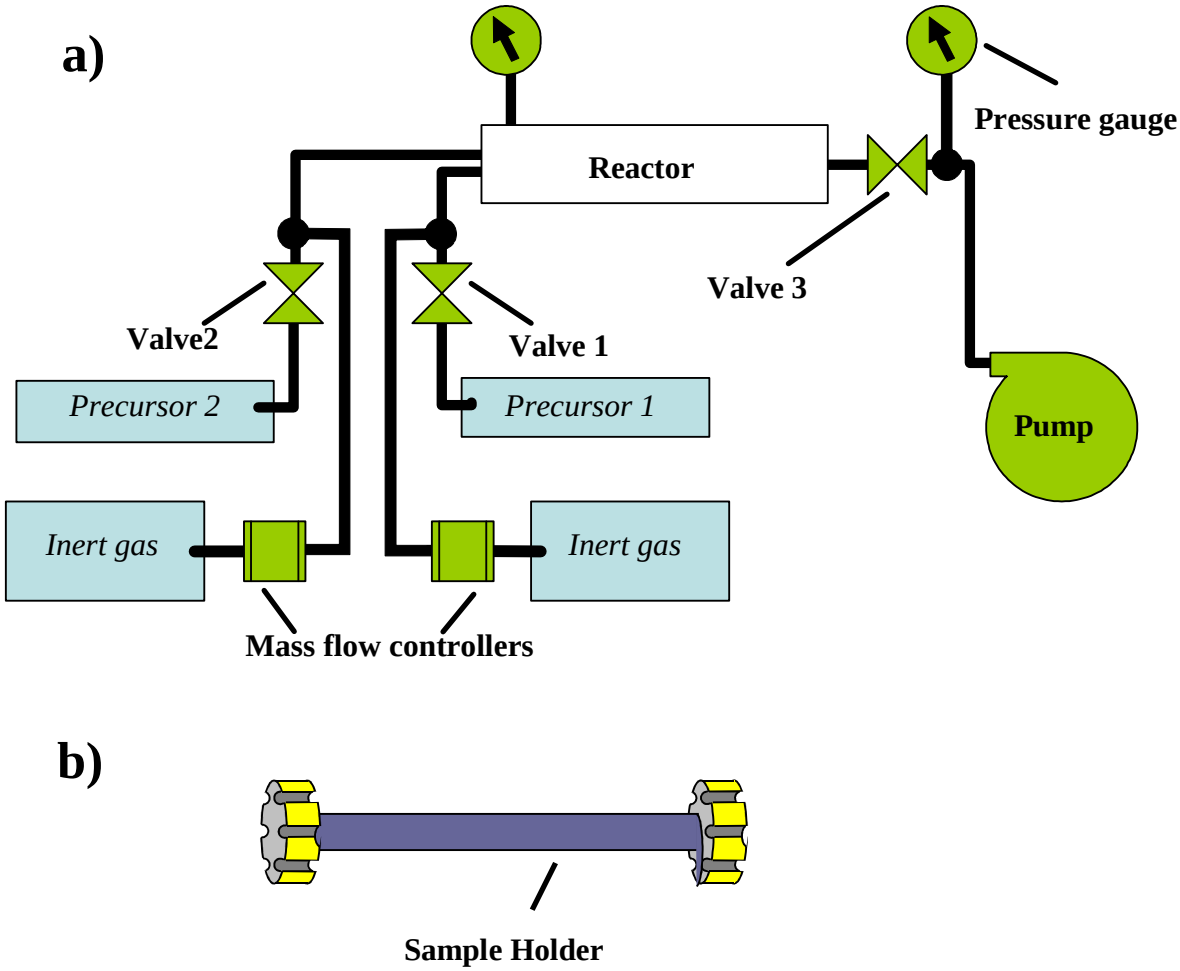


Figure 2: Flow-type ALD reactor designed for fiber coating. There are two separate precursor chambers connected to the main reactor separately by two computer controlled valves, valve 1 and valve 2. Each precursor chamber is connected to an inert gas supply that is controlled by a mass flow controller. There are two pressure measurement gauges for monitoring the pressure inside the reactor. Another computer controlled valve, valve 3 and the pump are controlling the pressure inside the reactor. (b) Scheme of the sample holder used to place the fibers within the furnace.

There are two separate precursor chambers separately connected with the reactor via tubes made out of stainless steel of 1/4" diameter. Precursor doses are controlled by pneumatic valves, valve 1 and valve 2 in Figure 2, which can switch within seconds. Each separate precursor tube is connected with inert gas supply that acts as carrier gas during precursor flow, otherwise, as a purge gas. Inert gas flow was controlled by mass flow controllers. Pressure inside the reactor is controlled by another pneumatic valve, valve 3 in Figure 2. Reactor evacuation was carried out by a rotary vane pump. There was a cooling trap before the pump in order to protect the pump from hazardous chemicals and corrosion. The pressure inside the reactor is measured by two pressure measurement gauges. The temperature of the main reactor is controlled by the tube furnace. Nitrogen was used for carrier as well as purge gas of a purity of 99.999%. This was further purified from oxygen and moisture by passing through specific absorber. All valves are controlled by a home written program with the help of 'LabVIEW' software from National Instrument.

2.5 Conclusions

ALD is a thin film processing technique, used mainly in the microelectronic industry. Solid thin films are deposited from gas phase precursors with very precise thickness control, generally, in the range of nanometers. From chemistry point of there are various types of precursors available, however, a particular type of precursor is not suitable for all kinds of depositions. It depends on the physical and chemical property of the individual materials and their available chemical sources. There are two types of reactors available, flow type reactor and ultrahigh vacuum reactor, flow type reactor is more advantageous compare to another one. In this thesis, a reactor has been designed, for atomic layer deposition onto bundle of reinforcing fibers.

2.6 References

1. Knez, M.; Niesch, K.; Niinisto, L., Synthesis and surface engineering of complex nanostructures by atomic layer deposition. *Advance Materials* **2007,** *19* (21), 3425-3438.

2. Suntola, T., Atomic Layer Epitaxy. *Thin Solid Films* **1992,** *216* (1), 84-89.

3. Niinisto, L.; Paivasaari, J.; Niinisto, J.; Putkonen, M.; Nieminen, M., Advanced electronic and optoelectronic materials by Atomic Layer Deposition: An overview with special emphasis on recent progress in processing of high-k dielectrics and other oxide materials. *Phiycas Status Solidi A* **2004,** *201* (7), 1443-1452.

4. Schumacher, M.; Baumann, P. K.; Seidel, T., AVD and ALD as two complementary technology solutions for next generation dielectric and conductive thin-film processing. *Chemical Vapor Deposition* **2006,** *12* (2-3), 99-108.

5. Leskela, M.; Ritala, M., Atomic layer deposition chemistry: Recent developments and future challenges. *Angewandte Chemie-International Edition* **2003,** *42* (45), 5548-5554.

6. Puurunen, R. L., Surface chemistry of atomic layer deposition: A case study for the trimethylaluminum/water process. *Journal of Applied Physics* **2005,** *97* (12), 121301-1213052.

7. Nafis, S.; Owyang, J.; Chatterji, S., The thin-film landscape for ALD processing. *Solid State Technology* **2006,** *49* (5), 37-42.

8. Musgrave, C. B.; Gordon, R..G.; Precursors for atomic layer deposition of high-k dielectrics. *Future Fab International* **2005**, *18* (18), Section 7: Process Gases, Chemicals and Materials.

9. T. Suntola, J. Antson, "Method for producing compound thin film," U.S. Patent no: 4058430, **1977**.

10. Liang, X. H.; George, S. M.; Weimer, A. W., Synthesis of a novel porous Polymer/Ceramic composite material by low-temperature atomic layer deposition. *Chemistry of Materials* **2007,** *19* (22), 5388-5394.

11. Dameron, A. A.; Davidson, S. D.; Burton, B. B.; Carcia, P. F.; McLean, R. S.; George, S. M., Gas diffusion barriers on polymers using multilayers fabricated by Al_2O_3 and rapid SiO2 atomic layer deposition. *The Journal of the Physical Chemistry C* **2008,** *112* (12), 4573-4580.

12. Farmer, D. B.; Gordon, R. G., Atomic layer deposition on suspended single-walled carbon nanotubes via gas-phase noncovalent functionalization. *Nano Letters* **2006,** *6* (4), 699-703.

13. Hyde, G. K.; Park, K. J.; Stewart, S. M.; Hinestroza, J. P.; Parsons, G. N., Atomic layer deposition of Conformal inorganic nanoscale coatings on three-dimensional natural fiber systems: Effect of surface topology on film growth characteristics. *Langmuir* **2007,** *23* (19), 9844-9849.

14. Lee, S. M.; Pippel, E.; Gosele, U.; Dresbach, C.; Qin, Y.; Chandran, C. V.; Brauniger, T.; Hause, G.; Knez, M., Greatly Increased Toughness of Infiltrated Spider Silk. *Science* **2009,** *324* (5926), 488-492.

15. Lim, B. S.; Rahtu, A.; Gordon, R. G., Atomic layer deposition of transition metals. *Nature Materials* **2003,** *2* (11), 749-754.

16. Elers, K. E.; Blomberg, T.; Peussa, M.; Aitchison, B.; Haukka, S.; Marcus, S., Film uniformity in atomic layer deposition. *Chemical Vapor Deposition* **2006,** *12* (1), 13-24.

17. Suntola, T. S.; Pakkala, A. J.; and Lindfors, S. G., US Patent 4413022, **1983**.

18. Ritala, M.; Leskela, M. In *Handbook of Thin Film Materials*, Vol. 1; Nawla, H. S., Ed.; Academic Press: San Diego, CA, **2001,** 108-113.

19. Roy, A. K.; Baumann, W.; Konig, I.; Baumann, G.; Schulze, S.; Hietschold, M.; Mader, T.; Nestler, D. J.; Wielage, B.; Goedel, W. A., Atomic layer deposition (ALD) as a coating tool for reinforcing fibers. *Analytical and Bioanaytical Chemistry* **2010,** *396* (5), 1913-1919.

20. Roy, A. K.; Baumann, W.; Schulze, S.; Hietschold, M.; Mäder, T.; Nestler, D. J.; Wielage, B.; Goedel, W. A., Atomic Layer Deposition of Alumina onto Carbon Fibers. *Journal of the American Ceramic Society* **2011**, DOI: 10.1111/j.1551-2916.2010.04340.x.

Chapter 3

3. Single layer oxide coatings*

3.1 State of the art

The initial goal of this thesis was to show that the principle of atomic layer deposition (ALD) may be applied to coat the reinforcing fibers. Polyacrilonitrile (PAN) based graphitic carbon fibers have been chosen because they are more promising compared to other reinforcing fibers as mentioned in the first chapter. It might be difficult to coat the carbon fibers because it may not contain any functional group (like hydroxyl, amine, carboxyl) at the surface[1, 2]. For a successful ALD process such groups usually are necessary which are acting as anchoring groups for the precursors and carry out the process from the first cycle. Nevertheless, conformal coating might be achieved if at least one of the precursors is absorbed on the surface or absorbed within a region of the substrate near the surface.

The next decision was about the coating materials. Inorganic oxides (alumina and titania) have been chosen because processing of inorganic oxides via ALD is well established, and found applications in the field of semiconductor industry within last few decades[1, 2]. In addition, inorganic oxide coating might be useful to improve the oxidation resistance of the carbon fiber which is an ongoing problem in the field of fiber reinforced composites. Recently, ALD of inorganic oxides onto delicate organic and polymeric materials has been reported[3-5]. The possibility to use low deposition temperatures makes this technique applicable for such delicate materials, also it might be applicable to carbon

* Most of the results of this chapter were published in the following articles:

Roy, A. K.; Baumann, W.; König, I.; Baumann, G.; Schulze, S.; Hietschold, M.; Mäder, T.; Nestler, D. J.; Wielage, B.; Goedel, W. A., Atomic layer deposition (ALD) as a coating tool for reinforcing fibers. *Analytical and Bioanalytical Chemistry* **2010,** *396* (5), 1913-1919**.**

Roy, A. K.; Baumann, W.; Schulze, S.; Hietschold, M.; Mäder, T.; Nestler, D. J.; Wielage, B.; Goedel, W. A., Atomic Layer Deposition of Alumina onto Carbon Fibers. *Journal of American Ceramic Society* **2011**, DOI: 10.1111/j.1551-2916.2010.04340.x.

fibers. In the following sections, depositions of alumina and titania onto carbon fibers are discussed in details.

3.2 Alumina coating using non-flammable precursors

3.2.1 Introduction

In past, alumina was deposited using aluminum trichloride and water by ALD[6, 7]. Recently, alumina has been deposited using trimethylaluminum and water as precursors[8]. However, trimethylaluminium is a pyrophoric material, (catches fire immediately in contact with air) and comparatively expensive. A beginner wants to start with precursors which are rather mild and inexpensive. Thus, alumina was deposited onto bundles of carbon fibers using aluminum trichloride and water. The carbon fibers are exposed to aluminum trichloride followed by purging. In the next step it is exposed to water followed by another purging. These four steps deposit a layer of certain thickness. Steps were repeated systematically to obtained desired coating thickness

3.2.2 Results and discussion

Bundles of carbon fibers were coated with alumina by sequential exposure to aluminum trichloride and water vapor. Coating was carried out at temperatures of 500 °C and 300 °C. The coated carbon fibers were characterized by scanning electron microscopy (SEM), transmission electron microscopy (TEM), and energy dispersive X-ray spectroscopy (EDXS). SEM images of the uncoated fibers show that they have corrugated surface bearing grooves parallel to the fiber axis (see Figure 1) and irregular protuberances; this morphology varies from fiber to fiber. According to the literature, the fibers are composed of amorphous and crystalline regions, the crystalline regions having to some extend preferential orientations with respect to the fiber axis[9]. SEM images of the coated fibers and fiber ends cut after the coating process are shown in Figure 2. The overview image (Figure 2a) reveals that the fibers within the bundle are still separated from each other, that no bridging was found, and that coatings have been deposited evenly on fibers. At the front of the fiber the coating was removed during the cutting process of sample preparation. Figure 2b shows the end of an individual fiber. There is an obvious contrast in the intensity of secondary electrons between the ~7 μm of the fiber

close to the end and the final part of the fiber that appears to be less bright in the SEM image. This indicates that the coating, which comprises the heavier element Al and thus gives rise to a stronger secondary electron emission, was removed from the front part of the fiber in the cutting process. Besides this intensity contrast, the surface of the coated region has a structure very similar to the surface of the uncoated regions. This fact is readily visible in the close up image of Figure 2c. Thus, the coatings are smooth, uniform and conformal. On the other hand, for a particular fiber bundle one can see few of the fibers are looking brighter than the others; this might be because they are directly expose to the electron beam or might be closer to the detector of the electron microscope.

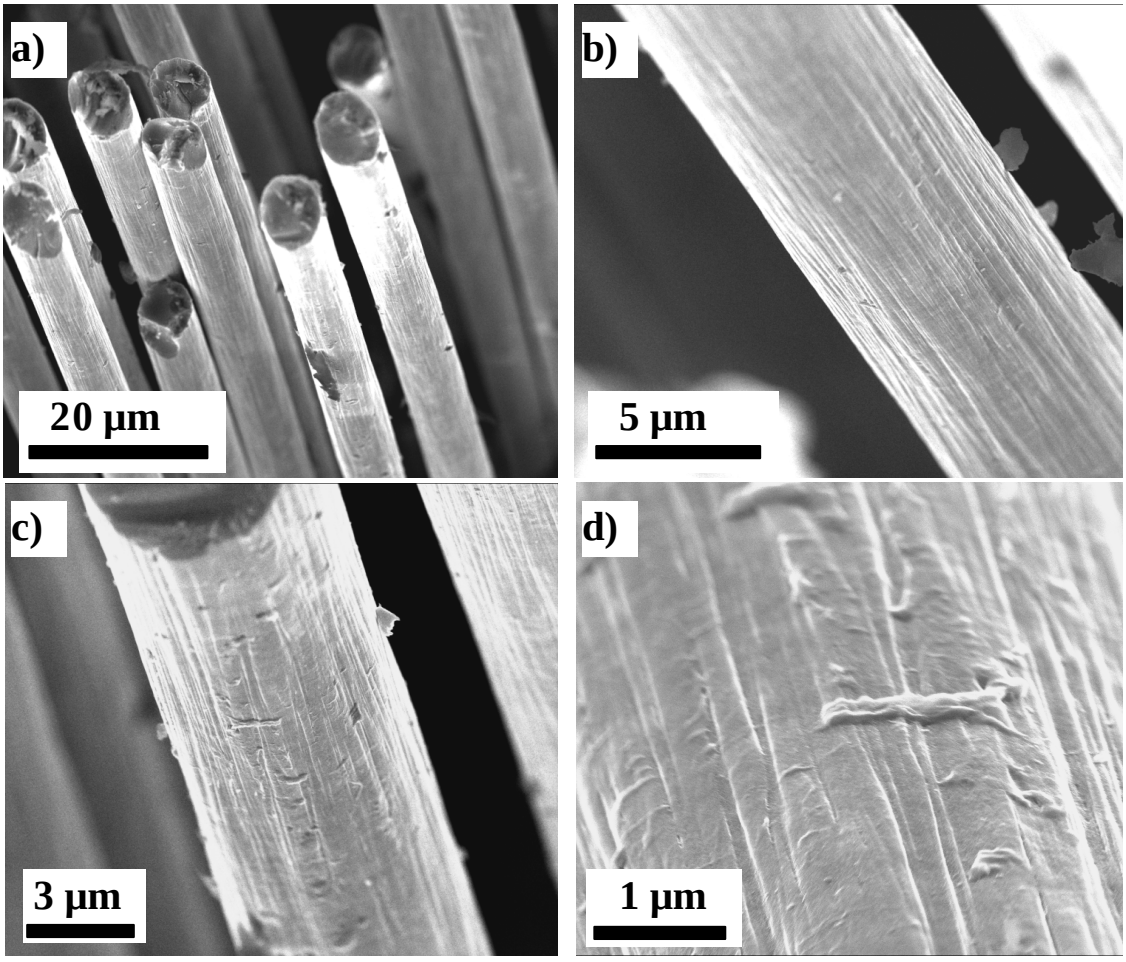


Figure 1: Scanning electron microscopy (SEM) images of uncoated fibers after removing the polymeric size: a) a part of a fiber bundle, b) and c) single fiber, irregular protrusions are visible on the fiber surface, and d) a close up view of a single fiber.

There are almost no regions—with the exceptions of the freshly cut ends—that indicate delamination of the coating; thus there seems to be good adhesion of the coating to the fiber (Figure 2d). In places, where delamination was caused by the cutting, one observes clear steps. One can estimate the coating thicknesses from these steps by analyzing these SEM images.

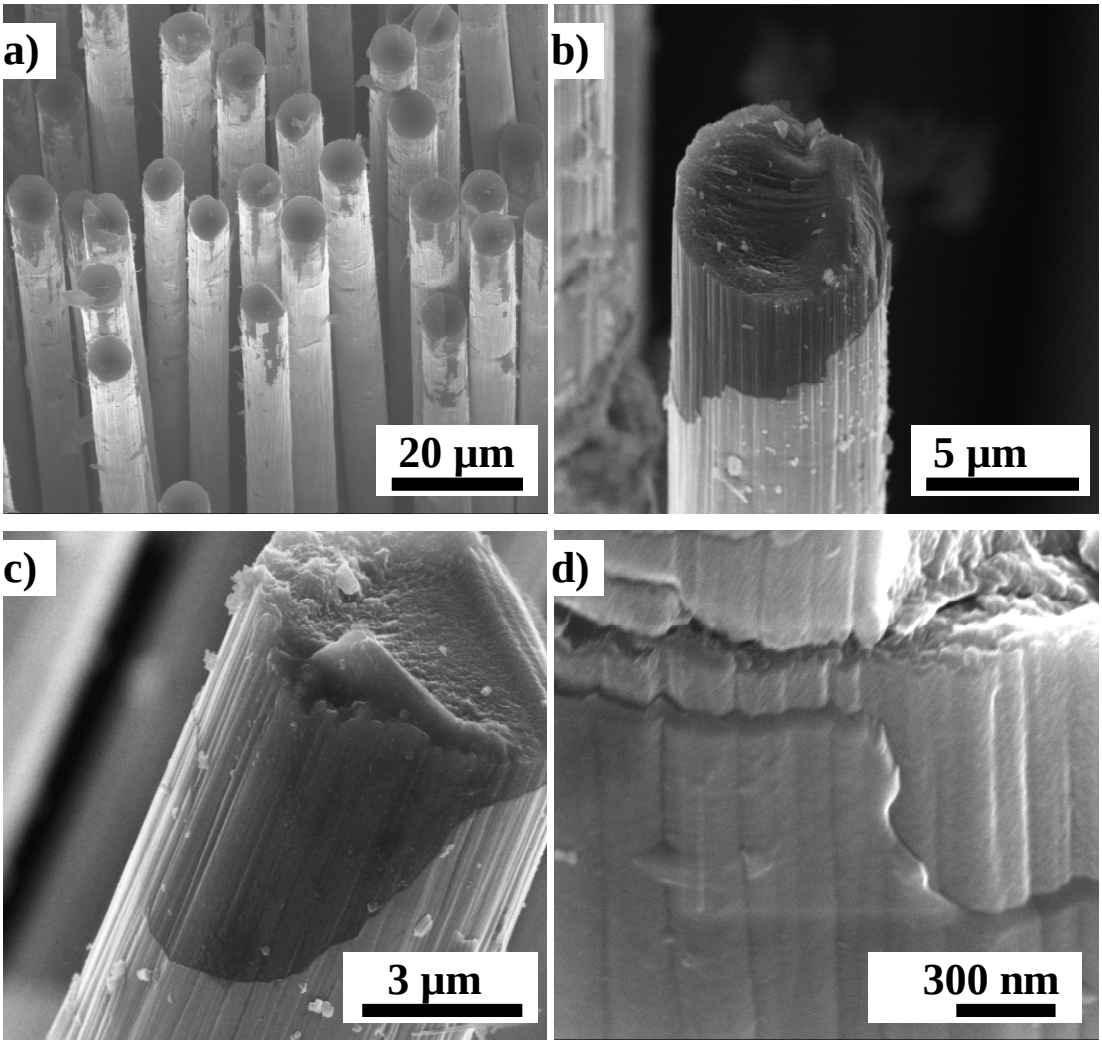


Figure 2: Scanning electron microscopic (SEM) images of alumina coated fibers: a) shows a part of a fiber bundle, b) a single fiber, dark gray part in front is the fiber and bright part is the coating, c) shows uniform and conformal coating onto the fiber surface, and d) shows good adhesion of the coating onto the fiber surface.

A cross-section of the fiber–coating interface was prepared by mechanical polishing and investigated by transmission electron microscopy (TEM). The detail of this sample preparation was reported elsewhere[10]. The resulting TEM image, shown in Figure 3, revealed that might be a sharp interface between the fiber and the coating, and it seems that the coating is not diffused into the fiber surface. The sample was not good enough for further high resolution TEM analysis.

Elemental analysis of the coated fiber by EDXS revealed that it contained a large amount of carbon aluminum, oxygen, and a small amount of chlorine. The large amount of carbon was expected because of the carbon fiber, the presence of aluminum and oxygen confirms the expected alumina coating.

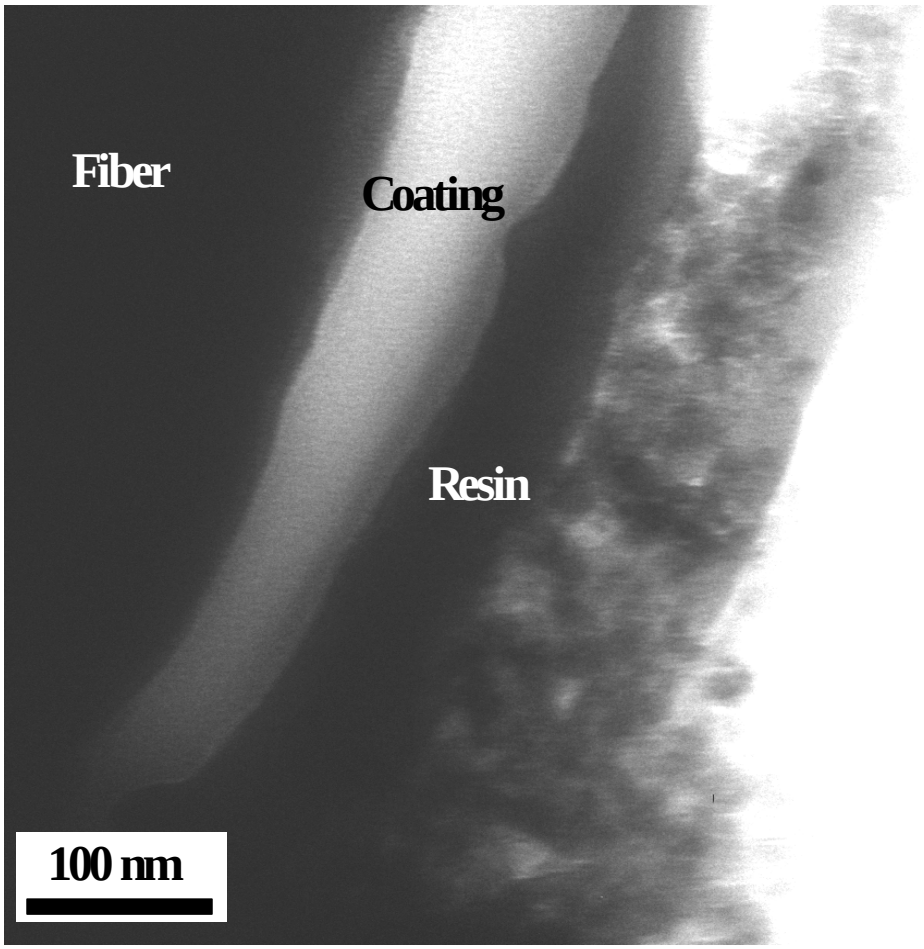


Figure 3: Transmission electron microscopic (TEM) image of a cross-sectional view trough the near surface region of a coated single fiber.

The small amount of chlorine can be estimated as an impurity from the aluminum trichloride precursor. If the fiber is removed by thermal oxidation in air, elemental analysis via EDXS of the residue indicates predominant aluminum and oxygen. The carbon, hydrogen, and nitrogen contain within the residues of the thermal oxidation were measured by elemental flash analysis. Results of this analysis indicate that the amount of carbon, hydrogen, and nitrogen within the residue of thermal oxidation were 0.424% carbon, and there were no hydrogen and nitrogen (if hydrogen and nitrogen were present that might be less than the detection limit, i.e., <0.01%). A small amount of carbon can be regarded as an irremovable part of the fiber.

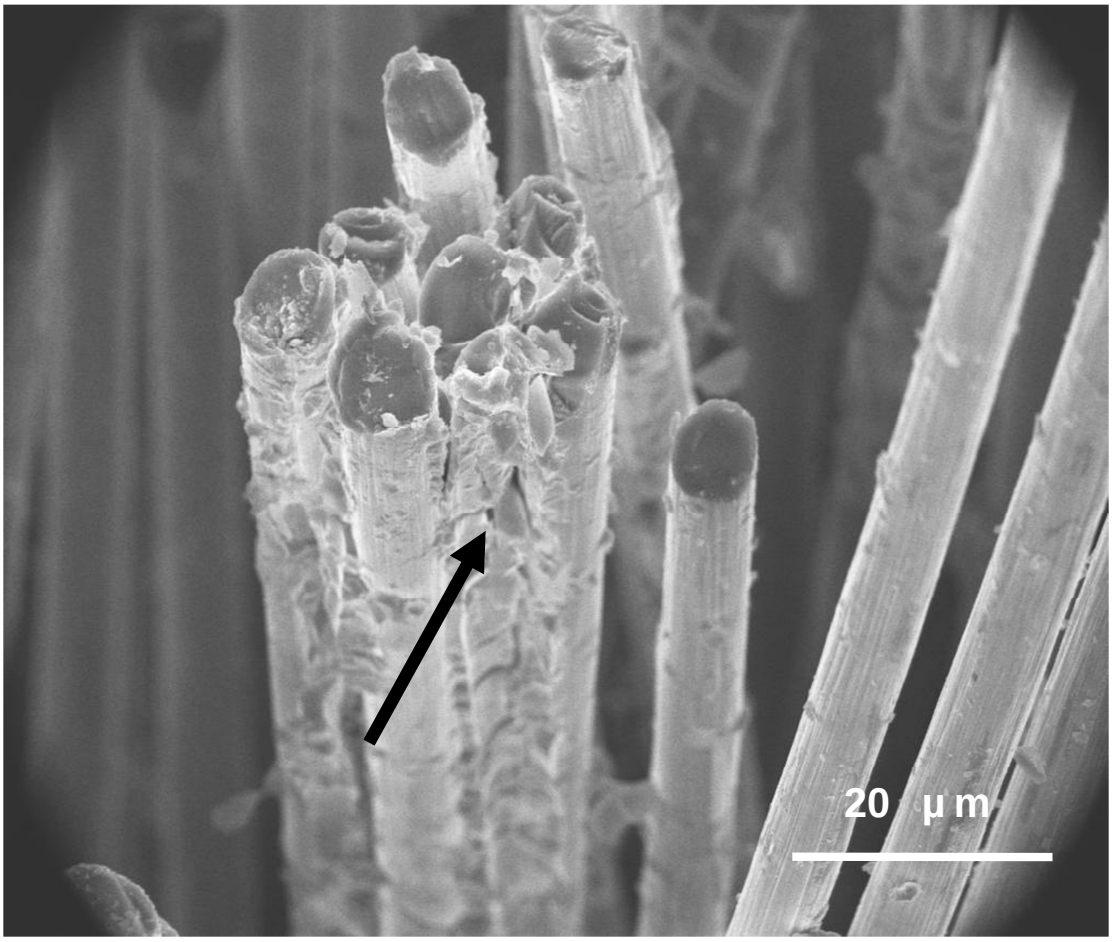


Figure 4: Scanning electron microscopic (SEM) image of a part of a fiber bundle after alumina deposition at temperature of 500 °C. The arrow indicates a residual coating still present although the corresponding fiber was degraded.

Initially, the coating was carried out at 500 °C; at this temperature the average coating deposition rate was approximately 0.06 nm per cycle (measures from steps visible in SEM). However, parts of the fibers are damaged as revealed in the SEM image shown in Figure 4. Fibers are damaged might be because of thermal oxidation. At the initial stage of the coating when there was not enough coating on the fiber, they might oxidize by water vapor at 500 °C. In the next series of experiments the temperature was reduced to 300 °C. At this temperature no damaged fibers were observed in the SEM images, the average deposition rate was approximately 0.033 nm per cycle. Thus, at 500 °C the deposition rate is higher, and fibers are affected. On the other hand, at 300 °C, the deposition rate is lower, but the fibers are unaffected.

One important aspect of alumina coating onto carbon fibers is to protect them from oxidation at elevated temperatures. Thus, the oxidation resistance of the alumina coated fibers is characterized by thermogravimetric analysis (TGA): 5 mm long coated fiber specimen were used for TGA. These specimens were heated from 30 °C to 900 °C with a heating rate of 5 °C/minute and subsequently held at 900 °C for 30 minutes in a flow of synthetic air. The results are shown in Figure 5. Oxidation onset temperature for the uncoated fiber and 45 thick coated fibers is approximately 630 °C and the fibers are completely burned at a temperature of approximately 825 °C and 880 °C, respectively. Thus, there might be a moderate oxidation protection of the fibres by the alumina coatings.

Although ALD deposition of alumina clearly has the merits detailed above, there was one difficulty to control the aluminum trichloride precursor dose. Aluminum trichloride is solid at room temperature but ALD is a gas-phase method. Sufficient vapor pressure was achieved by heating the aluminum trichloride to a temperature of 150 °C. However, these vapors are often deposited inside the carrier tube. Additionally, aluminum trichloride reacts rapidly with oxygen and/or moisture, and forms aluminum oxide. Aluminum oxide and chloride mixtures formed very hard, high temperature stable solid material. This solid material often blocked the carrier tube of aluminum trichloride. As a result the deposition process often had to be terminated midway, although there was still enough $AlCl_3$ inside the precursor chamber. Further investigation is needed to control the aluminum trichloride dose efficiently. Nevertheless, it was proved that the

atomic layer deposition of alumina can be applied to carbon fibers and also proved that the homemade reactor was functioning properly.

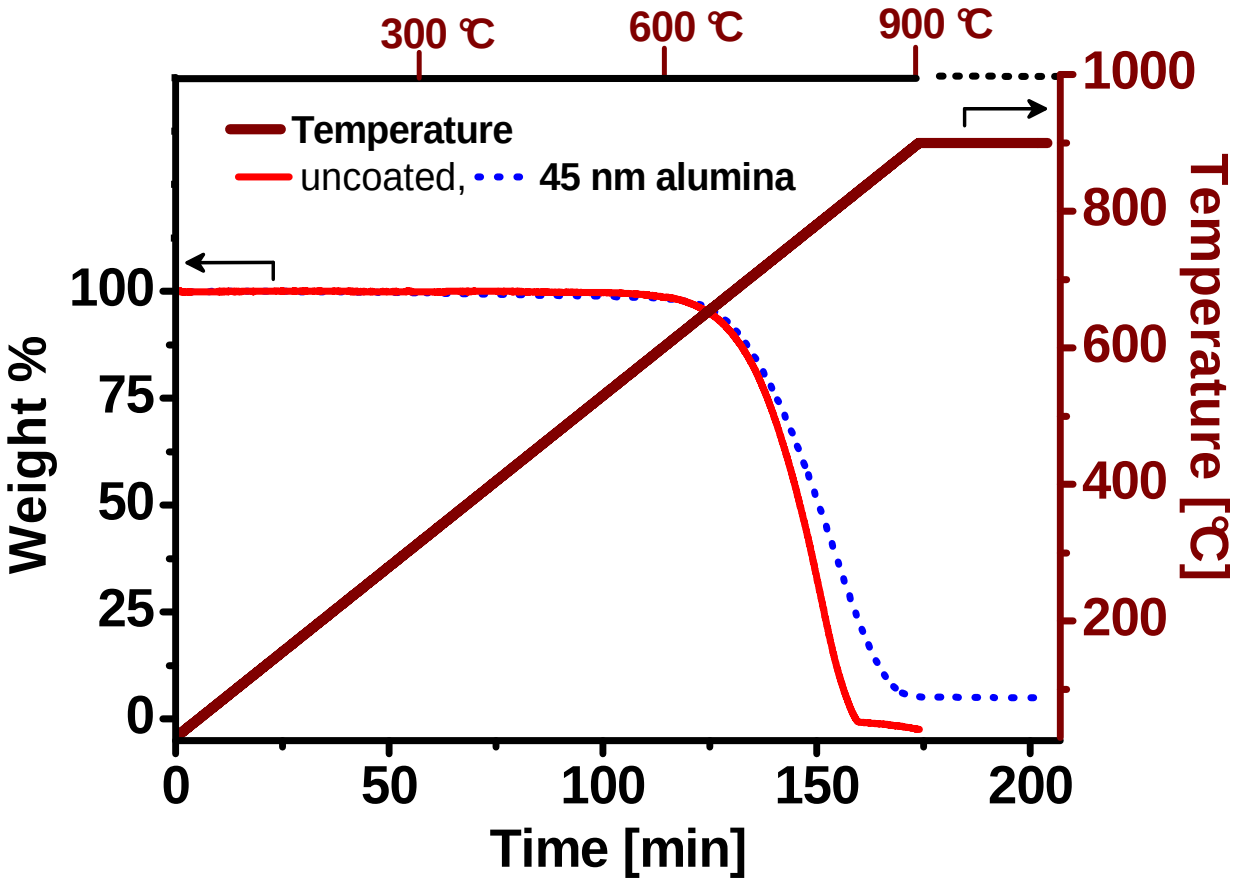


Figure 5: Thermogravimetric analysis (TGA) of the uncoated and alumina coated fibers. Coated fibers were heated from 30 °C to 900 °C with a heating rate of 5 °C min^{-1} and subsequently held at 900 °C for 30 min in a flow of synthetic air.

3.3 Alumina coating using organometallic precursor

3.3.2 Introduction

Atomic Layer Deposition (ALD) of alumina using aluminum trichloride and water as precursors is limited because of a) the difficulty to control the aluminum trichloride precursor b) the high deposition temperature (500 °C and 300 °C) which might damaged the substrate, especially, delicate materials, (e.g., carbon fibers were damaged during deposition at 500 °C), c) the chloride impurity in the coating, and d) the formation of HCl as byproduct which is corrosive, and affected the reactor badly. As for example, the valve responsible for delivering the aluminum trichloride was damaged (within six months). It was not possible to repair according to the manufacturer. Thus, the precursor has been changed but alumina depositions have been continued. There are reports of alumina deposition using trimethylaluminum and water at low temperatures (below 100 °C)3, [11]. Atomic layer deposition was applied to delicate materials, such as biological materials and polymer materials. Thus, ALD of alumina has been applied onto carbon fibers using trimethylaluminum and water at a temperature of 77 °C.

3.3.3 Results and discussion

Bundles of carbon fiber were coated with alumina by sequential exposure to trimethylaluminum and water vapor at reduced pressure and a temperature of 77 °C; the coated carbon fibers were characterized by scanning electron microscopy (SEM), transmission electron microscopy (TEM), energy dispersive X-ray spectroscopy (EDXS), atomic absorption spectroscopy (AAS), and thermogravimetric analysis (TGA). SEM images of coated fibers and fiber ends cut after the coating process are shown in Figure 6. The overview image (Figure 6a) reveals that the fibers within the bundle are still separated from each other, no bridging has been observed, and that coatings have been deposited evenly on fibers. Figure 6b shows the end of one individual fiber the surface of the coated region has a structure very similar to the surface of the non coated regions. Thus, the coatings are smooth, uniform and conformal. Seldom there were flakes of coating on the fiber surfaces that might be because of mainly two reasons: a) During removable of sample holder, coating that deposited inside the reactor, often plugged out and formed flakes on fibers (because sample holder was designed in such a way which

can just fits into the reactor). b) They were also forming during the SEM sample preparation, coating that remove from the front parts of the fibers during the segregation of samples can also forming flakes. There are almost no regions with the exceptions of the freshly cut ends that indicate delamination of the coating. Thus, there seems to be good adhesion of the coating to the fiber.

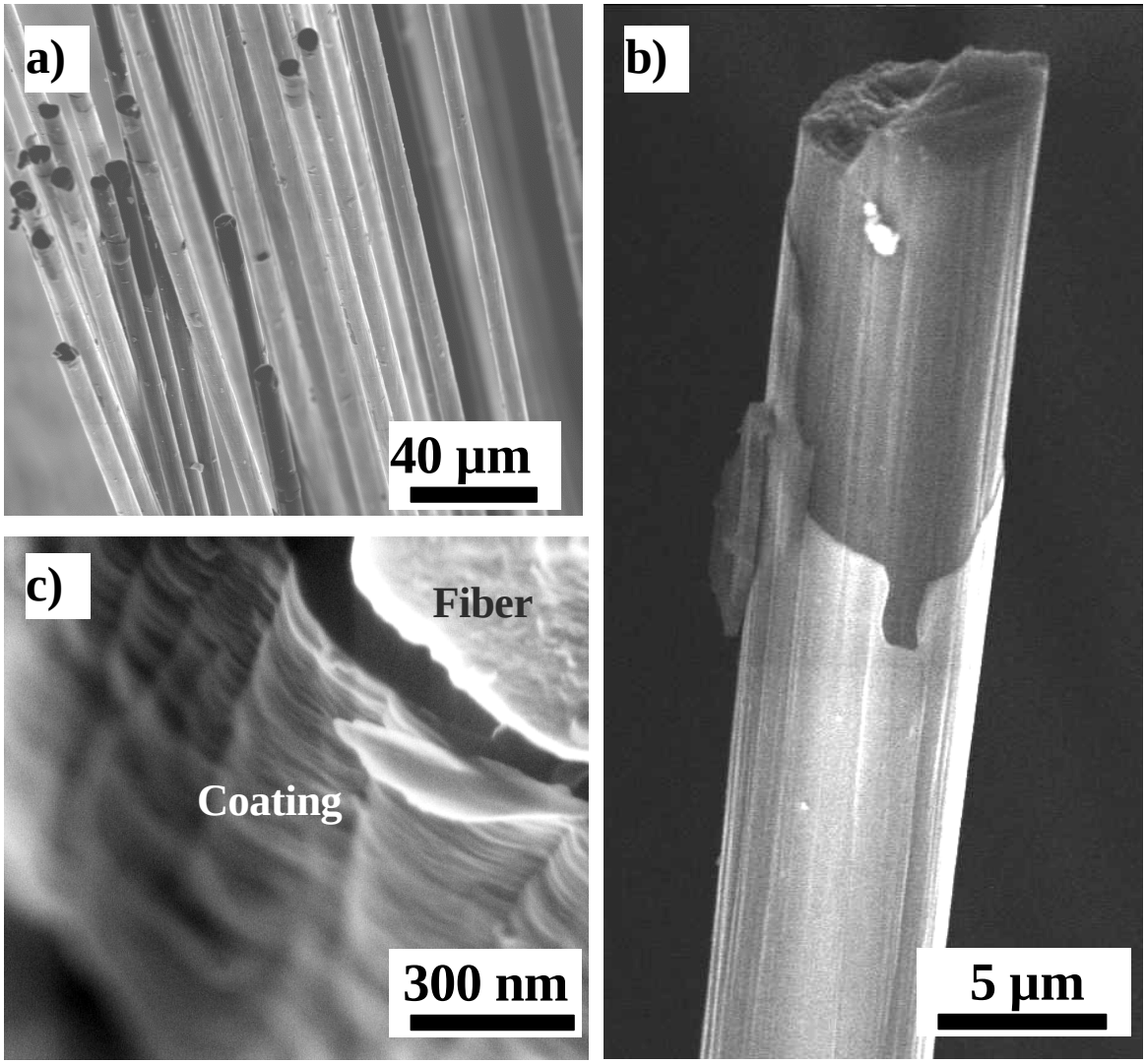


Figure 6: Scanning electron microscopic (SEM) images of fibers coated with layers of alumina obtained after 350 cycles: a) overview of a part of a fiber bundle coated with alumina, b) a single fiber coated with alumina, dark gray part in front is the carbon fiber and bright part is the alumina coating, and c) magnified images with an axis of view almost perpendicular to the cut end. One can see uniform and conformal coating and good adhesion of the coating.

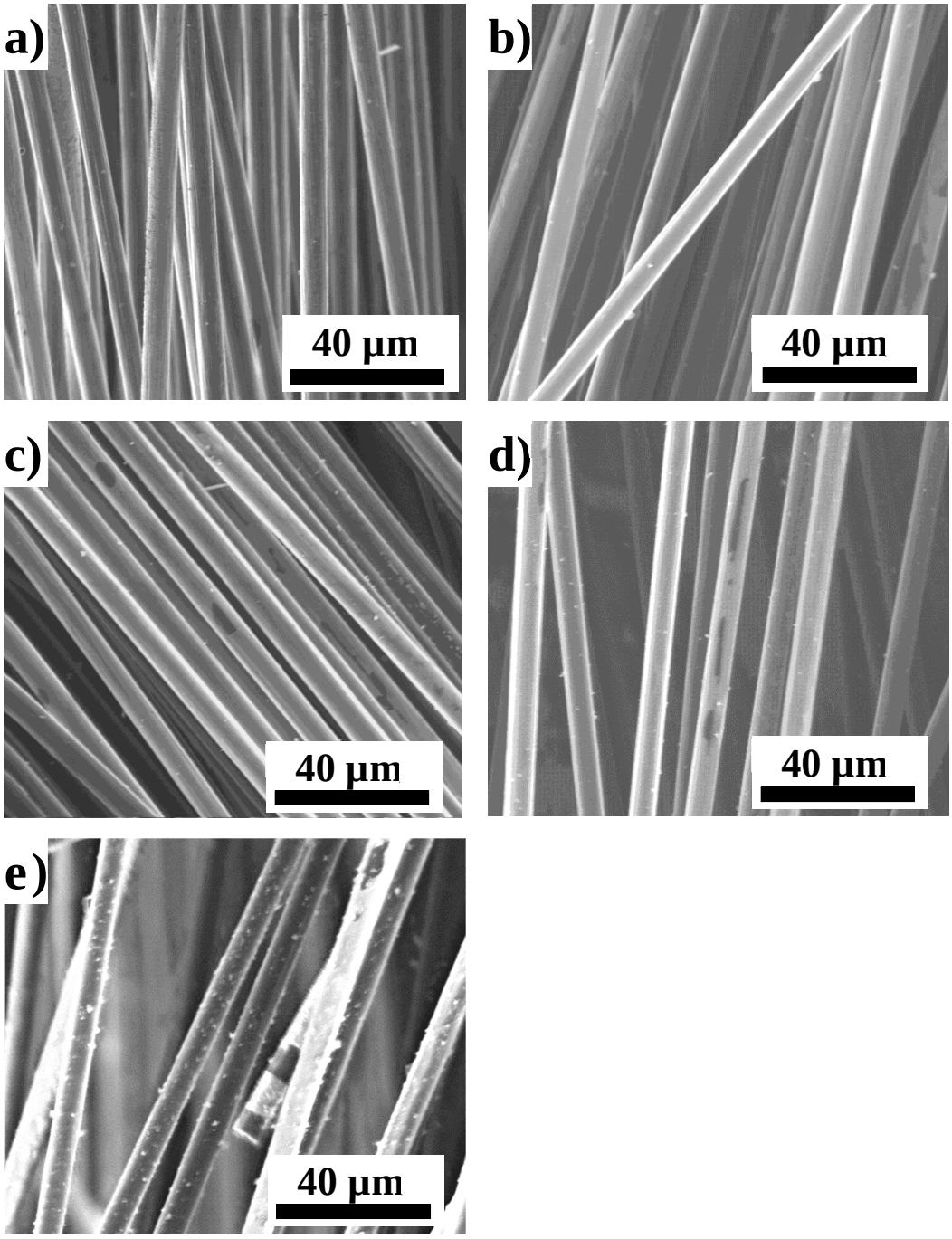


Figure 7: Carbon fibers coated with 50 nm thick alumina were bend around cylinders of decreasing radius of a) 37.5 mm ; b) 12.5 mm c) 7.5 mm d) 0.75 mm. e): fibers were bend around a razor blade. The fibers were subsequently straightened again and imaged via electron microscopy.

In places where the cutting induced delaminations were formed, one can observes clear steps (see Figure 6c). These indicate that cohesion within the coating is stronger than the adhesion.

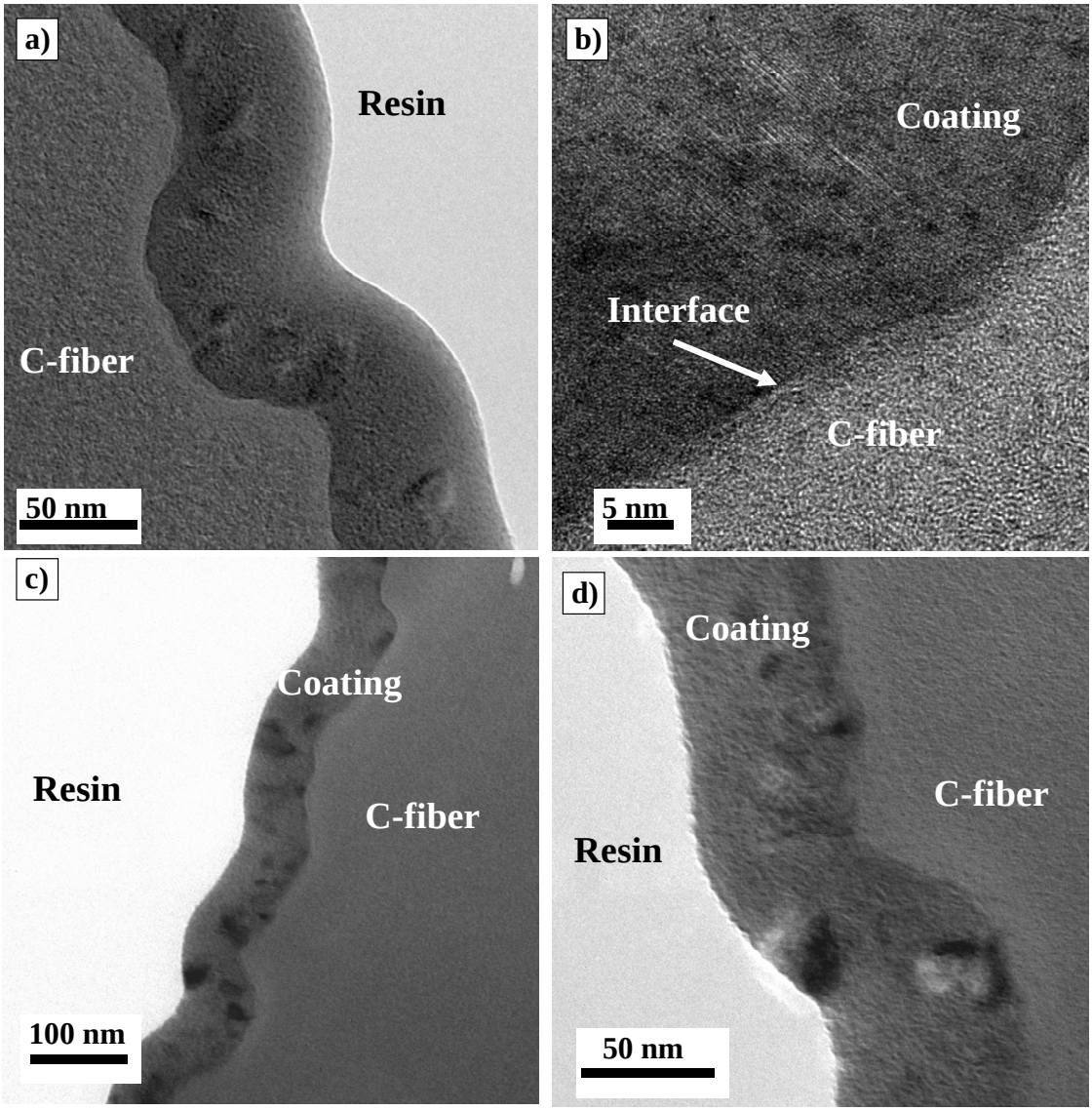


Figure 8: (a) Transmission electron microscopic (TEM) images of a cross section perpendicular to the fiber axis through a near surface region of a single fiber coated with alumina (and embedded into an auxiliary resin). (b) Enlarged image of the interface between the fiber and the coating (arrow). (c) and (d) Dark-field images. The variations in gray shades in the images indicate some degree of crystallinity, albeit there seems to be coexistence of several polymorphs. The degree of crystallinity seems not to be a function of the distance from the interface.

In addition, the occurrence of these well-defined steps allows to estimate the layer thicknesses. To get a bit more insight into the adhesion strength, fibers were bent around cylinders of decreasing radius (see Figure 7). If the fibers are bent around cylinders of radii down to 12.5 mm, no significant delamination was observed. Slight delamination (less than one percent of the total area) occurred, if the bending radius was in between 7.5 mm and 0.75 mm. However, severe delamination of more than half of the total area occurred only if the fibers were bent around the edge of a razor blade. This bending around a razor blade caused most fibers to break and delamination occurred in the proximity of the break points. Adhesion is a function of residual mechanical stress and of defects within the material. Residual stress might arise from mismatch of thermal expansion coefficients, if deposition is done at an elevated temperature and the fibers are subsequently cooled down. Defects might arise from thermally induced recrystallisation after deposition that causes fault lines and grain borders within the material. The process depicted here is conducted at a comparatively low temperature, thus it is likely that there is a low amount of residual stress and defects (e.g. the TEM in Figure 8 indicates some degree of crystallinity), which favors the adhesion of the coatings to the fibers.

A TEM image of a cross section of the interface between fiber and coating (prepared using a focused ion beam) shows that the coating is conformal; the distance between the two interfaces is almost independent on the position despite the corrugated surface (see Figure 8). The magnified image Figure 8b, reveals that the interface between fiber and coating is sharp: if there is a zone of inter-diffusion it has a thickness of less than 3 nm (approximately).

Elemental analysis of the coated fiber by EDXS (Figure 9) revealed that it contained a large amount of carbon as well as aluminum and oxygen. The large amount of carbon was expected because of the carbon fiber, the presence of aluminum and oxygen confirms the expected alumina coating. Because EDXS does not always yield accurate quantitative chemical compositions, coated fibers were burned selectively by thermal oxidation in air. The carbon, nitrogen and hydrogen content of the residue were measured via elemental flash analysis. Results of this analysis indicate that the amount of carbon, hydrogen within the residue of thermal oxidation were 1.6%, 0.06% respectively and there was no nitrogen (if nitrogen is present that might be less than the detection

limit, i.e., <0.01%). Possibly, this small amount of hydrogen and a part of the carbon can be attributed to decomposition products of the trimethylaluminum, and the rest of the carbon to an irremovable part of the fiber. The ratios of mass to length of uncoated and coated fibers were obtained by gravimetry.

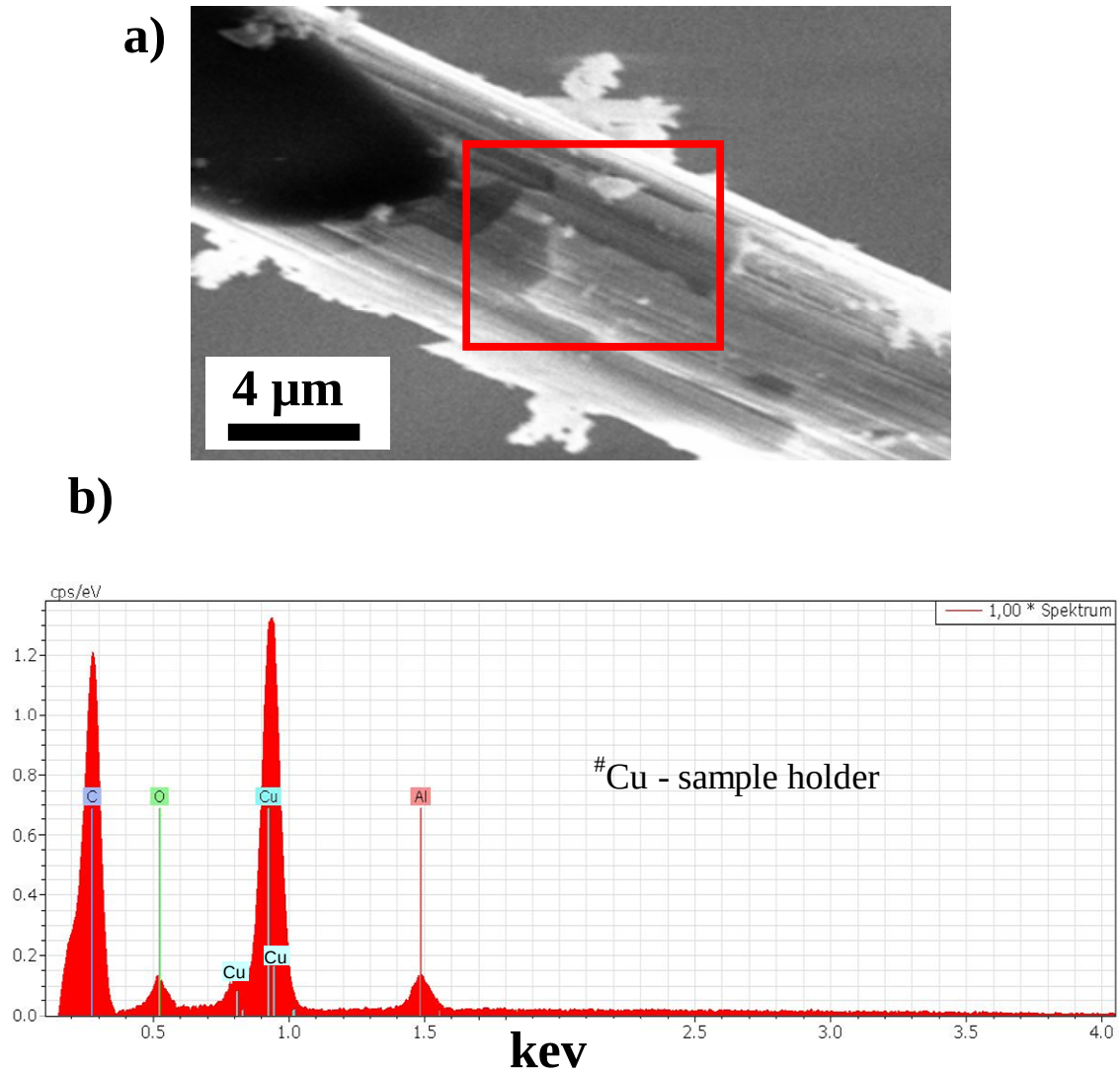


Figure 9: Elemental analysis of a coated carbon fiber by energy dispersive X-ray spectroscopy (EDXS). a): the area selected for EDXS analysis. b): EDXS-spectrum indicating that there are four elements present in that selected area. There is a signal for copper that is due to the sample holder used for this analysis. There is a dominating signal for carbon originating from the fiber, and signal for aluminum and oxygen as expected from the alumina coating.

As well as the ratio of the mass of the deposited alumina to the length of the fiber was obtained independently from elemental analysis by atomic absorption spectroscopy. If this value is subtracted from the weight/length of the coated fiber, one obtains a weight/length that differs from the original weight/length of the uncoated fiber by only 0.7%. Thus, one can conclude that the carbon fibers did not significantly lose weight even though the process involved the presence of moisture. This preservation of the fiber might be due to low process temperature of 77 °C.

To determine, whether fibers of a bundle were coated evenly and regardless of the position within or along the bundle, a bundle (coated at 77 °C using 450 deposition cycles) was split into parts originating from regions close to the centre of the bundle and close to the perimeter of the bundle and cut into segments originating from the part that faced the gas supply, a middle part and a part that faced the pump during the coating process. For each of these segments the amount of aluminum (Al) was measured via elemental analysis by AAS as described above: the aluminum weight fraction varies from 5.3 weight % at the part facing the pump to 6.5 weight% at the part facing the gas supply and from 7.4 weight% at the fraction taken from the perimeter to 4.8 weight% at the fraction taken out of the centre of the bundle. This translates into an estimated coating thickness (respectively deposition rate) which varied along the fiber from the end facing the gas supply to the end facing the pump from166 nm to 126 nm (0.37 nm/cycle to 0.28 nm/cycle) and from center to perimeter from 114 nm to 183 nm (0.25 nm/cycle to 0.40 nm/cycle).

The coating thickness of the same fiber bundle was measured from SEM images at various positions along the length and also along the cross-section of the fiber bundle. SEM images revealed the general trend but the average coating thickness was 126 nm. Discrepancies between the results in these two methods can be attributed to experimental error and the uncertainties of the parameters used for calculating the coating thickness (e.g. the value taken for the density). The variations in coating thickness observed here indicate that conditions for ALD might not have been fully achieved. The coating thickness increases with decreasing distance of the fiber parts to the precursor source. This observation, combined with an observed deposition rate above the usual value, might indicate that there is in addition to chemical reaction of the precursors some

degree of physisorption taking place in a non-equilibrium manner and being influenced by the flow characteristics of the reactor.

The coating deposition rate was measured by the analysis of SEM images of ends of fibers that were exposed to various numbers of coating cycles and cut in the middle after the process such as the one shown in Figure 6. As can be seen from Figure 10, there is a linear relationship between the coating thickness and the number of cycles with an average deposition rate of (0.25 ± 0.02) nm per cycle. The deposition rate is lower than the value that can be estimated theoretically for a monomolecular layer of alumina but larger than the rates usually reported in the literature[12]. Purge times were increased up to 100 s (keeping the flow of purge gas constant at 40 sccm) and subsequently the flow of purging was increased to 100 sccm (keeping the purge time at 100 s). Both variations had no significant effect on the amount deposited per cycle.

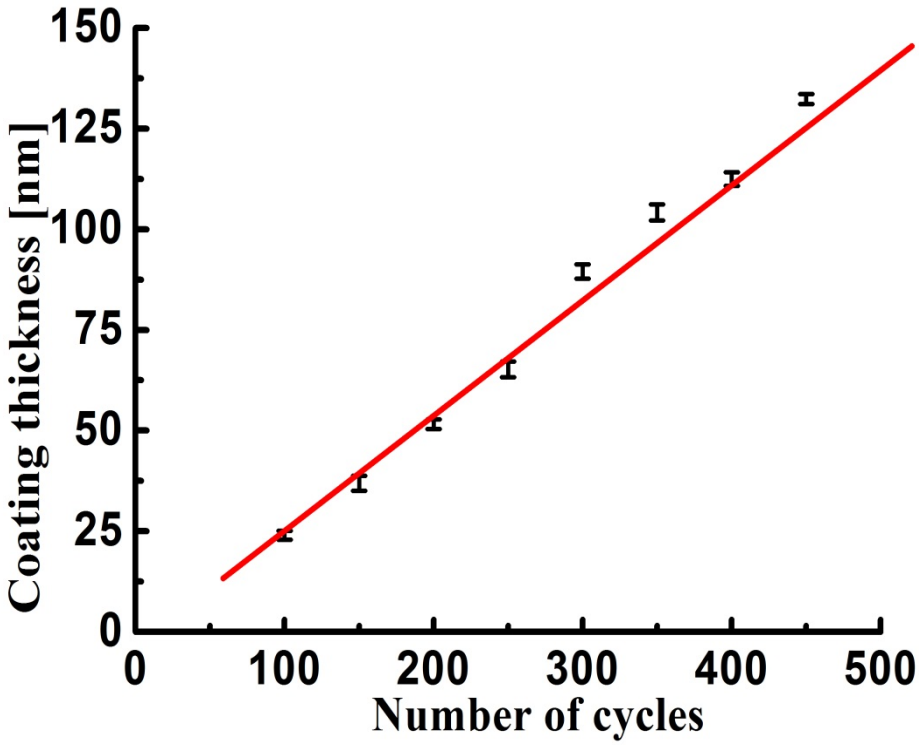


Figure 10: Coating thickness as a function of the number of cycles. The coating thickness increases almost linearly with the number of cycles at an average deposition rate of (0.25 ± 0.02) nm per cycle.

The growth per cycle decreased to (0.17 ± 0.03) nm/cycle, however, if the temperature was raised to 150 °C. The explanation for the growth per cycle observed here thus might be the comparatively low deposition temperature used in our experiments. In most reports in the literature, the deposition temperature is significantly higher than the 77 °C used here. Thus, part of the deposition may be due to physisorbed water that is present in a larger amount if the temperature is low, but becomes less if the temperature is increased. Since growth per layer is independent of purge time in our case, one might conclude that purging of an excess of gaseous precursors was complete in each cycle and that physisorbed water was either completely removed as well or desorbed with such a low rate that further purging did not change the residual water content.

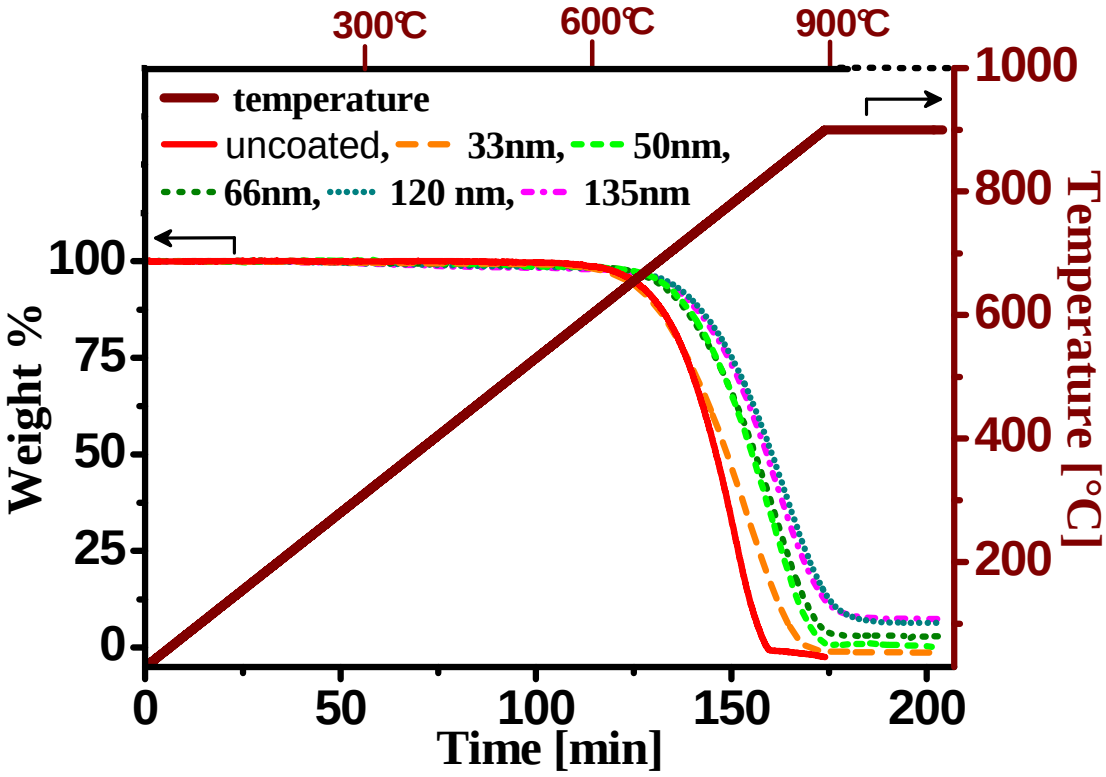


Figure 11: Thermogravimetric analysis (TGA) of coated fibers with various coating thicknesses. The specimens were heated from 30 °C to 900 °C with a heating rate of 5 °C/minute and subsequently held at 900 °C for 30 minutes in synthetic air. Oxidation onset temperature of the coated fiber increases with the increase of coating thickness and levels off for coating thicknesses exceeding approximately 100 nm.

There are indeed reports showing that outgassing of physisorbed water in low temperature ALD processes applied to substrates of high surface area like powders and nanotubes may need times even longer than half an hour[13]. In Figure 10, the data can be represented by a line passing through the origin of the graph. This indicates that the coating starts spontaneously from the first cycle without a nucleation period, or in other words that a continuous layer of limited growth or a dense array of tiny seed particles are formed already at a very early stage of the coating process. This interpretation is further supported by the smooth and conformal appearance of the coating. To some extent, this might be unexpected because (i) carbon fibers presumably have a comparatively low concentration of reactive functional groups like hydroxyl groups on the surface and (ii) there are reports that carbon nanotubes seem to resist coating by ALD unless pretreated by azo compounds, nitric oxide or surfactants. On the other hand, the surface of a carbon fiber is not a smooth defect free graphitic basal plane as one usually presumes in the case of carbon nanotubes: it might expose to the gas phase at least to some extend polar groups created via oxidation and edges of disrupted graphitic planes. Furthermore, there are reports of significant adsorption of trimethylaluminum onto graphitic carbon[14]. This physical adsorption might be the reason for the fast induction and comparatively high initial deposition rate of the coating process.

Oxidation resistance of the alumina coated fibers is characterized by thermogravimetric analysis (TGA) as described in the previous section: The results are shown in Figure 11; the oxidation onset temperature (approximately 3% weight loss) for the uncoated fiber is approximately 630 °C and the fibers are completely burned at temperatures of approximately 825 °C. In case of fibers coated with a 33 nm thick layer of alumina, the oxidation starts at a temperature of approximately 600 °C and the fibers are burned completely at a temperature of approximately 800 °C. With increasing thickness of the coating the oxidation onset temperature increases slightly and also the amount of ash. Oxidation onset temperature reached a plateau value of 660 °C for fibers bearing a coating of a thickness of a 120 nm or more. Thus, alumina coating improves the oxidation resistance of the carbon fibers to a moderate extend.

As mentioned above, 5 mm long specimens were used for the oxidation test. These specimens were cut from the fiber bundle; however, at the freshly cut ends, the

coating was removed during cutting process (as shown in Figure 6b). Thus, there is the possibility that oxidation starts from the unprotected ends, and actually will be less prominent in defect free endless fibers. To test this hypothesis, one 5 mm long specimen was coated after cutting in such a way that both ends were covered with the coating. The oxidation resistance of these end protected fibers was compared to fibers with unprotected ends (see Figure 12). Both specimens were heated from 30 °C to 500 °C with a heating rate of 5 °C per minute and subsequently held at 500 °C for 300 minutes in synthetic air. In case of unprotected ends, fiber oxidation starts already at the very beginning, fibers with both ends protected are stable up to temperature of approximately 200 °C. At the end of this experiment, fibers with unprotected ends lost approximately 9% of their mass, the fibers with protected ends lost 7%. Thus, these results indicate that an endless fiber may be more resistant to oxidation than fibers with unprotected ends. We notice, however, that the effect is not very prominent. Thus, there must be as well a mechanism of oxygen diffusion through the coating. Figure 11 seems to indicate that the oxidation protection levels off at layer thicknesses exceeding 100 nm. Layers of any thickness exceeding this threshold seem to fail at temperatures around 660 °C regardless of their thickness. Thus, one might come to the conclusion, that the layers become significantly more permeable at that temperature, allowing oxygen diffusion perpendicular to the layer surface. One possible explanation for this fact might be a mismatch of the coefficients of thermal expansion of fiber and coating, as for example has been shown in the case of alumina coating as an oxidation barrier for iron particles[15, 16]. In that case the coefficient of thermal expansion of the iron particle was larger than the corresponding coefficient of the coating. Thus, thermal expansion leads to extensional stress on the coating and finally cracks formation[17]. In our case, the coefficient of expansion of the fiber has a lower value than the corresponding value of the coating. Thus, in our case the coating will experience compressive stress upon heating. This might probably seal cracks instead of opening them up. Another process that has the potential to increase permeability may be change in structure from amorphous to crystalline, which might induce shrinkage of the coating due to the densification that is associated with crystallization and may give rise to grain boundaries that act as pores passing through the coating. In order to investigate this detail, coated fibers were

subjected to complete oxidation in air, one sample at a temperature of 900 °C, another one at a temperature of 550 °C (complete oxidation of fibers took 4 hours in the first and 12 hours in the latter case). The coatings that remain after these treatments were investigated via transmission electron microscopy (see Figure 13). The image shows a still low degree of crystallinity in the sample obtained via oxidation at 550 °C whereas the sample obtained via oxidation at 900 °C showed a significant degree of crystallization even exposing details that may be interpreted as cracks within the coating. In case of oxidations at 900 °C, grains size are bigger larger than at 550 °C.

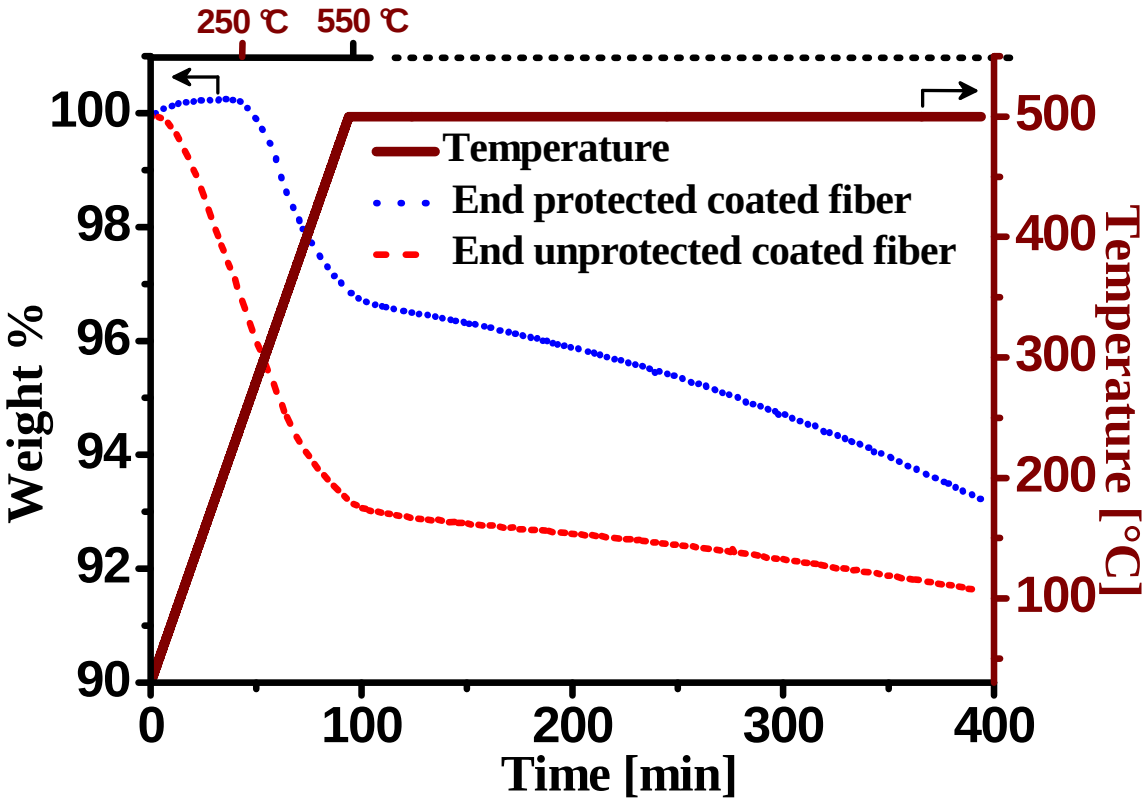


Figure 12: Thermogravimetric analysis (TGA) of both end protected, and both end unprotected coated fibers with a coating thickness of 135 nm. The specimens were heated from 30 °C to 500 °C with a heating rate of 5 °C/minute and subsequently held at 500 °C for 300 minutes in synthetic air. End unprotected coated fibers started to oxidize from the very beginning and within 400 minutes lost approximately 9% weight; end protected coated fibers started oxidation approximately after 40 minutes and within 400 minutes lost approximately 7%.

Thus, it is likely that the observed lowering of the oxidation stability at higher temperatures is due to crystallization. Oxidation thus might be delayed, if compounds are included into the coating that delay crystallization or preferentially fill the gaps between the crystal grains.

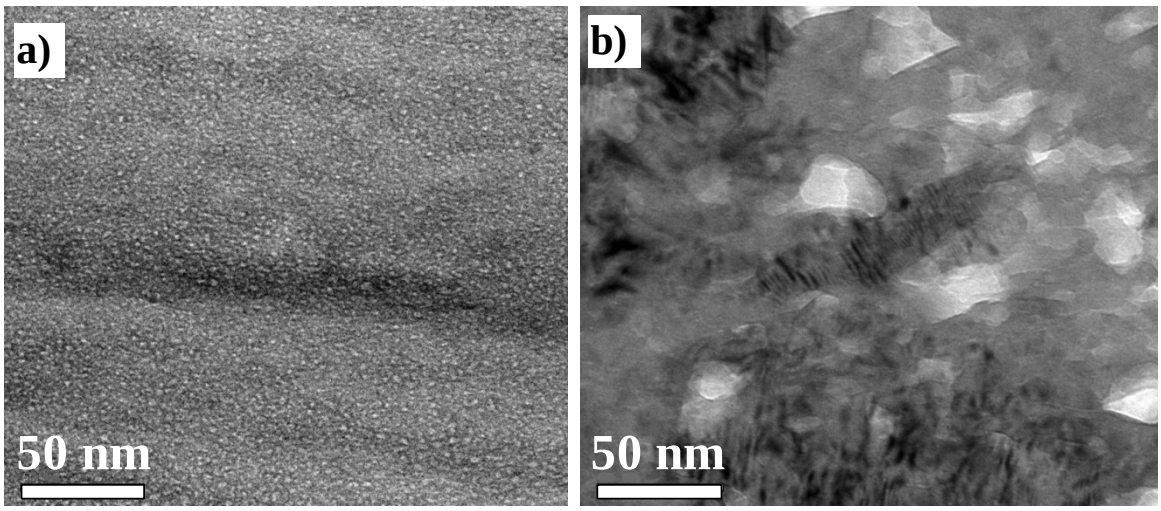


Figure 13: Transmission electron microscopy images of residual coatings after complete oxidation of the fibers in air at an oxidation temperature of a) 550 °C and b) 900 °C. Whereas sample a) still has a low degree of crystallinity, sample b) has crystallized during the heat treatment, possibly opening up pores and pathways for oxygen diffusion perpendicular to the layer.

3.4 Titania coating using titanium tetrachloride and water

3.4.1 Introduction

Alumina coating can improve oxidation onset temperature up to 660 °C whereas uncoated fibers started to oxidize at 630 °C. However, oxidation protection levels off at layer thicknesses exceeding 100 nm; regardless of their thickness alumina seem to fail at temperatures around 660 °C. Thus, a coating is needed which can improve the oxidation resistance further. Titanium oxide (titania) layers prepared by sol-gel methods have been used for oxidation protection of carbon fibers[18].

In addition, thin films of titania have several applications such as insulating layers for electronic and optoelectronic devices, active layer for solid state chemical sensors[19], solar cells, and photo catalysis to remove toxic and carcinogenic organic impurities from water[20]. Titania is also used as white pigments because of its brightness and high refractive index (2.5-2.9). Thin layers of titania are used here as oxidation barriers coating for carbon fibers.

Atomic layer depositions (ALD) of titania onto various substrates other than fibers have been reported using titanium tetrachloride and water[21]. In another report titania has been deposited using two separate methods titanium isopropoxide and water, as well as titanium isopropoxide and hydrogen per oxide[22]. Here, titania was deposited onto carbon fibers by sequential exposure to titanium tetrachloride ($TiCl_4$) and water vapor at reduced pressure and an ambient temperature. Coating was characterized by scanning electron microscopy (SEM), transmission electron microscopy, energy dispersive X-ray spectroscopy (EDXS), and thermogravimetric analysis (TGA).

3.4.2 Results and discussion

Carbon fibers were coated with titania by exposing them to the pulses of titanium tetrachloride ($TiCl_4$) and water vapor at a temperature of 200 °C. Two sets of experiment were carried out with two separate purge times 15 s and 40 s. In case of 15 s purge time coating was rough and uneven as revealed in scanning electron microscopic (SEM) images in Figure 14, the surface of the coating does not reflect the original structure of the fiber. Figure 14a shows that the coating was delaminated from the middle of the fibers and Figure 14b shows that cracks are formed within the coating, probably

this happens during handling of the specimens, thus, adhesion is poor. These rough films may be due to bulk gas phase reaction which may give rise to solid titania precipitation onto fibers. The film deposition rate was measured by the analysis of SEM images; it was 12 nm/cycle whereas the thickness of a monolayer is 0.28 nm[21a].

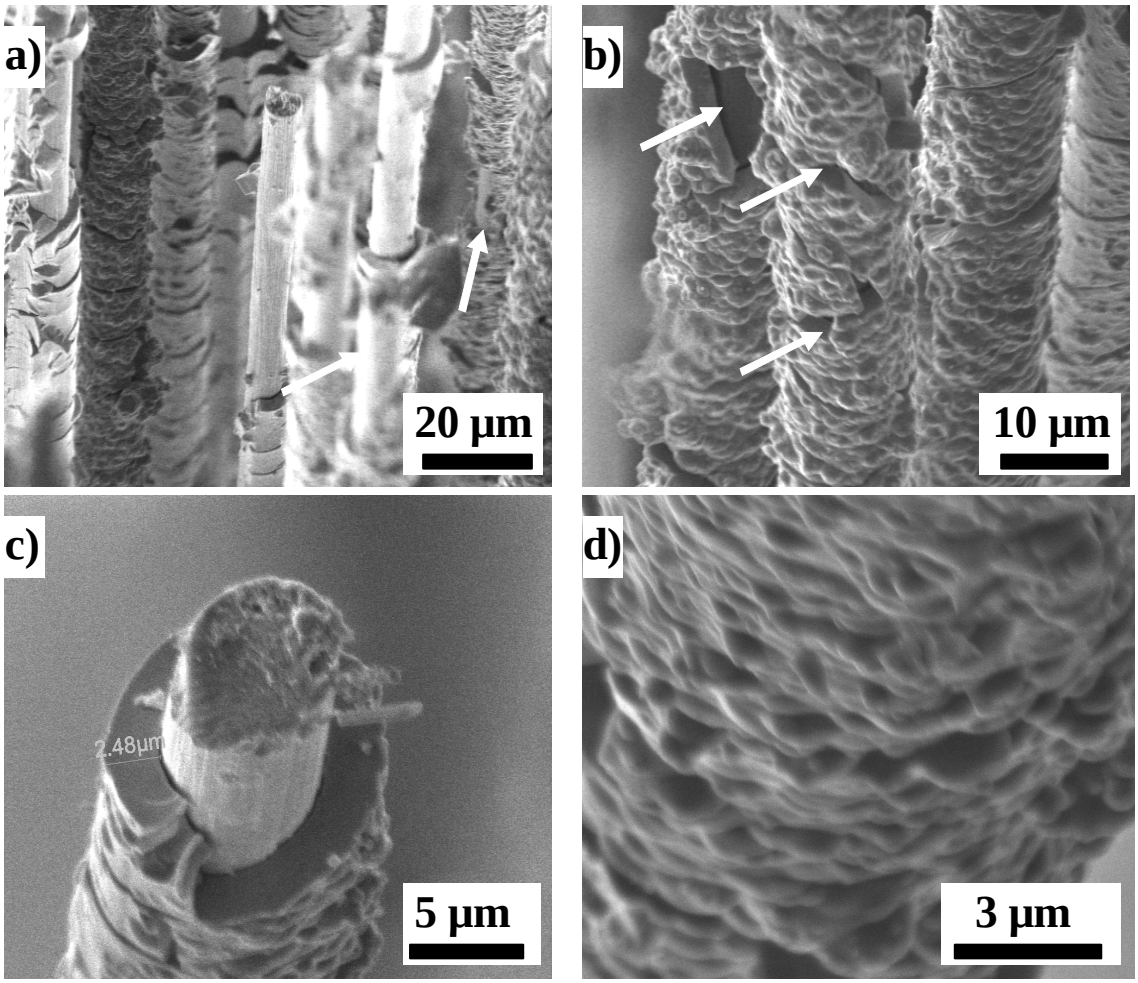


Figure 14: Scanning electron microscopic (SEM) images of titania coated fibers, coating was carried out for 200 cycles with 15 s purge time: a) part of the fiber bundle coated with titanium oxide, arrows indiacate delaminated part of the coating b) a close up view of the fiber bundle coated with titanium oxide, arrows indiacate cracks within the coating c) a step of the coating on the fiber surface d) non-uniform and non-conformal coating on the fiber surface.

Thickness of these films was more than a monolayer might be because of precursors mixing already in the gas phase. Thus, 15 s purge time leads to non-uniform and non-conformal coatings through gas phase precipitation (for the detail, see chapter 4).

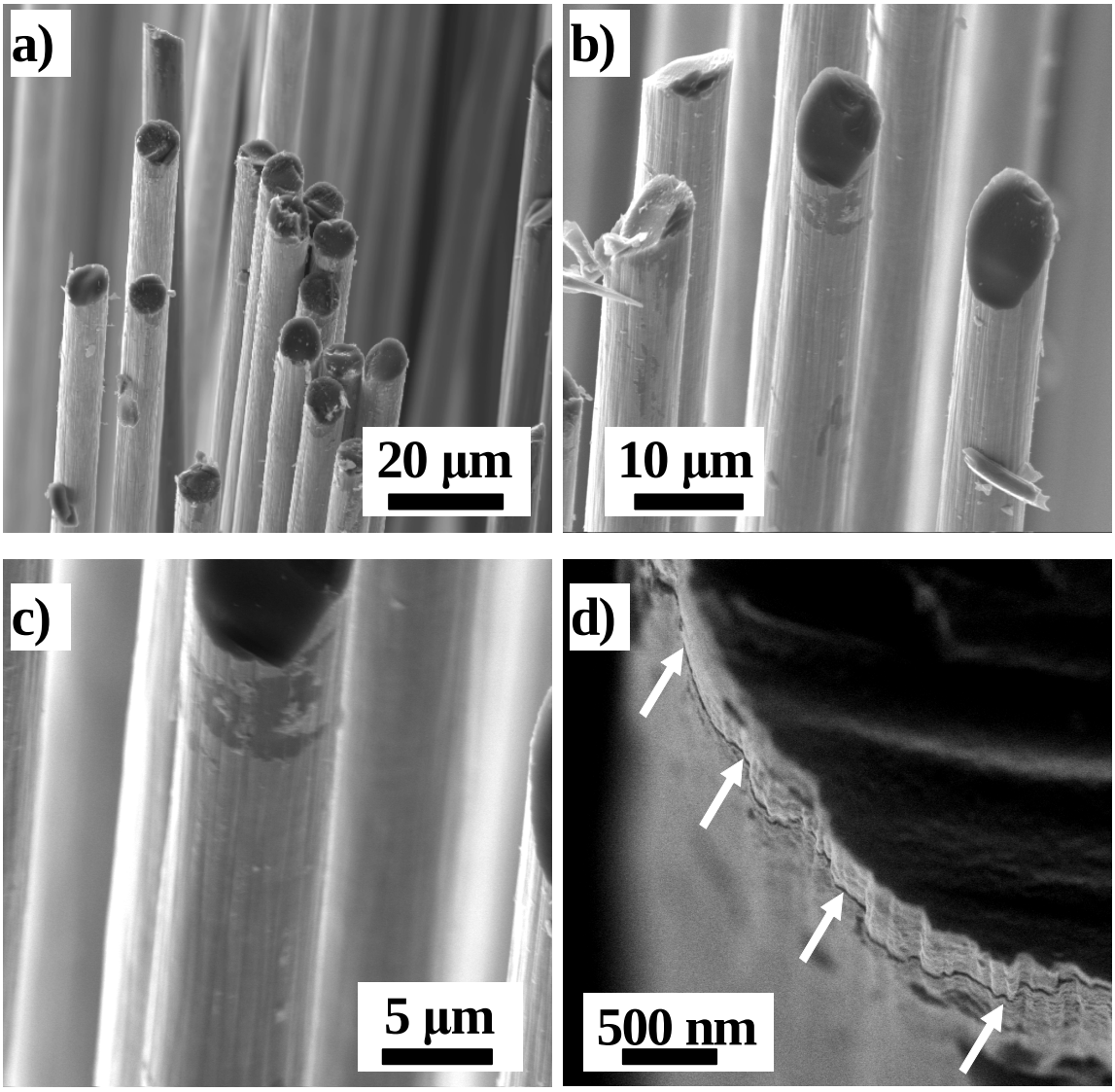


Figure 15: Scanning electron microscopic (SEM) images of titania coated fibers, coating was carried out for 150 cycles with 40 s purge time: a) part of fiber bundle coated with titania; (b) a close up view of the fiber bundle coated with titania; the dark gray part in front is the carbon fiber and the bright part is the titania coating; (c) uniform and conformal coating on the fiber surface; (d) a step of the coating on the fiber surface (indicated by arrows).

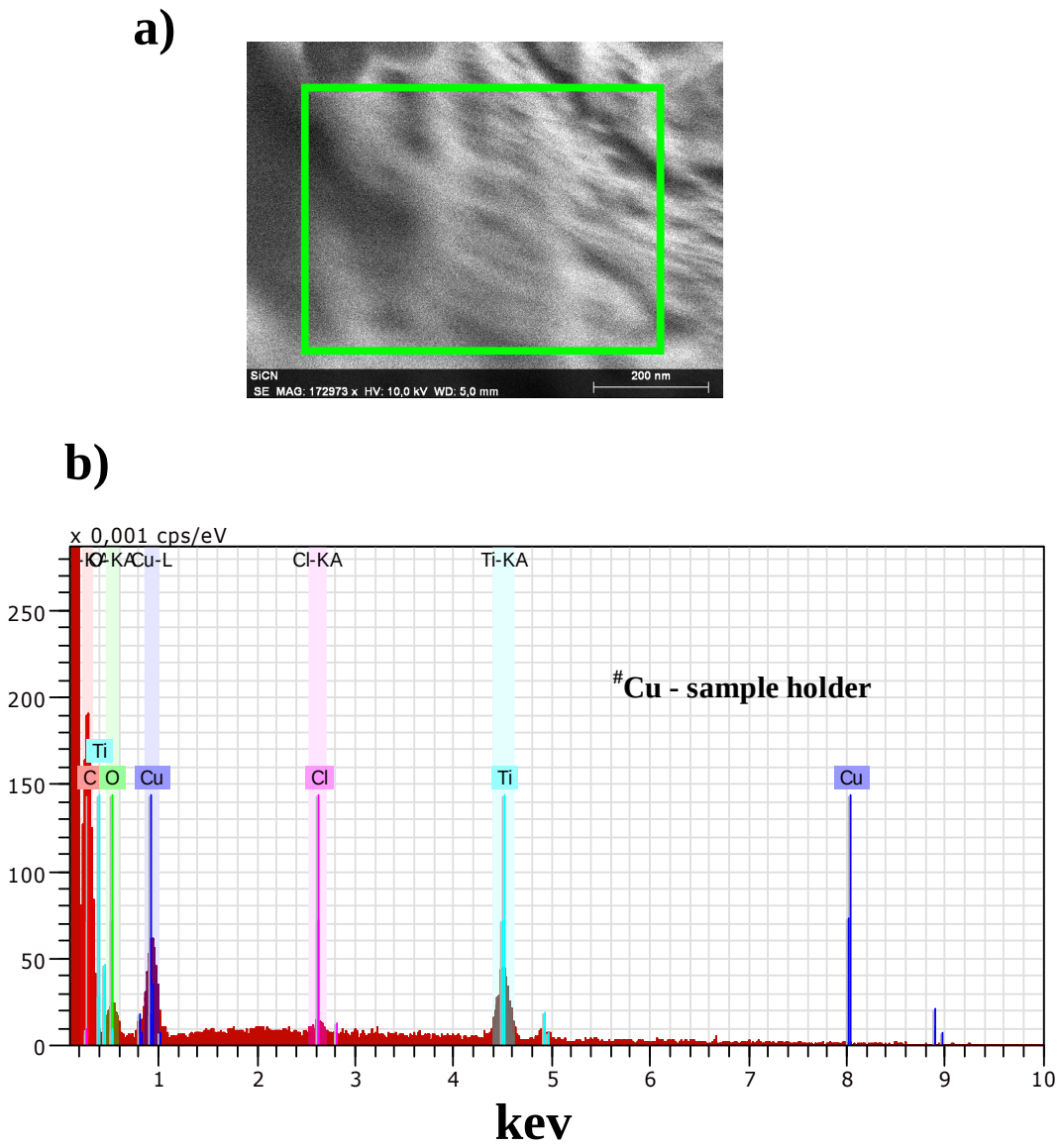


Figure 16: Energy dispersive X-ray spectroscopy (EDXS) of the coated fibers after 150 cycles: a) a part of the selected single fiber for EDXS (b) Energy dispersive X-ray spectroscopy (EDXS) of the selected part.

SEM images of coated fibers with 40 s purge time are shown in Figure 15. The overview image (Figure 15a and b) reveals that the fibers within the bundle are still separated from each other, no bridging has been formed, and that coatings have been deposited evenly onto fibers. Figure 15b shows the end of individual fibers, where one can see a contrast between fiber and coating. Besides this intensity contrast, the surface of the coated region

has a structure very similar to the surface of the non coated regions. This fact is as well visible in the close up images Figure 15c and 15d. Thus, the coatings are smooth, uniform and conformal.

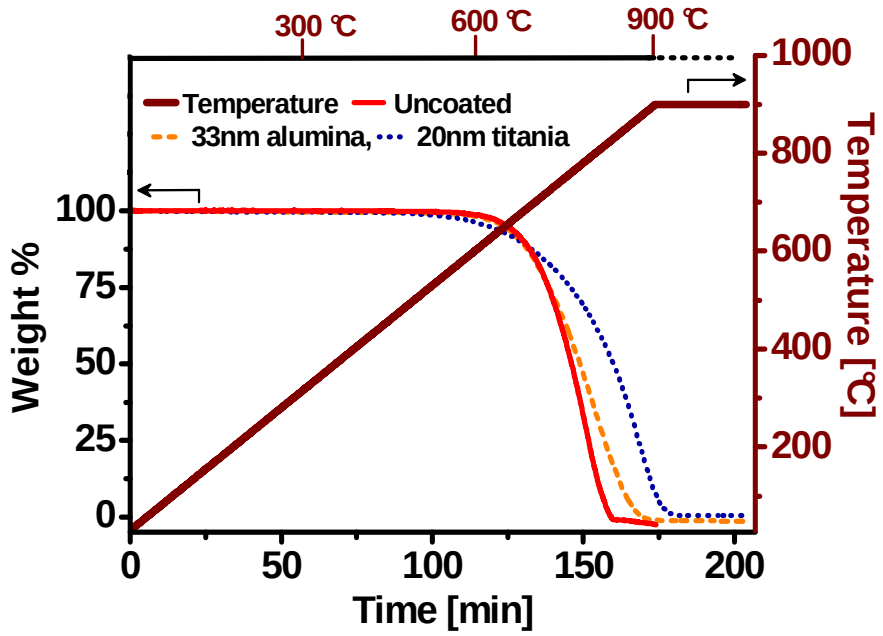


Figure 17: Thermogravimetric analysis (TGA) of the titanium oxide, aluminum oxide coated fibers. The specimens were heated from 30 °C to 900 °C with a heating rate of 5 °C/minute and subsequently held at 900 °C in synthetic air.

There are almost no regions with the exceptions of the freshly cut ends that indicate delamination of the coating. Thus, there seems to be good adhesion of the coating to the fiber. In places where the cutting induced delamination occurred, one observes clear steps (see Figure 15d). These indicate that cohesion within the coating is stronger than the adhesion. In addition, from these well-defined steps one can measure the layer thickness. Thickness of the titania layer was 20 nm for 150 cycle deposition, which translate into deposition rate of 0.13 nm per cycle (thickness of a monolayer 0.28 nm/cycle)[21a]. Deposition rate is well below compare to the thickness of a monolayer, which indicates that this process is an atomic layer deposition. Elemental analysis of the coated fiber by energy dispersive X-ray spectroscopy (EDXS) (see Figure 16) revealed dominating carbon content, titanium, oxygen, and a small amount of chlorine.

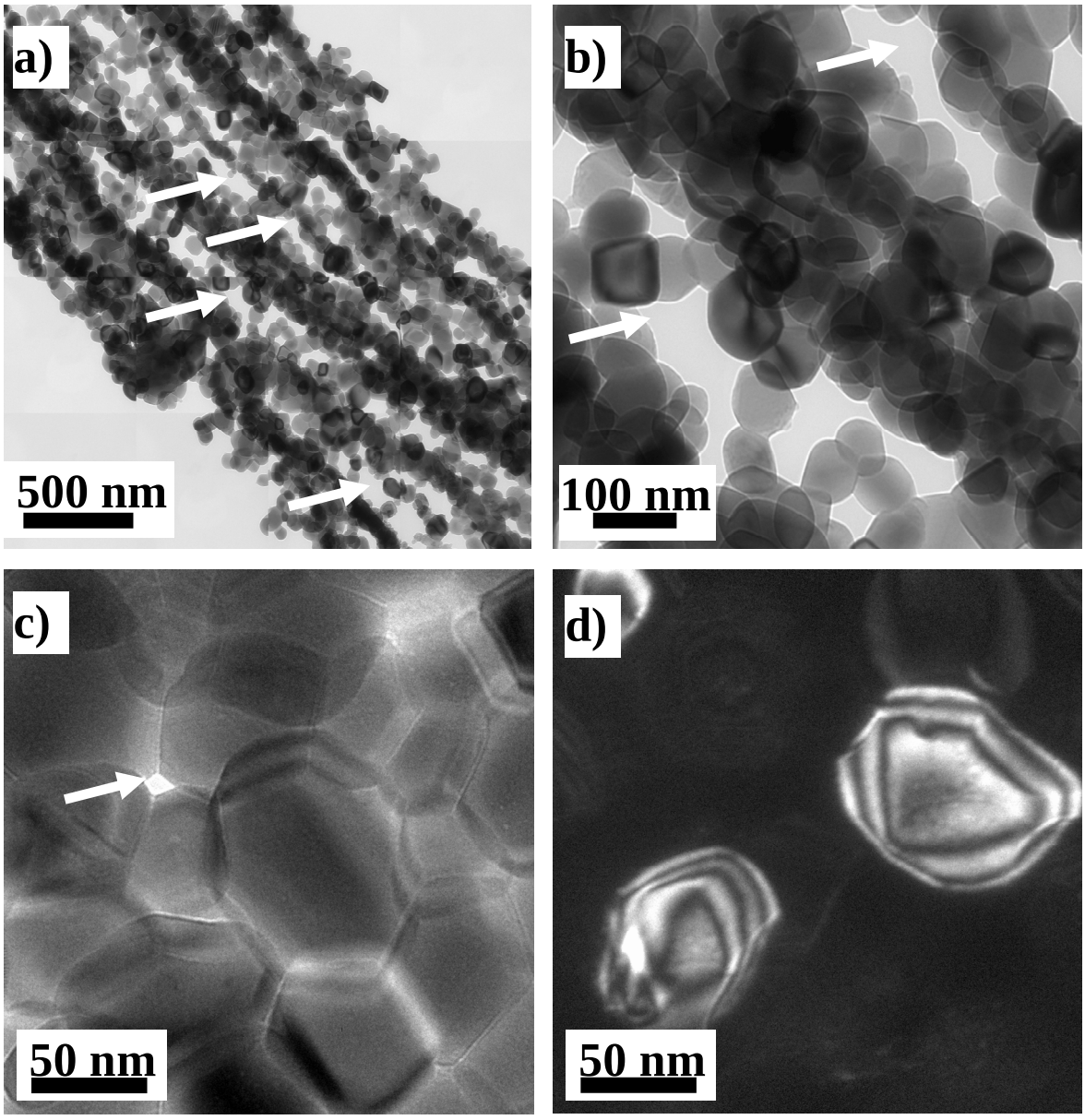


Figure 18: Transmission electron microscopic (TEM) image of the residue left after thermogravimetric analysis (TGA) of the 20 nm thick titania coated carbon fiber, a) 20 nm thick uniform layer transform into crystal grains, arrows indicate voids between grains b) close up view of crystal grain of the titania, arrows indicate voids between grains c) even close up view of the grains, size of a crystal grain can be estimated d) dark-field image of the residue there are two bright crystal grains oriented according to Bragg`s conditions.

The dominating amount of carbon was expected because of the carbon fiber, the presence of titanium, and oxygen confirms the expected titania coating. The small amount of chlorine can be estimated as an impurity from the titanium tetrachloride precursor.

Oxidation resistance of the titania coated fibers is characterized by thermogravimetric analysis (TGA) as described in the previous section. The results are shown in Figure 17; the oxidation onset temperature (approximately 3 % weight loss) for the uncoated fiber is approximately 630 °C and the fibers are completely burned at temperatures of approximately 825 °C. In case of fibers coated with a 33 nm thick layer of aluminum oxide, the oxidation starts at a temperature of approximately 630 °C and the fibers are burned completely at a temperature of approximately 870 °C. Although oxidation onset temperature of titania coated carbon fibers start earlier compare to alumina coated fibers but titania (20 nm thick) improves the oxidation resistance slightly than aluminum oxide. In case of 20 nm titania, the oxidation starts at a temperature of approximately 590 °C and the fibers are burned completely at a temperature of approximately 900 °C. Thus, titania coatings can act an oxidation barrier for carbon fibers to a little extend The residues that remain after TGA experiment were investigated via transmission electron microscopy (TEM) (see Figure 18). The images show a high degree of coarse structure, large grains are clearly visible, as deposited smooth and uniform layer transformed into crystal grains during the TGA experiment. There are voids visible between the grains as indicated by arrows in Figure 18a and b. During TGA, oxygen might diffuse through these voids and oxidized the carbon fibers, especially, at temperatures exceeding 590 °C. Diffraction pattern (see Figure 19) of these grains indicates that these materials have a crystal structure which resembles anatase polymorphs.

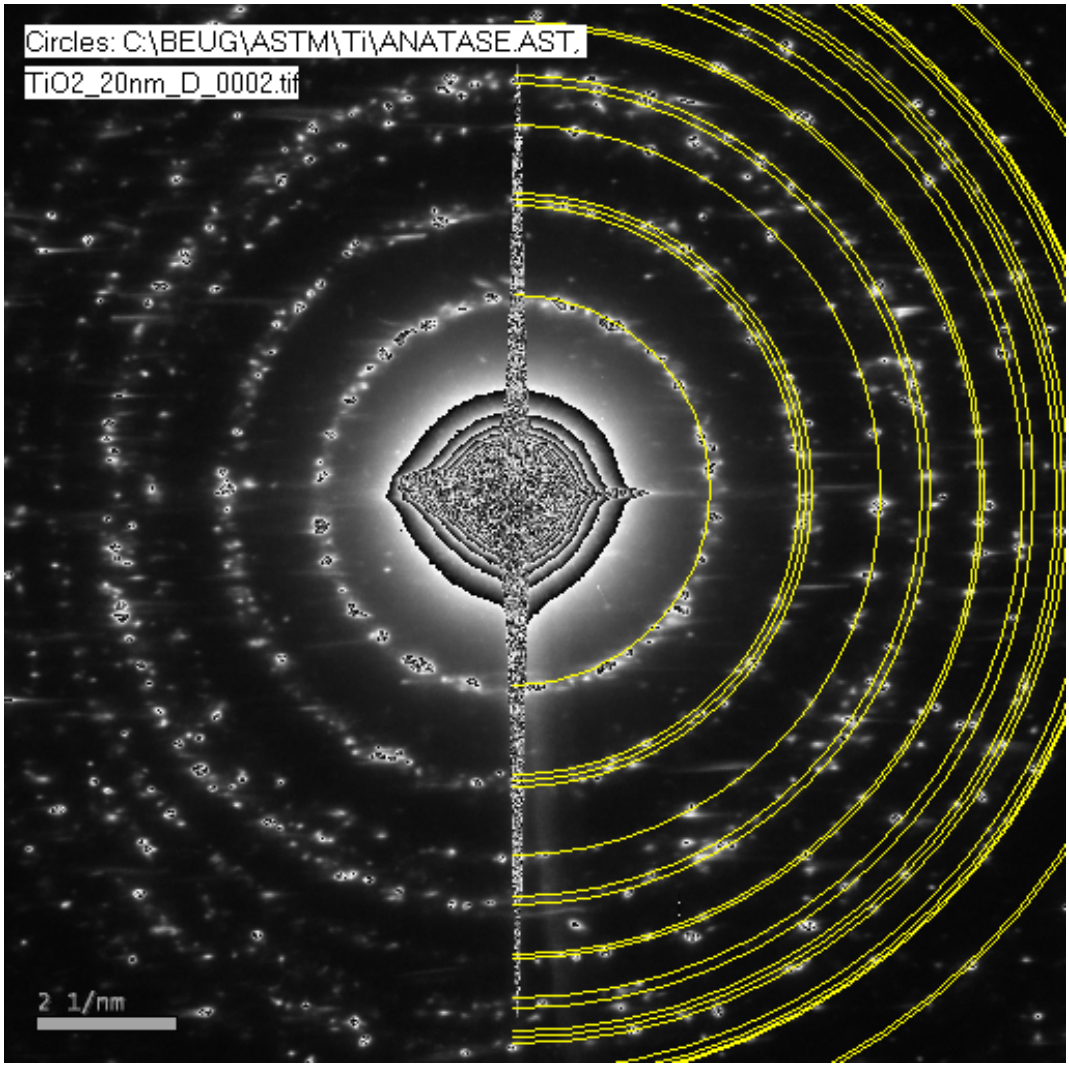


Figure 19: Differection pattern of the titania grains, which fits with the anatase titania crystal structure.

3.5 Experimental part

3.5.1 General experiments

All depositions were carried out in a home-built reactor (see Figure 20). The detailed description of this reactor is as follows: A reaction tube, 1 m long and 4 cm in diameter, made out of stainless steel is placed inside a 70 cm long tube furnace. The fiber holder is 30 cm long with 12 channels made out of stainless steel. There are two separate precursor chambers separately connected with the reactor via tubes made out of stainless steel of 1/4" diameter. Precursor doses are controlled by pneumatic valves (Swagelok, 6LVV-ALD3TMR4-P-CV), that can switch within seconds. Each separate precursor tube is connected with inert gas supply that acts as carrier gas during precursor flow, otherwise, as a purge gas. Inert gas flow was controlled by mass flow controllers (MKS instruments, Mode 247D). Pressure inside the reactor is controlled by another pneumatic valve (BOC EDWARDS, IPV25PKS). Reactor evacuation was carried out by a rotary vane pump (PFEIFFER VACUUM, Duo 5, Mod. Nr. PK D61 705 AA). There was a cooling trap before the pump in order to protect the pump from hazardous chemicals and corrosion. The pressure inside the reactor is measured by two pressure measurement gauges. The temperature of the main reactor is controlled by the tube furnace (CARBOLITE, Model: HST 12/-/600). Nitrogen was used as carrier and purge gas of a purity of 99.999%. This was further purified from moisture and oxygen by passing through specific absorber (HYDROSORB and OXYSORB from Messer Griesheim Gmbh, Düsseldrof), respectively. All valves are controlled by a home written program with the help of 'LabVIEW' software from National Instrument. Tenax HTA 5331 6 K, Polyacrilonitrile (PAN) based carbon fiber with 6000 fibers, was purchased from Toho Tenax (Toho Tenax Europe GmbH, Wuppertal, Germany). Polymeric size on this fiber was removed by thermal treatment at 700 °C in a N_2 atmosphere. Segments of this fiber, 3.6 m long, were mounted onto the fiber holder in such a way that they were longitudinally oriented parallel to the tubing and gently bent by 180° at the ends facing the precursor flow and the pump. This fiber holder was placed inside the reactor mentioned before.

To characterize the coating on the fibers directly after deposition, scanning electron microscopy (SEM) and energy dispersive X-ray spectroscopy (EDXS) were

recorded using a Nova NanoSEM (FEI, PHILIPS, Eindhoven, Netherlands), specimens were taken from the bundles. Transmission electron microscopy (TEM) was recorded using a PHILIPS CM 20 FEG (PHILIPS, Eindhoven, Netherlands), taking directly the microtubes. TEM images were recorded in transmission perpendicular to the natural surface of the coating.

Elemental flash analysis was performed via flash pyrolysis/oxidation of the sample, coupled to a chromatographic separation and detection of the gaseous oxidation products using a FLASHAE 1112 (Thermo Fischer Scientific, Waltham, Massachusetts, USA).

Thermogravimetry was performed using a TGA7 from Perkin–Elmer (PerkinElmer, Waltham, Massachusetts, USA). Coated fiber specimens of a length of approximately 5 mm (weight 3 mg to 4 mg) were heated from 30 °C to 900 °C with a heating rate of 5 °C min^{-1} and subsequently held at 900 °C for 30 min in 20 mL min^{-1} synthetic air flow.



Figure 20: Flow-type atomic layer deposition (ALD) reactor, especially designed for coating deposition onto meters long bundle of fibers.

3.5.2 Alumina coating using aluminum trichloride and water

Fibers are coated with alumina at temperatures of 500 °C and 300 °C and at a reduced pressure of 0.1 mbar using aluminum trichloride (98% from Sigma Aldrich Chemie Gmbh, Munich) and double distilled water as precursors. Aluminum trichloride was heated to 150 °C and the water temperature was maintained at 30 °C. Nitrogen was used as inert gas. Both mass flow controllers were set at 20 standard cubic centimeters per minute (sccm). In the first half cycle the fiber bundle was exposed to aluminium trichloride for 45 s followed by purge step with nitrogen for 20 s. In the second half cycle it was exposed to water vapor for 15 s followed by another purge step with nitrogen for 20 s. One complete cycle consisted of 100 s. Steps are repeated for an appropriate number of times to obtain systematically varied coating thicknesses.

3.5.3 Alumina coating using trimethylaluminum and water

Fibers were coated by alumina at a temperature of 77 °C and at a reduced pressure of 0.1 mbar using trimethylaluminum (98% from ABCR GmbH & co. KG, Karlsruhe) and deionised water as precursors. Trimethylaluminum was heated to 70 °C and the temperature of the water was maintained at 50 °C. Nitrogen was used as an inert gas. Both mass flow controllers were set at 20 standard cubic centimeters per minute (sccm). Thus, in purge cycles there was a flow of 40 standard cubic centimeters per minute. In the 1^{st} half cycle, the fiber bundle was exposed to trimethylaluminum for 20 s followed by purge the reactor with nitrogen for 30 s. In the second half cycle, it was exposed to water vapor for 20 s followed by purging the reactor with nitrogen for 30 s. One complete cycle consisted of 100 s. Steps are repeated for an appropriate number of times to obtain systematically varied coating thicknesses. Purge times were increased up to 100 s. In a separate set of deposition experiments the flow of purge gas was increased up to 100 sccm, while keeping the purge time constant at 100 s.

Aluminum contains of the coating deposited at various positions of the bundle were analyzed via atomic absorption spectroscopy (AAS). One alumina coated bundle was manually split along the fiber axis into four bundles in such a way that fibers were collected predominantly from the outer region, from the core origin and from two regions in between. Another bundle was cut perpendicular to its length into four sections of equal

length. Then the mass of these eight samples was measured. The samples were dissolved in concentrated nitric acid separately, the aluminum content of these solutions was determined by AAS and the equivalent alumina content of each the samples was calculated. AAS was carried out by an analytical company (BERGHOF Aalytik + umweltengineering GmbH & Co. KG, Chemnitz, Germany) using flame absorption spectrometry.

Thus, for each sample we know the total mass, m_t and the mass of the alumina coating m_a, in addition we know its radius, $r = 3.5 \times 10^{-4}$ cm, its length, L, and the number of fibers, N, and take values for the density of the carbon, $\rho_c = 1.76$ g cm^{-3} provided by the manufacturer, and of the density of the alumina, $\rho_a = 2.6$ g cm^{-3} from the literature3.

We assumed that a single fiber is a cylinder of radius r and length L coated by a coating of thickness d (see Figure 21).

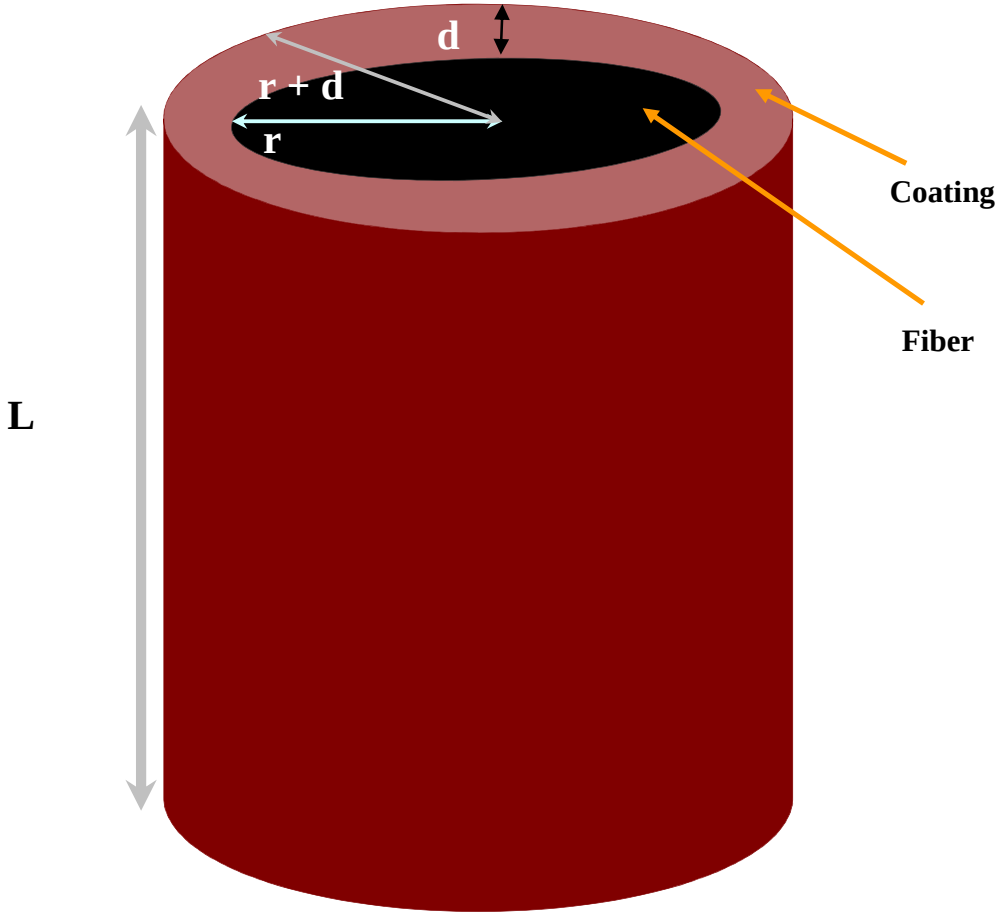


Figure 21: Schematic diagram of a coated fiber

The Volume of the carbon fiber, V_c, is given by the difference between the total mass, m_t, and the mass of the coating, m_a, divided by the carbon density, ρ_c

$$V_c = \frac{m_c}{\rho_c} = \frac{m_t - m_a}{\rho_c} \qquad \text{E 1}$$

It can as well be calculated from the fiber geometry:

$$V_c = \pi r^2 NL \qquad \text{E 2}$$

The Volume of the alumina coating is given by its mass and density

$$V_a = \frac{m_a}{\rho_a} \qquad \text{E 3}$$

It is as well given by geometrical calculations:

$$V_a = \pi(r+d)^2 NL - V_c \qquad \text{E 4}$$

Rearranging E 4 yields:

$$d = r\left(\sqrt{\frac{V_c + V_a}{\pi r^2 NL}} - 1\right) \qquad \text{E 5}$$

Applying E 2 to E 5 yields

$$d = r\left(\sqrt{1 + \frac{V_a}{\pi r^2 NL}} - 1\right) \qquad \text{E 6}$$

and

$$d = r\left(\sqrt{1 + \frac{V_a}{V_c}} - 1\right) \qquad \text{E 7}$$

Applying E 3 to E 6 yields

$$d = r\left(\sqrt{1 + \frac{m_a/\rho_a}{\pi r^2 NL}} - 1\right) \qquad \text{E 8}$$

Applying E 3 and E 1 to E 7 yields

$$d = r\left(\sqrt{1+\frac{m_a \rho_c}{\rho_a (m_t - m_a)}} - 1\right) \qquad \text{E 9}$$

Thus, we may either take equation E 8 or E 9 to calculate the thickness of our layer. Both equations should give identical results, though the errors may be different, e.g. eq. E 8 is sensitive to uncertainties in the number of fibers per bundle, while E 9 is sensitive to uncertainties in the density of the carbon fiber. (Both methods gave almost identical results).

3.5.4 Titania coating

Fibers were coated by titania at a temperature of 200 °C and at a reduce pressure using titanium tetrachloride ($TiCl_4$) (98% from ABCR GmbH & co. KG, Karlsruhe) and deionised water as precursors. Titanium tetrachloride was heated to 70 °C and the temperature of the water was maintained at 50 °C. Nitrogen was used as an inert gas. Both mass flow controllers were set at 20 standard cubic centimeters per minute (sccm). Thus, in purge cycles there was a flow of nitrogen at 40 standard cubic centimeters per minute. In a first set of experiment, 1st half cycle, the fiber bundle was exposed to titanium tetrachloride for 30 s followed by purging the reactor with nitrogen for 15 s. In the second half cycle, it was exposed to water vapor for 30 s followed by purging the reactor with nitrogen for 15 s. Another set of experiment exposure time for both the precursors were same, only purge time increases to 40 s. One complete cycle consisted of 140 s. Steps are repeated for an appropriate number of times to obtain systematically varied coating thicknesses.

3.6 Conclusions

Alumina and titania has been successfully deposited onto carbon fibers. In general, all these coatings were uniform and conformal on the fiber surfaces. Alumina depositions using both the precursors were successfully.

Initially, alumina has been deposited onto carbon fibers at a deposition temperature of 500 °C using non-flammable precursors, aluminum trichloride ($AlCl_3$) and water. This process was quite successful but there were few problems. At the deposition

conditions few of the fibers were damaged. When deposition temperature was decreased down to 300 °C, carbon fibers were intact as revealed in scanning electron microscopic (SEM) images. At 500 °C average coating deposition rate was 0.06 nm per cycle whereas it was 0.033 nm per cycle at 300 °C. Controlling the aluminum trichloride dose was another problem. At room temperature aluminum trichloride is a solid but ALD is a gas-phase method. To obtained sufficient vapor pressure thermal evaporation is one of the ways. Sufficient vapor pressure was achieved by heating the aluminum trichloride to a temperature of 150 °C. However, these vapors are often deposited inside the carrier tube. Additionally, aluminum trichloride reacts rapidly with oxygen and/or moisture, and forms aluminum oxide. Aluminum oxide and chloride mixtures formed very hard, high temperature stable solid material. This solid material often blocked the carrier tube of aluminum trichloride. As a result the deposition process often had to be terminated midway, although there was still enough aluminum trichloride inside the precursor chamber. In this process hydrochloric acid is formed as a byproduct which is a corrosive substance and thus can affect the reactor. After first alumina deposition, it has been proven that the ALD can be applied for reinforcing fibers and also proven that the home-built reactor was functioning properly.

Alumina deposition was continued by replacing the aluminum trichloride with trimethylaluminum ($Al(CH_3)_3$) at a lower temperature (77 °C) than the previous cases. After deposition, there was a weight loss of carbon fibers of about 1%. One can conclude that the carbon fibers are almost intact even though there was water involved in the process. This preservation of the fiber might be due to low process temperature of 77 °C. A qualitative adhesion test has been conducted by bending alumina coated fibers around cylinders of radii. Results indicated that the coatings were well adhesion to the fiber surfaces. An average deposition rate was (0.25 ± 0.02) nm per cycle at 77 °C which was comparatively higher than reported in literature, when the deposition temperature raised to 150 °C, growth per cycle decreased to (0.17 ± 0.03) nm/cycle. One of the reasons for higher growth rate at lower temperature (77 °C) might be because of physically adsorbed water molecules. Physically adsorbed water molecules facilitate additional growth on ALD layer during the next pulse of trimethylalumium.

Titania has been deposited onto carbon fibers were coated with titania by exposing them to the pulses of titanium tetrachloride ($TiCl_4$) at a temperature of 200 °C. Two sets of experiment were carried out with two separate purge times 15 s and 40 s. In case of 15 s purge time coating was rough and uneven. Cracks are formed within the coating; probably this happens during handling of the specimens thus the adhesion is poor. These rough films may be due to bulk gas phase reaction which may give rise to solid titania precipitation onto fibers. The film deposition rate was measured by the analysis of SEM images; it was 12 nm/cycle whereas the thickness of a monolayer is 0.28 nm. Thus, 15 s purge time leads to non-uniform and non-conformal films through gas phase precipitation.

In case of reaction purge time 40 s, coatings were smooth, uniform and conformal. There are almost no regions with the exceptions of the freshly cut ends that indicate delamination of the coating. Thus, there seems to be good adhesion of the coating to the fiber. In places where the cutting induced delamination, one observes clear steps (see Figure 15d). These indicate that cohesion within the coating is stronger than the adhesion. In addition, from these well defined steps one can measure the layer thickness. Thickness of the titania layer was 20 nm for 150 cycle deposition, which translate into deposition rate of 0.13 nm per cycle (thickness of a monolayer 0.28 nm/cycle)[21a]. Deposition rate is well below compare to the thickness of a monolayer, which indicates that this process is an atomic layer deposition.

Thus, alumina and titania have successfully been deposited onto carbon fibers and this coating improved oxidation resistance to a little extent.

3.7 References

1. Leskela, M.; Ritala, M., Atomic layer deposition chemistry: Recent developments and future challenges. *Angewandte Chemie-International Edition* **2003,** *42* (45), 5548-5554.

2. Niinisto, L.; Paivasaari, J.; Niinisto, J.; Putkonen, M.; Nieminen, M., Advanced electronic and optoelectronic materials by Atomic Layer Deposition: An overview with special emphasis on recent progress in processing of high-k dielectrics and other oxide materials. *Physica Status Solidi A* **2004,** *201* (7), 1443-1452.

3. Groner, M. D.; Fabreguette, F. H.; Elam, J. W.; and George, S. M.:Low-temperature Al_2O_3 atomic layer deposition, *Chemistry of Materials* **2004**, *16* (4), 639-645.

4. Kemell M, Pore V, Ritala M, Leskela M, Linden M. Atomic layer deposition in nanometer-level replication of cellulosic substances and preparation of photocatalytic TiO_2/cellulose composites. *Journal of the American Chemical Society* **2005**, *127*(41), 14178-14179.

5. Hyde GK, Park KJ, Stewart SM, Hinestroza JP, Parsons GN. Atomic layer deposition of Conformal inorganic nanoscale coatings on three-dimensional natural fiber systems: Effect of surface topology on film growth characteristics. *Langmuir* **2007**, *23*(19), 9844-9849.

6. Koltsov, S. I.; Kopylov, V. B.; Smirnov, V. M.; Aleskovskii, V. B., Synthesis and Investigation of Aluminum-Oxygen Layers on Surface of Silica. *Journal of Appllied Chemistry-USSR* **1976,** *49* (3), 525-528.

7. Antson, H.; Grasserbauer, M.; Hamilo, M.; Hiltunen, L.; Koskinen, T.; Leskela, M.; Niinisto, L.; Stingeder, G.; Tammenmaa, M., Characterization of Thin-Film Electroluminescent Structures by Sims and Other Analytical Techniques. *Fresenius´ Journal of Analytical Chemistry* **1985,** *322* (2), 175-180.

8. Puurunen, R. L., Surface chemistry of atomic layer deposition: A case study for the trimethylaluminum/water process. *Journal of Applied Physics* **2005,** *97* (12), 121301–52.

9. Bai, Y. J.; Wang, C. G.; Lun, N.; Wang, Y. X.; Yu, M. J.; Zhu, B., HRTEM microstructures of PAN precursor fibers. *Carbon* **2006,** *44* (9), 1773-1778.

10. Anderson, R.; Klepeis, S.; Benedict, J.; Vandygrift, W. G.; Orndorff, M., Recent Developments in the Preparation of Semiconductor Device Materials for the Transmission Electron Microscope. *Institute of Physics Conference Series* **1989,** (100), 491-500.

11. a) Ferguson, J. D.; Weimer, A. W.; George, S. M., Atomic layer deposition of Al_2O_3 films on polyethylene particles. *Chemistry of Materials* **2004,** *16* (26), 5602-5609. b) Knez, M.; Kadri, A.; Wege, C.; Gosele, U.; Jeske, H.; Nielsch, K., Atomic layer deposition on biological macromolecules: Metal oxide coating of tobacco mosaic virus and ferritin. *Nano Letters* **2006,** *6* (6), 1172-1177.

12. Puurunen, R. L., Growth per cycle in atomic layer deposition: Real application examples of a theoretical model. *Chemial Vapor Deposition* **2003,** *9* (6), 327-332.

13. a) King, D. M.; Liang, X. H.; Li, P.; Weimer, A. W., Low-temperature atomic layer deposition of ZnO films on particles in a fluidized bed reactor. *Thin Solid Films* **2008,** *516* (23), 8517-8523. b) King, D. M.; Spencer, J. A.; Liang, X.; Hakim, L. F.; Weimer, A. W., Atomic layer deposition on particles using a fluidized bed reactor with in situ mass spectrometry. *Surface and Coatings Technology* **2007,** *201* (22-23), 9163-9171. c) Cavanagh, A. S.; Wilson, C. A.; Weimer, A. W.; George, S. M., Atomic layer deposition on gram quantities of multi-walled carbon nanotubes. *Nanotechnology* **2009,** *20* (25), 255602-255609.

14. a) Kisker, D. W.; Stevenson, D. A.; Miller, J. N.; Stringfellow, G. B., The Vapor-Phase Interaction of Trimethylaluminum with Graphite during OMVPE. *Journal De Physique* **1982,** *43* (NC-5), 221-227. b) Kisker, D. W.; Stevenson, D. A., Mechanism of Graphite Baffle Gettering in Organometallic Vapor-Phase Epitaxy; Adsorption of Trimethylaluminum on Graphite. *Journal of Electronic Materials* **1983,** *12* (2), 459-482.

15. Pradere, C.; Sauder, C., Transverse and longitudinal coefficient of thermal expansion of carbon fibers at high temperatures (300-2500 K). *Carbon* **2008,** *46* (14), 1874-1884.

16. a) Moghtaderi, B.; Shames, I.; Doroodchi, E., Combustion prevention of iron powders by a novel coating method. *Chemical Engineering &Technology* **2006,** *29* (1), 97-103. b) Hakim, L. F.; Vaughn, C. L.; Dunsheath, H. J.; Carney, C. S.; Liang, X.; Li, P.; Weimer, A. W., Synthesis of oxidation-resistant metal nanoparticles via atomic layer deposition. *Nanotechnology* **2007,** *18* (34), 345603-345609.

17. Alumina: isotropic linear coefficient of expansion of $\approx 9 \times 10^{-6}K^{-1}$ =1/3 of the cubic coefficient of expansion of $27.6 \times 10^{-6}K^{-1}$ given in ref 16a, Carbon Fibre: longitudinal coefficient of expansion $\approx 0\ K^{-1}$, transverse coefficient of expansion $\approx 5 \times 10^{-6}K^{-1}$ extracted from Figure 5 of: Pradere C.; Sauder C. Transverse and longitudinal coefficient of thermal expansion of carbon fibers at high temperatures (300–2500 K). *Carbon* **2008**, *46*, 1874-1884.

18. Hashishin, T.; Murashita, J.; Joyama, A; Kaneko, Y., Oxidation-resistant coating of carbon fibers with TiO_2 by sol-gel method. *Journal of the Ceramic Society of Japan* **1998**, *106*(1), 1-5.

19. a) Boccuzzi, F.; Guglielminotti, E.; Chiorino, A., Ir Study of Gas-Sensor Materials: NO Interaction on ZnO and TiO_2, Pure or Modified by Metals. *Sensors and Actuatuators B* **1992,** *7* (1-3), 645-650. b) Takao, Y.; Iwanaga, Y.; Shimizu, Y.; Egashira, M., Trimethylamine-sensing mechanism of TiO_2-based sensors 1. Effects of metal additives on trimethylamine-sensing properties of TiO_2 sensors. *Sensors and Actuatuators B* **1993,** *10* (3), 229-234. c) Huusko, J.; Lantto, V.; Torvela, H., TiO_2 thick-film gas sensors and their suitability for NO*x* monitoring. *Sensors and Actuatuators B* **1993,** *16* (1-3), 245-248.

20. a) Wold, A., Photocatalytic Properties of TiO_2. *Chemistry of Materials* **1993,** *5* (3), 280-283; b) Papp, J.; Shen, H. S.; Kershaw, R.; Dwight, K.; Wold, A., Titanium (iv) Oxide Photocatalysts with Palladium. *Chemistry of Materials* **1993,** *5* (3), 284-288.

21. a) Desu, S. B., Ultra-Thin TiO_2 Films by a Novel Method. *Mat Sci Eng B-Solid* **1992**, *13* (4), 299-303. b) Aarik, J.; Aidla, A.; Uustare, T.; Sammelselg, V., Morphology and Structure of TiO_2 Thin-Films Grown by Atomic Layer Deposition. *Journal of Crystal Growth* **1995**, *148* (3), 268-275. c) Aarik, J.; Aidla, A.; Kiisler, A. A.; Uustare, T.; Sammelselg, V., Effect of crystal structure on optical properties of TiO_2 films grown by atomic layer deposition. *Thin Solid Films* **1997**, *305* (1-2), 270-273.

22. Aarik, J.; Aidla, A.; Uustare, T.; Ritala, M.; Leskela, M., Titanium isopropoxide as a precursor for atomic layer deposition: characterization of titanium dioxide growth process. *Applied Surface Science* **2000**, *161* (3-4), 385-395.

Chapter 4

4. Coating thickness and morphology*

4.1 Introduction

In chemical vapor deposition (CVD) a surface is exposed to precursors, more precisely a mixture of gaseous components which react to form a solid deposit on the surface. In principle, the components of the process might react already in the gas phase; however, it is of significant advantage to control the process in such a way that chemical reactions occur only at the solid/gas interface. Even in the latter case we have to distinguish two extremes: if the rate determining factor of the process is the reaction at the surface, one can expect uniform thickness of the deposited coatings even deep down in trenches e.g. in the preparation of a capacitor in a microelectronic circuit or deep in porous structures e.g. a porous membrane or a bundle of fibers. However, if the rate of the process is controlled by the diffusion of the precursors to the surface, one obtains a non-uniform coating thickness, especially if there is a non-uniform diffusion path from the source of the precursors to the surface. Thus, a process controlled by the surface reaction rate is preferred. However, any process controlled by the surface reaction rate eventually becomes controlled by diffusion if the diffusion path gets extensively non uniform, e.g. if the surface exposes very deep trenches or if one desires to coat thick bundles of fibers. One elegant way to obtain uniform coating thicknesses even in geometries that require deep infiltration is pulsed chemical vapor deposition (pulsed CVD)[1] especially atomic layer deposition (ALD)[2]. In this process there are two precursors that are delivered into a reaction chamber sequentially by separate pulses; these pulses are separated by a purging step with an inert gas. One exposure and subsequent purging is called a half cycle; the succession of the two half cycles is one complete cycle. Usually, several cycles are applied subsequently. In the first half cycle the surface is saturated with the first precursor, for example with one monolayer of chemically or physically adsorbed molecules. In the second half cycle these molecules react with the second precursor to form a well-defined layer[3]. Purging of the reaction chamber in between the pulses removes all

* Most of the results of this chapter were published in the following articles:
Roy, A. K.; Goedel, W. A. Control of thickness and morphology of thin alumina coatings deposited via Pulsed Chemical Vapor Deposition (Pulsed CVD) through variation of purge times, *Surface and Coating Technology* **2011,** *205* (17-18) 4177-4182.

excess of precursors and byproducts after each precursor pulse. The amount deposited may vary between more than a monolayer or a fraction of a monolayer but definitively reaches a surface saturation limit if one exceeds a certain precursor dose and if the duration of the precursor pulse is long enough to allow the precursor to diffuse even into trenches and pores. Further increase of purge time will not affect the amount deposited per cycle. Thus, a precursor dose which is above surface saturation limit (with respect to the amount and duration) and a sufficient purge time will deposit a uniform coating of a certain thickness in each cycle. In case of atomic layer deposition, saturation occurs due to the formation of covalent bonds and one expects the deposition rate to be equivalent to a monolayer; however, it is usually less than a monolayer due to steric hindrance[4]. If saturation occurs due to physisorption it is possible as well that more than a monolayer of precursor is adsorbed. As long as the layer growth is limited by surface saturation and the pumping speed and the flow of the purge gas are sufficient to prevent the mixing of the precursors inside the reaction chamber, the increase of coating thickness per cycle will be uniform and the deposited coating will be conformal to the substrate — even if the geometry of the surface is complicated.

Pulsed CVD may deviate from this principle in two ways: (i) one of the precursors may not be a reagent but a catalyst which triggers a limited deposition of a solid coating via reaction of the second precursor. In this case, coatings of well limited catalyzed growth larger than a monolayer may form per cycle[5]. (ii) If the purge time is chosen rather short, one may observe: (a) the formation of more than a monolayer in a single cycle, (b) diffusion controlled reaction and (c) spontaneous bulk gas phase reaction inside the reactor. Thus, one can expect in pulsed CVD a deviation from conformal growth upon shortening the purge time further and further. However, pulsed CVD is also carried out at a low pressure which facilitates surface confined growth due to faster precursor diffusion and slower gas phase reaction rate even though the precursors might mix in the gas phase to a certain extent[6]. High reactivity of the precursors and low deposition pressure might allow to deposit deep into trenches. Thus, by tuning the pulsed CVD process, one can achieve an optimum deposition behavior and conformal growth at conditions that lead to growth rates of more than a monolayer per cycle.

However, when the precursors are mixed to a large extend, there is a possibility of deposition from bulk gas phase reaction. This increases the deposition rate further, but usually adversely affects the morphology of the deposited coatings. Surface confined growths always produce smooth, uniform coatings whereas gas phase precipitation usually deposits rough

coatings and thus should be avoided. In addition, the structure of the deposited coating may be influenced by the reaction parameters like temperature, and pressure etc. which might induce a change in the morphology simultaneously with in the deposition.

This is one very carefully done publication comparing pulsed plasma-enhanced chemical vapor deposition (PECVD) to plasma-enhanced atomic layer deposition (PEALD) onto silicon wafers[7]. In this work it was shown that one can obtain self-limiting growth of alumina in pulsed plasma-enhanced chemical vapor deposition. The growth rate per cycle levels off with increasing pulse duration and increases linear with the partial pressure of the gaseous precursor. The extrapolation of the alumina growth rate in pulsed PECVD towards negligible partial pressure of the precursor coincides with the growth rate observed in PEALD.

In this chapter, results of alumina depositions onto carbon fibers via pulsed CVD have been discussed, especially the variation of coating thickness and morphology as a function of extent of two precursors mixing inside the reactor have been discussed. It was aim to isolate the transitions between process conditions controlled by surface saturation and conditions that do not rigorously exclude mixing of precursors in the gas phase. Thus, it was investigated changes in morphology of the coatings formed by vapor deposition with various purge times while keeping the other parameters constant.

4.2 Results and discussion

Bundles of carbon fibers were coated with alumina by sequential exposure to pulses of trimethylaluminum and water vapor at reduced pressure and a temperature of 77 °C, varying the purge time. The low deposition temperature is of advantage, first of all because it makes the deposition process gentle to the fiber. Furthermore, at high temperatures the deposited thin coating may already undergo structural rearrangement in situ. Thus, a low deposition temperature helps to observe the morphology in the ‘as deposited’ state. In addition, the fibers chosen have a corrugated surface. This allows to judge conformality of the deposited coatings as a function of purge times. In the first half cycle, the fiber bundle was exposed to trimethylaluminum for 20 s followed by purging the reactor with nitrogen. In the second half cycle, it was exposed to water vapor for 20 s followed by another purging. The purge times were varied systematically. The coated carbon fibers were characterized by scanning electron microscopy (SEM), and energy dispersive X-ray spectroscopy (EDXS). Elemental analysis of the coated fiber by EDXS revealed in all cases a carbon content and aluminum and oxygen. The

carbon content was expected because of the carbon fiber, the presence of aluminum and oxygen confirms the expected alumina coating. EDXS results for all kinds of fibers were similar. In the following, the results are depicted in the order of increasing purge time.

4.2.1 Purge time 15 s

SEM images in figure1a-d show a part of the coated fiber bundle using 15 s purge time. Figure 1a reveals that all the fibers are coated separately and some of them are coated smoothly; however, there are fibers which bear a rather rough coating. SEM images in Figure 1b and 1c indicate that there is a continuous coating on the fiber; the surface of the coating not necessarily reflects the original morphology of the fiber. These rough coatings may be due to bulk gas phase reaction which may give rise to solid alumina precipitated from the gas phase. The uniform coating visible on some of the fibers may be explained by surface confined growth. The morphology differs substantially from fiber to fiber; this might indicate that variations in the packing density of the fiber in the bundle influence the mechanism of deposition. The layer thickness was measured by the analysis of SEM images. Fibers exposed to various numbers of deposition cycles were cut after the deposition to expose cross-sections of the coatings for SEM analysis. This analysis revealed that not all of the fibers bear the same coating thickness; on some of the fibers, coating thicknesses were higher than on the others. In addition, Figure 1c and especially 1d reveal a gap between the fiber and the coating, thus, adhesion is poor. Furthermore, the fibers at the perimeter of the bundle are coated with a thicker alumina coating compared to the fibers inside the bundle (see Figure 2a). The thickness increases with increasing number of deposition cycles. Using these data, average deposition rates can be calculated. The deposition rates depend to some extent on the mathematical method of averaging (see Table 1). Nevertheless, it is obvious that the coating deposition rate obtained for fibers inside the bundle of about (0.83 ± 0.10) nm per cycle is much larger than the theoretical value expected for a monolayer (~ 0.32 nm, calculated considering the density of alumina at 77 °C, reported by S. M. George and coworkers)[8].

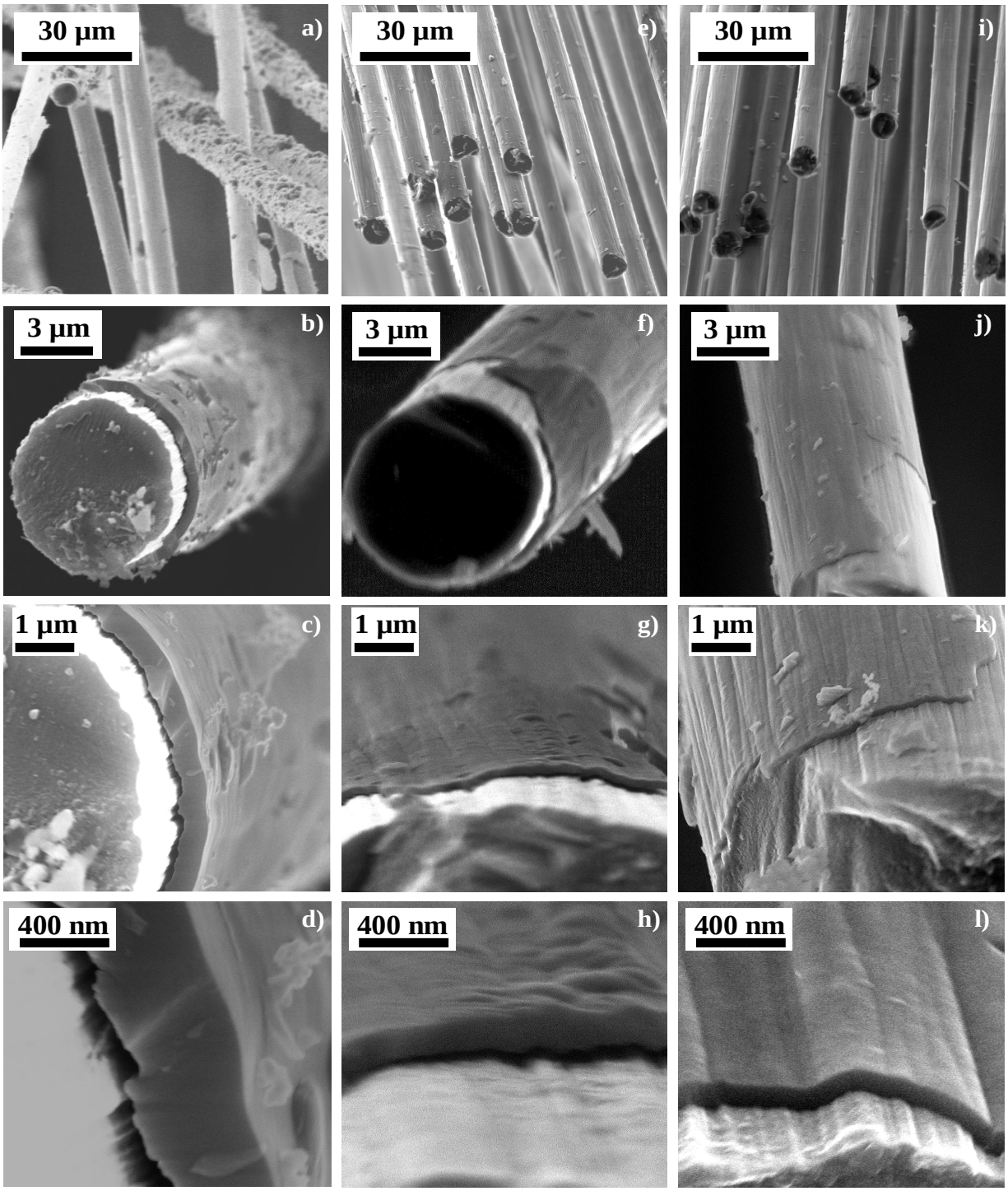


Figure 1: Scanning electron microscopic (SEM) images of alumina coated carbon fibers, after 350 cycles of deposition; the purge time increases from left to right from 15 s [image a)-d)] to 30 s [image e)-h)] to 100 s [image i)-l)].

Table 1: Deposition rates as a function of purge times.

	Deposition rate (nm/cycle)					
	Purge times = 15 s	Purge times = 15 s	Purge times = 30 s	Purge times = 45 s	Purge times = 100 s	Purge times = 100 s
	Pumping speed = 5 m^3/h (perimeter of the bundle)	Pumping speed = 5 m^3/h (inside the bundle)	(Pumping speed = 5 m^3/h)	(Pumping speed = 5 m^3/h)	(Pumping speed = 5 m^3/h)	(Pumping speed =20 m^3/h)
Average of deposition rate calculated individually for each point	1.429 ± 0.092	0.828 ± 0.100	0.339 ± 0.031	0.298 ± 0.21	0.275 ± 0.019	0.266 ± 0.022
Slope of the linear fit forced through origin	1.412 ± 0.056	0.868 ± 0.030	0.339 ± 0.005	0.298 ± 0.011	0.287 ± 0.008	0.284 ± 0.002
Slope of the linear fit allowing intercept	1.419 ± 0.351	0.4244 ± 0.229	0.344 ± 0.030	0.275 ± 0.025	0.313 ± 0.019	0.314 ± 0.008

The thickness of these uniform coatings, exceeding a monolayer per cycle may be because of the precursors mixing already in the gas phase. Thus, 15 s purge time leads to non-uniform, non-conformal poor adhesion of coatings onto fibers, and a sharp variation in thicknesses from perimeter to inside the bundle.

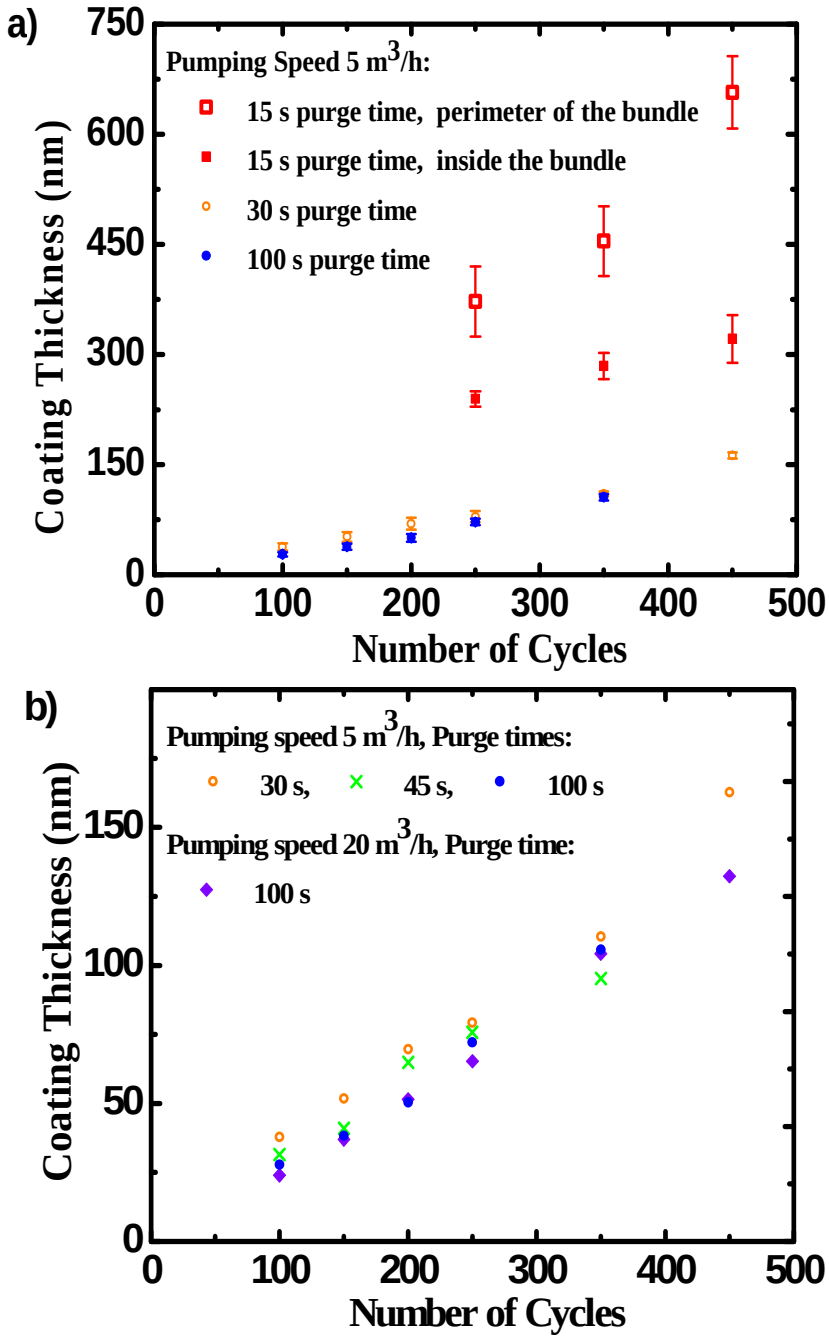


Figure 2: Coating thicknesses as a function of number of deposition cycles and of a variation of purge time. Data of at least 20 individual fibers are analysed, error bars indicate standard deviations. a) overview showing experiments using 15 s, 30 s and 100 s purge time with pumping speed of 5 m^3/h. b) Enlarged section of a) for the case of 30 s, 45 s, 100 s purge time with pumping speed of 5 m^3/h, and for 100 s purge time with a pumping speed of 20 m^3/h.

4.2.2 Purge time 30 s

The purge time was increased from 15 s to 30 s, all other parameters remained unchanged: The coatings on the fibers were more uniform (see Figure 1e-h). The overview SEM image of a fiber bundle shows that coatings were deposited on all of the fibers, they were smooth and uniform, no significant roughness exceeding the original morphology of the fibers was observed. Figure 1f to 1h show a cut end of a single fiber at various magnifications. A clear step indicates that a coating coats the fiber in a conformal way. Compared to Figure 1d, there is almost no gap between the coating and the fiber. Thus, coating adhesion is improved significantly. This good quality of the coating can only be attributed to surface limited growth: Most of the extra precursor after surface saturation was removed from the reactor and thus, gas phase reactions became negligible. The coating deposition rate was measured by the analysis of SEM images. Variation of coating thickness from fiber to fiber was significantly lower than in the previous case (see Figure 2a). As can be seen from Figure 2b, there is an almost linear relationship between the coating thickness and the number of cycles with an average deposition rate of (0.34 ± 0.03) nm per cycle (see table 1). The average deposition rate is marginally higher than the theoretical value of a monolayer (~ 0.32 nm). Usually however, a complete ALD cycle deposits only a fraction of a monolayer, The deposition rate thus might indicate that the process was not an atomic layer deposition although it gave rise to uniform and conformal coatings.

4.2.3 Purge time 45 s to 100 s

Using a purge time of 45 s gave rise to an average deposition rate of (0.30 ± 0.021) nm per cycle which is almost equivalent to the thickness of a monolayer. Increasing the purge time further to 60 s, 75 s and 100 s did not significantly change the deposition rate. Figure 1i to 1l shows coatings deposited with a purge time of 100 s. Average deposition rate was (0.28 ± 0.019) nm per cycle, in case of 100 s purge time. Furthermore, increasing the pumping speed from 5 m^3/h to 20 m^3/h for the purge time of 100 s gave no significant reduction of deposition rate. In case of a pumping speed of 20 m^3/h, an average deposition rate of (0.27 ± 0.02) nm per cycle was obtained.

The limiting average deposition rate obtained even at long purge times of (0.27 ± 0.02) nm per cycle for alumina is higher than the deposition rate between 0.13 nm and 0.09 nm per cycle usually reported for ALD of alumina [9,] which is just below the value of ~ 0.32 nm estimated for a monolayer. With the exception of a few[10c, d], these depositions were carried out at

elevated temperatures (between 177 °C and 300 °C). Additionally, in these articles, substrates other than carbon are used. One can expect significant adsorption of water to alumina; additionally, there might be a favorable interaction between trimethylaluminum and the carbon fiber which facilitates deposition of aluminum oxide onto carbon fibers at the initial stage. At least there are reports about the adsorption of trimethylaluminum onto a graphitic surface[11]. Thus, it is likely that the process depicted here works at surface saturation conditions, but that surface saturation is obtained via physical adsorption rather than via chemical reaction. We expect that at elevated temperatures conditions may be shifted towards saturation achieved by chemical reaction. Thus, another set of experiments was conducted at 150 °C with 100 s purge time. In this case, the deposited coating looked similar as it was in 100 s purge time at 77 °C but the average deposition rate was decreased down to (0.17 ± 0.03) nm per cycle. Thus, adsorption of trimethylaluminum onto carbon fibers at the initial stage and an increased degree of physical absorption of water molecules onto the alumina surface at reduced temperature may be a possible explanation for the observed higher deposition rate at lower temperature.

The morphology using 30 s purge time was almost the same, as in the case of extended purge time. Especially, compared to Figure 1a-d there were no flakes deposited on the fiber (the few flakes on Figure 1i-1l). Seldom there were flakes of coating on the fiber surfaces that might be because of mainly three reasons: (I) During removable of sample holder, coating that deposited inside the reactor, often plugged out and formed flakes on fibers (because sample holder was designed in such a way which can just fits into the reactor). (II) They were also forming during the SEM sample preparation, coating that removed from the front parts of the fibers during the segregation of samples can also formed flakes. (III) Often process had to be terminated, because it was needed to collect intermediate specimens and there was no possibility to run the process overnight. After specimen collection, depositions were resumed. Flakes which are formed because of the above two reasons might be embedded into coating and revealed as rough coating.

Flakes which are formed by the first two ways were removed to a certain extent by using a soft brash or by blowing air. Flakes which were embedded to the coatings are not possible to remove. Thus, the rough coatings are not always because of deposition process, it may come from other sources too, In general, pulsed CVD gives rise to smooth and conformal coatings and no formation of bridges even if the criteria of ALD are not strictly fulfilled (as one can see in Figure 1e-h).

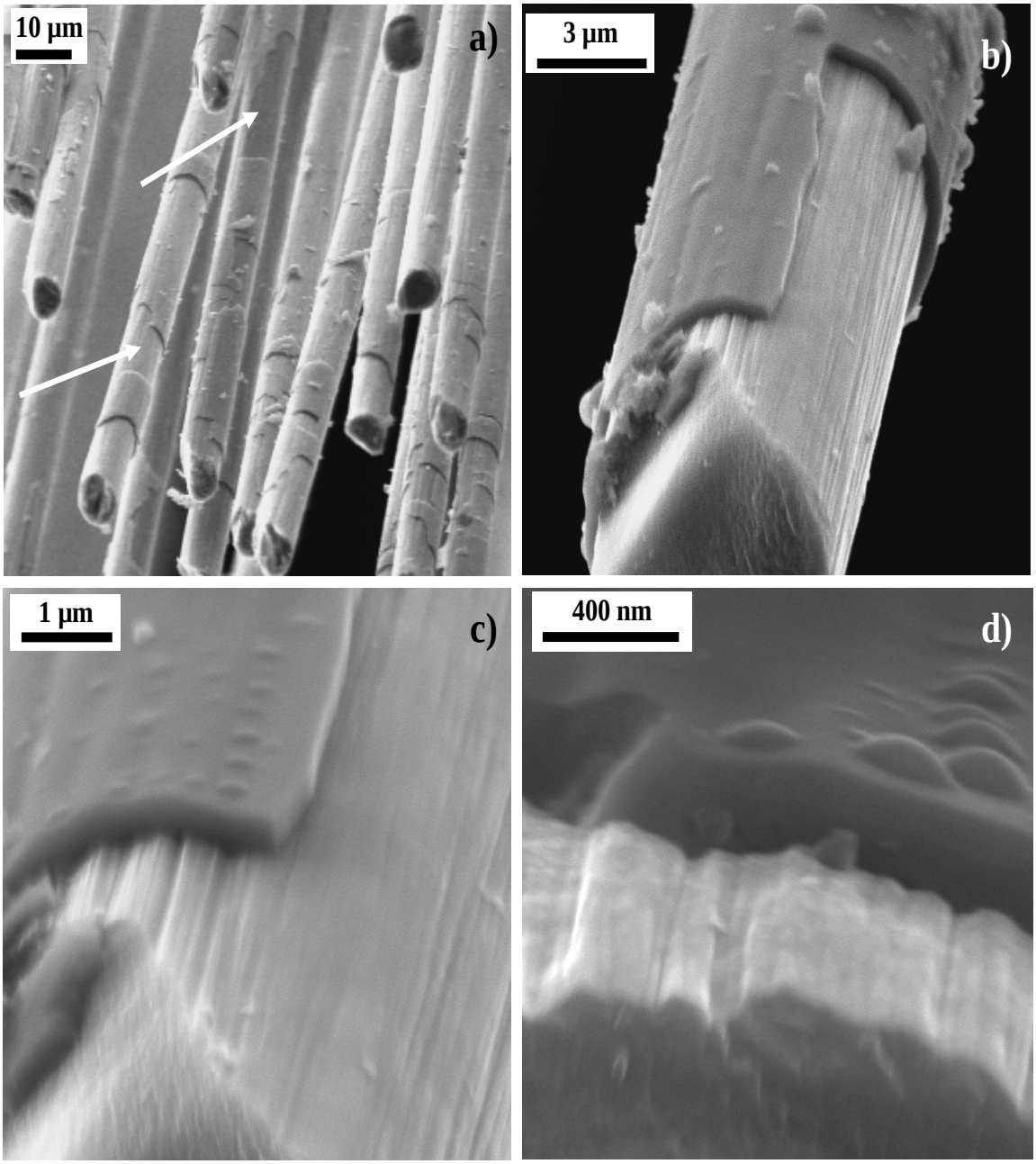


Figure 3: a)-d): Scanning electron microscopic (SEM) images of alumina coated fibers, using 15 s purge time and 450 cycles of deposition followed by annealing at 650 °C for 3 hours. The overview [image a)] indicates that the coating is non-uniform in some of the filaments and that it is removed from many parts of the filaments (arrows). Magnified images [b)-d)] indicate that there is almost no gap between the fiber and the coating and that the coating is significantly more smooth and conformal than the similar coating shown in Figure 1a)-d, just after depositions).

To investigate, whether annealing might be used to increase the smoothness of the deposited coatings, the coated fibers were annealed at a temperature of 650 °C in vacuum. A coating deposited using 15 s purge time that was initially inhomogeneous and rough as one can see in Figure 1a-d became significantly more conformal and smooth upon annealing (see Figure 3c and 3d). On the other hand, after annealing, coatings split off from the fiber upon normal handling (see Figure 3a). This was observed irrespective of purge time. This splitting off, is in accordance with an increased rate of oxidation at temperatures exceeding 600 °C, that was already observed previously in case of alumina coated carbon fibers. It is possible that this splintering off is triggered by a mismatch of coefficients of thermal expansion (the carbon fiber extends less upon heating than the coating). On the other hand, it might be because of increasing the crystallinity[10c, 12] which gives rise to mechanical stress due to densification[10d]. Therefore, either annealing after deposition or in situ (if the deposition is carried out at elevated temperature) might give rise to more smooth and conformal coatings irrespective of purge time. However, this implies the danger of damaging the fiber and the formation of coatings that are more brittle and less adhering. Thus, the low deposition temperature used here (77 °C) helps us to identify the morphology of the coatings and the deposition mechanisms during various gas phase deposition processes, and as well might give rise to coatings of advantageous mechanical properties.

4.3 Experimental Part

The reaction chamber and sample holder were identical to the one described in chapter 3. Same type of carbon fibers were used for coating after thermal desized. Fibers were coated with alumina at a temperature of 77 °C using pulses of trimethylaluminum (98% from Strem chemicals) and of deionised water as precursors in a homebuilt reactor. The supply vessel of trimethylaluminum was heated to 60 °C. The temperature of the water supply was maintained at 50 °C. Two streams of nitrogen were used as carrier for trimethylaluminum and water respectively, and as purge gas, their flow was controlled by two mass flow controllers each set to 20 standard cubic centimeters per minute (sccm). In the first half cycle, the fiber bundle was exposed to trimethylaluminum for 20 s followed by purging the reactor with nitrogen. In the second half cycle it was exposed to water vapor for 20 s followed by purging the reactor with nitrogen. In both exposures the valve in front of the pump was closed, it was opened fully during the purge time. Nominal pumping speed (as specified by the manufacturer) during the purging cycle was 5 m^3/h (PFEIFFER VACUUM, Duo 5, Mod. Nr.: PK D61 705 AA) in most

experiments and was increased to 20 m^3/ h (PFEIFFER VACUUM, Duo 20, Mod. Nr.: PK D63 021) in a second set of experiments. The purge times after exposure to one precursor were chosen to be identical to the purge time after exposure to the other one. A series of experiments was performed by varying only the purge time with durations of 15 s, 30 s, 45 s, 60 s, 75 s and 100 s, while the other parameters remained unchanged. Coated fibers were annealed using a tube furnace in vacuum.

Scanning electron microscopy (SEM) was carried out using a Nova NanoSEM (FEI, PHILIPS), directly taking the specimens from the bundles after deposition.

4.4 Conclusions

One can control the deposition mechanism of alumina during pulsed chemical vapor deposition (Pulsed CVD) from 'gas phase precipitation' to deposition controlled by surface saturation by varying the purge time. Even if the criteria of atomic layer deposition are not met, especially if the deposition rate exceeds a monolayer thickness, conformal coatings of smooth morphology can be obtained with a further advantage of increased deposition rate.

4.5 References

1. a) Avedisian, T.; Raj, R., Method and Apparatus for CVD using Liquid Delivery System with Ultrasonic Nozzle. U.S. Patent 5451260, **1995**. b) Dupel, P.; Pailler, R.; Langlais, F., Pulse chemical vapour deposition and infiltration of pyrocarbon in model pores with rectangular cross-sections. *Journal of Materials Science* **1994**, *29* (5), 1341-1347. c) Krumdieck, S.; Raj, R., Conversion efficiency or alkoxide precursor to oxide coatings grown by an ultrasonic-assisted, pulsed liquid injection, metalorganic chemical vapor deposition (pulsed-CVD) process. *Journal of American Ceramic Society* **1999,** *82* (6), 1605-1607.

2. Suntola, T.; Antson, J., Methods for Producing Compound Thin Coatings, U.S. Patent 4058430, **1977**.

3. Puurunen, R. L., Surface chemistry of atomic layer deposition: A case study for the trimethylaluminum/water process. *Journal of Applied Physics* **2005,** *97* (12), 121301–52.

4. Leskela, M.; Ritala, M., Atomic layer deposition chemistry: Recent developments and future challenges. *Angewandte Chemie-International Edition* **2003,** *42* (45), 5548-5554.

5. Hausmann, D.; Becker, J.; Wang, S. L.; Gordon, R. G., Rapid vapor deposition of highly conformal silica nanolaminates. *Science* **2002,** *298* (5592), 402-406.

6. H.O. Pierson, in: R.F. Bunshah, G.E. McGuire, S.M. Rossnagel (Eds.), Handbook of chemical vapor deposition (CVD), Principle, Technology, and Applications. 2nd edition, Noyes publications, Park Ridge, New Jersey, USA. **1997**, p. 44, chapter 2, ISBN 978-0-8155-1432-9.

7. Seman, M. T.; Richards, D. N.; Rowlette, P.; Wolden, C. A., An Analysis of the Deposition Mechanisms involved during Self-Limiting Growth of Aluminum Oxide by Pulsed PECVD. *Chemical Vapor Deposition* **2008,** *14* (9-10), 296-302.

8.Groner, M. D.; Fabreguette, F. H.; Elam, J. W.; George, S. M., Low-temperature Al_2O_3 atomic layer deposition. *Chemistry of Materials* **2004,** *16* (4), 639-645.

9. a) Puurunen, R. L., Growth per cycle in atomic layer deposition: A theoretical model. *Chemical Vapor Deposition* **2003,** *9* (5), 249-257. b) Puurunen, R. L., Growth per cycle in atomic layer deposition: Real application examples of a theoretical model. *Chemical Vapor Deposition* **2003,** *9* (6), 327-332.

10. a) Jensen, J. M.; Oelkers, A. B.; Toivola, R.; Johnson, D. C.; Elam, J. W.; George, S. M., X-ray reflectivity characterization of ZnO/Al_2O_3 multilayers prepared by atomic layer deposition. *Chemistry of Materials* **2002,** *14* (5), 2276-2282. b) Sneh, O.; Clark-Phelps, R. B.; Londergan, A. R.; Winkler, J.; Seidel, T. E., Thin coating atomic layer deposition equipment for semiconductor processing. *Thin Solid Films* **2002,** *402* (1-2), 248-261. c) Yun, S. J.; Lee, K. H.; Skarp, J.; Kim, H. R.; Nam, K. S., Dependence of atomic layer-deposited Al_2O_3 coatings characteristics on growth temperature and Al precursors of $Al(CH_3)_3$ and $AlCl_3$. *Journal of Vacuum Science & Technology A* **1997,** *15* (6), 2993-2997. d) Groner, M. D.; Fabreguette, F. H.; Elam, J. W.; George, S. M., Low-temperature Al_2O_3 atomic layer deposition. *Chemistry of Materials* **2004,** *16* (4), 639-645.

11. a) Kisker, D. W.; Stevenson, D. A.; Miller, J. N.; Stringfellow, G. B., The Vapor Phase Interaction of Trimethylaluminum with Graphite during OMVPE. *Journal De Physique* **1982,** *43* (NC-5), 221-227. b) Kisker, D. W.; Stevenson, D. A., Mechanism of Graphite Baffle Gettering in Organometallic Vapor-Phase Epitaxy; Adsorption of Trimethylaluminum on Graphite. *Journal of Electronic Materials* **1983,** *12* (2), 459-482.

12. Jakschik, S.; Schroeder, U.; Hecht, T.; Gutsche, M.; Seidl, H.; Bartha, J. W., Crystallization behavior of thin ALD-Al_2O_3 films. *Thin Solid Films* **2003,** *425* (1-2), 216-220.

5. Alumina and titania double layer coatings*

5.1 Introduction

As mentioned in chapter 3, alumina and titania coatings can improve oxidation resistance of the carbon fibers to a little extent (see in chapter 3 and also in the corresponding erratum of the references[1, 2]): While uncoated and 33 nm thick alumina coated fibers started to oxidize already at 630 °C, and increased gradually with increasing coating thickness up to 660 °C at a thickness of 120 nm. However, oxidation protection levels off at layer thicknesses exceeding 100 nm regardless of the coating thickness. Alumina seems to fail at temperatures around 660 °C. On the other hand, the oxidation onset temperature of carbon fibers coated with 20 nm thick titania was 590 °C but the rate of oxidation was slower than alumina coated fibers. Thus, new coatings are needed which can improve the oxidation resistance further.

There are several approaches to protect the carbon fibers by covering them with coatings such as nitrides (BN[3], TiN[4]), carbides (B_4C[5], SiC [6], TiC5), Oxides (SiO_2[7], Al_2O_3[8], TiO_2[9], $ZrO_2$8, Al_2O_3-SiO_2 mixed layer[10]), phosphoric acid (H_3PO_4)[11] and also with double layer (ZrC/ZrO_2)8 coatings. Most of these coatings have been deposited either by sol-gel or by chemical vapor deposition (CVD). Fiber coating via these methods may be affected because of significant process limitations.

To the best of my knowledge, oxidation behavior of double layer coatings made out of alumina and titania has not been reported so far. Thus, double layer coatings of titania and alumina were applied to the carbon fibers using identical methods as described in chapter 3. Alumina followed by titania (alumina/titania) and titania followed by alumina (titania/alumina) both layers are separately applied to the carbon fibers. The oxidation resistances of the coated fibers were characterized by thermogravimetry and the residues left after complete oxidation were characterized by electron microscopy.

* Most of the results of this chapter were submitted for publication in the following manuscript:
Roy, A. K.; Goedel, W. A. Oxidation protection of carbon fibers by coatings with alumina and titania using atomic layer deposition.

5.2 Results and discussion

Carbon fibers were coated with single layers of alumina, titania, and with double layers of either titania/alumina, or alumina/titania. Alumina coating was deposited by sequential exposure of the fibers to trimethylaluminum and deionised water at a temperature of 77 °C. The properties and the appearance of the alumina coated fibers were identical to the results presented in chapter 3. Titania coatings were deposited by sequential exposure to titanium tetrachloride ($TiCl_4$) and water vapor at a temperature of 200 °C. SEM images of single layer alumina and titania coated fibers were shown in chapter 3 of Figure 6 and Figure 15, respectively.

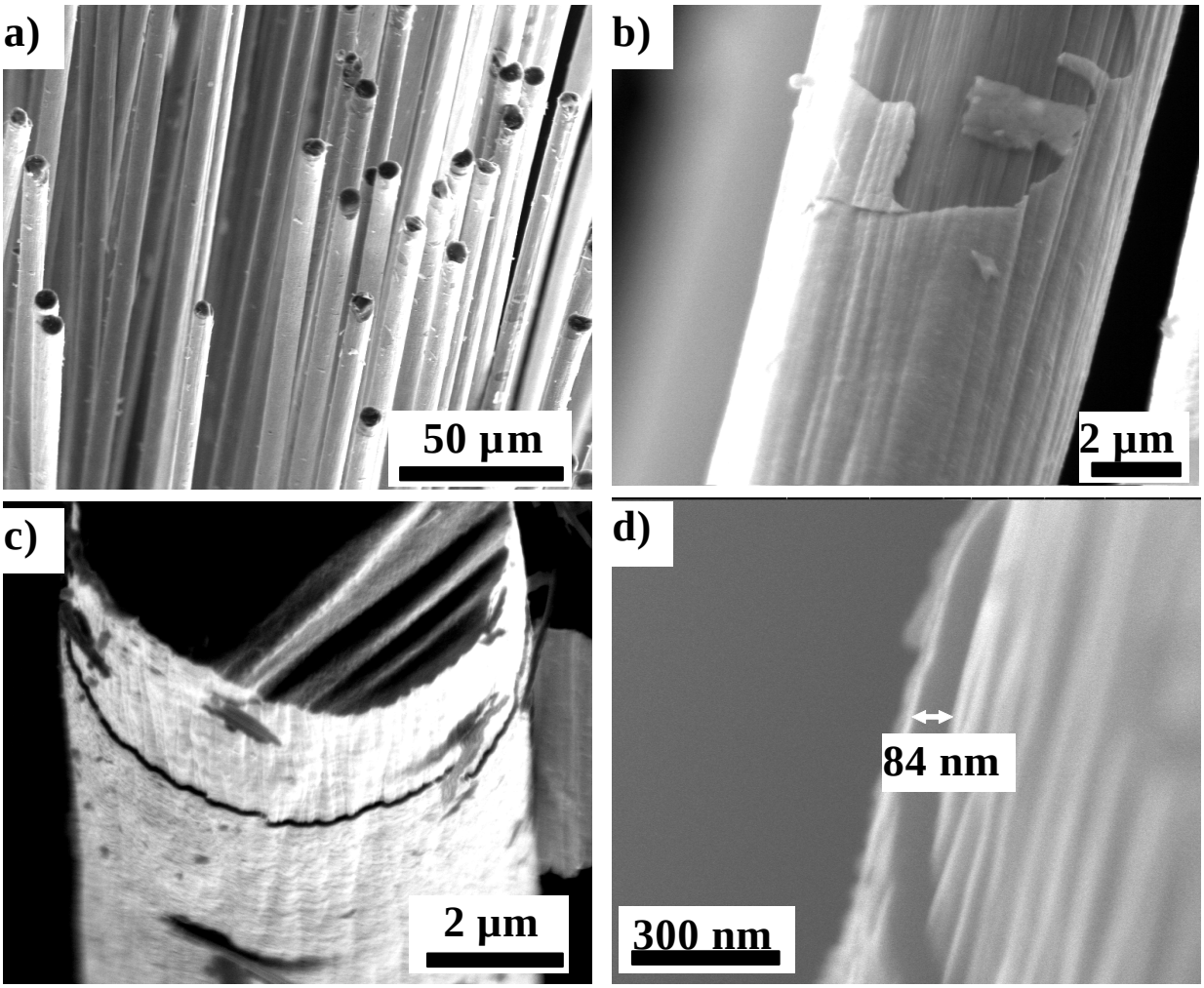


Figure 1: Scanning electron microscopic (SEM) images of fibers coated with 200 cycles of alumina followed by 300 cycles of titania: a) part of a fiber bundle; b) a close up view of a single fiber; c) detail revealing the uniform and conformal coating on the fiber surface; d) a step formed by delamination of the coating from the fiber surface.

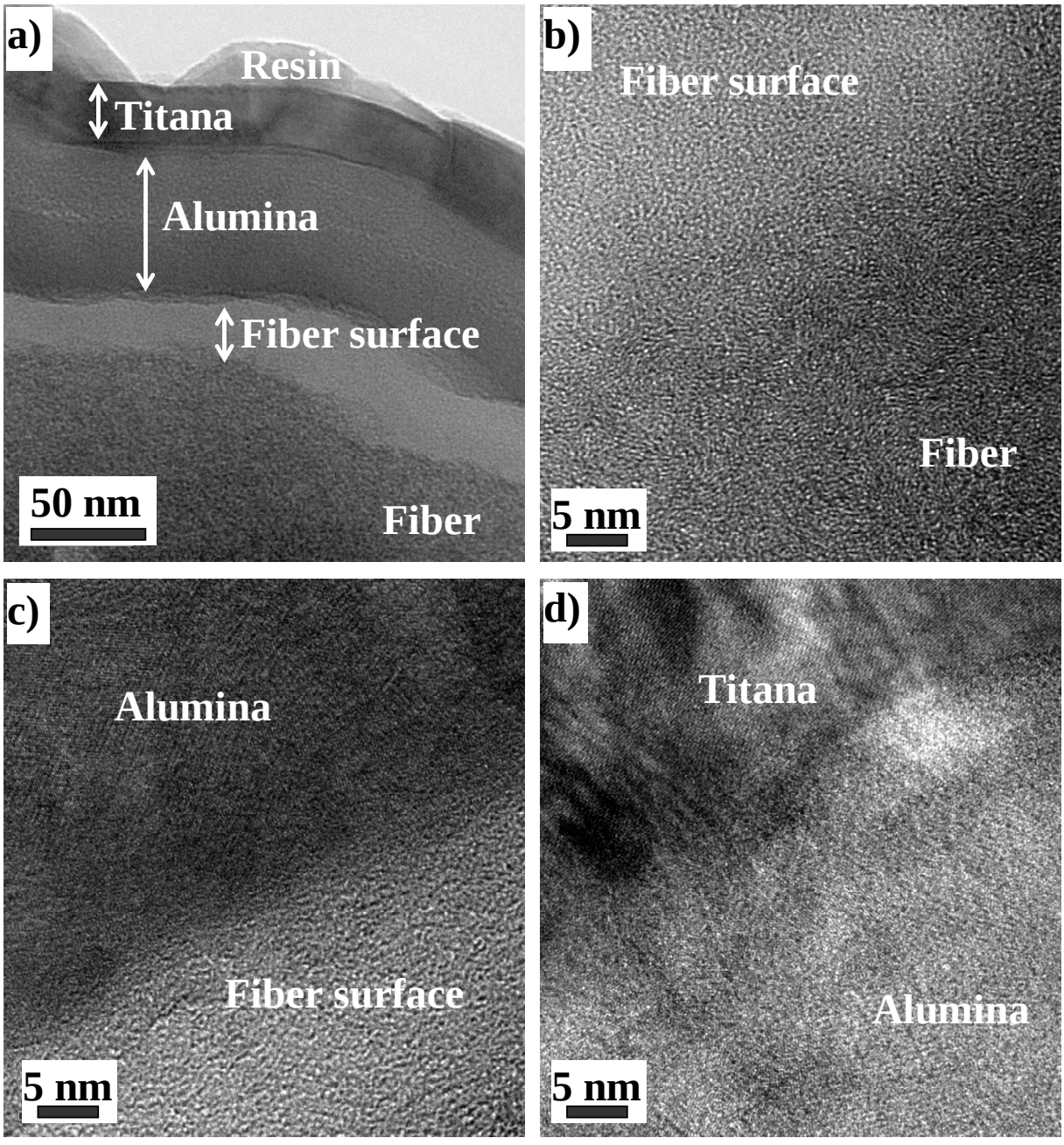


Figure 2: Transmission electron microscopic (TEM) images of a single fiber (cross-sectional view) coated with 200 cycles of alumina followed by 300 cycles of titania: a) overview of the cross-section, b), c), and d) are high resolution images of, fiber-fiber surface, fiber surface-alumina, and alumina-titania, respectively.

Briefly, both of these coated fibers were still separated from each other within the bundle, no bridging has been formed, and the coatings have been deposited evenly on the fibers. The coatings were smooth, uniform and conformal. There were almost no regions with the exceptions of the freshly cut ends that indicate delamination of the coating. Thus, there seem to be good adhesion of the coatings to the fibers. In places where the cutting induced delamination, one observes clear steps. These indicate that cohesion within the coating was stronger than the adhesion. In addition, the occurrence of these well-defined steps allows to estimate the layer thickness. Such as, titania deposition of 150 cycles yields a layer thickness of 20 nm. Assuming a linear dependency between thickness and number of cycles, this translates to a deposition rate of 0.13 nm per cycle. The deposition rate of the titania was significantly lower than the deposition rate of the alumina (deposition rate of 0.25 nm per cycle). This, however, we attribute primarily to the different temperatures used rather than the differences in the reactivity of precursors (at lower temperature often high deposition rates occur due to physical adsorption of water).

Fibers that were coated with a double layer of first 200 cycles of alumina followed by 300 cycles of titana are shown in Figure 1. The physical appearance of these fibers was similar to single layer coating of alumina or titania. The coating thickness that was measured after 200 cycles of alumina deposition from the steps observed in SEM was approximately 50 nm, which translate into a deposition rate of 0.25 nm/cycle. The observed deposition rate is in good agreement with our previous results in chapter 3. Subsequently applied 300 cycles of titana deposition, increased the coating thickness from 50 nm to 90 nm, which translates into a deposition rate of approximately 0.13 nm/cycle. Thus titana deposition rates do not depend on whether deposition starts directly from the fiber or from the alumina coated fiber (at least not in the regime investigated). A cross-section of the fiber–coating interface was prepared by mechanical polishing and investigated by transmission electron microscopy (TEM). Details of the sample preparation were reported elsewhere[12]. The resulting TEM image, shown in Figure 2, two layers alumina and titania are distinctly visible. There is an interface zone between fiber and alumina layers, named as “fiber surface” either this zone was before coating deposition or appeared during deposition. It is difficult to specify one particular possibility. On the other hand, in the previous TEM image (Figure 8 in chapter 3), this type of zone was not visible. One can estimate the coating thickness of alumina and titania layers from Figure 2a, which are approximately 60 nm and 30 nm, respectively. There is a discrepancy in the coating thickness estimation from SEM and TEM images. One reason might be the estimation of SEM is an average of several fibers, whereas the estimation from TEM image is a single event. In addition,

SEM images were not so sharp like the TEM, especially in the range of nanometers, so, manual errors could not be excluded. High resolution images Figure 2 c and d indicate that both alumina and titania coatings were partially crystalline.

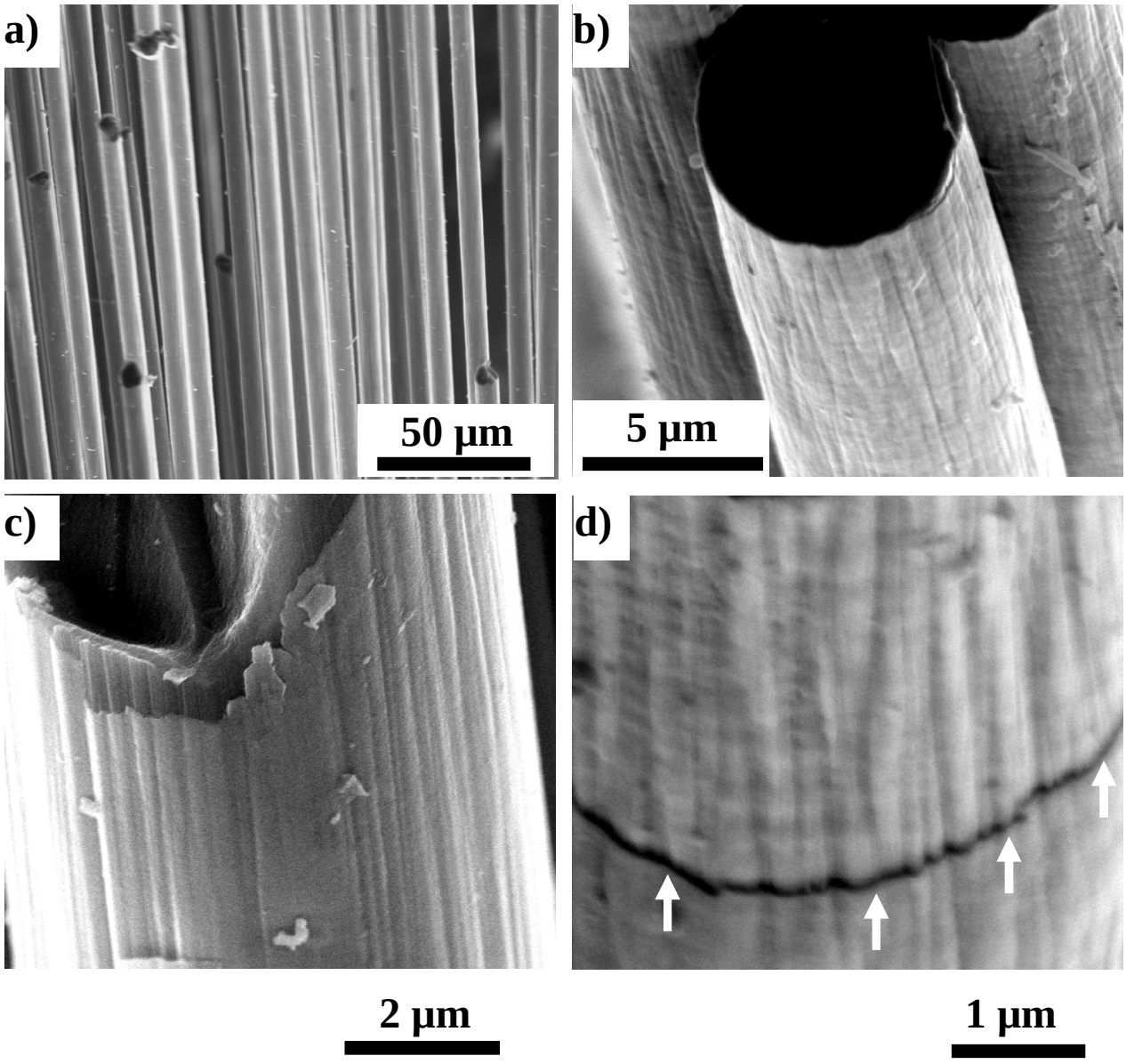


Figure 3: Scanning electron microscopic (SEM) images of fibers coated with 150 cycles of titania followed by 125 cycles of alumina: a) part of a fiber bundle; b) a close up view of a coated fiber bundle; c) detail revealing the uniform and conformal coating on the fiber surface; d) a step formed by delamination of the coating from the fiber surface, indicated by arrows.

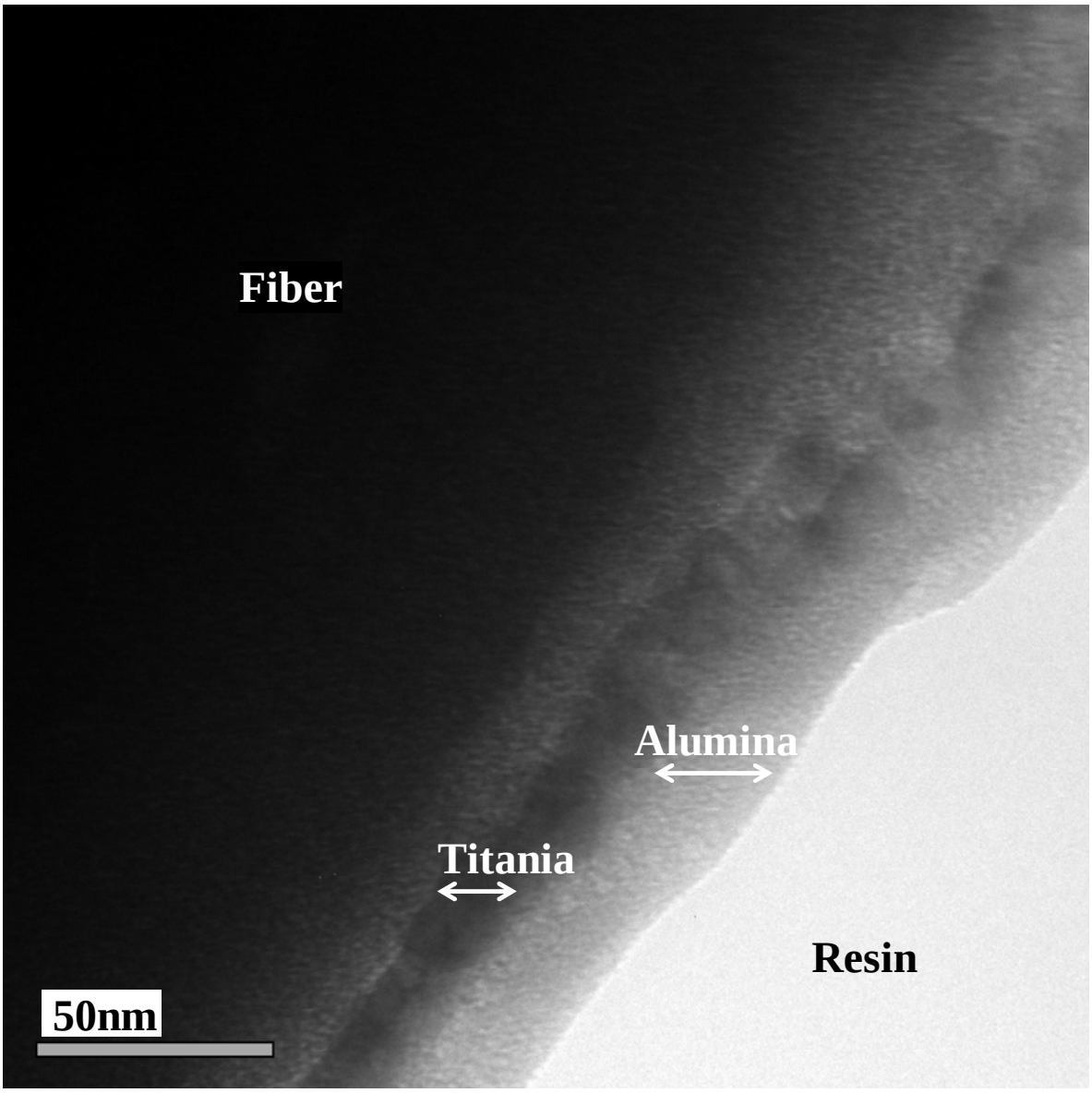


Figure 4: Transmission electron microscopic (TEM) images of a single fiber (cross-sectional view) coated with 150 cycles of titania followed by 125 cycles of alumina

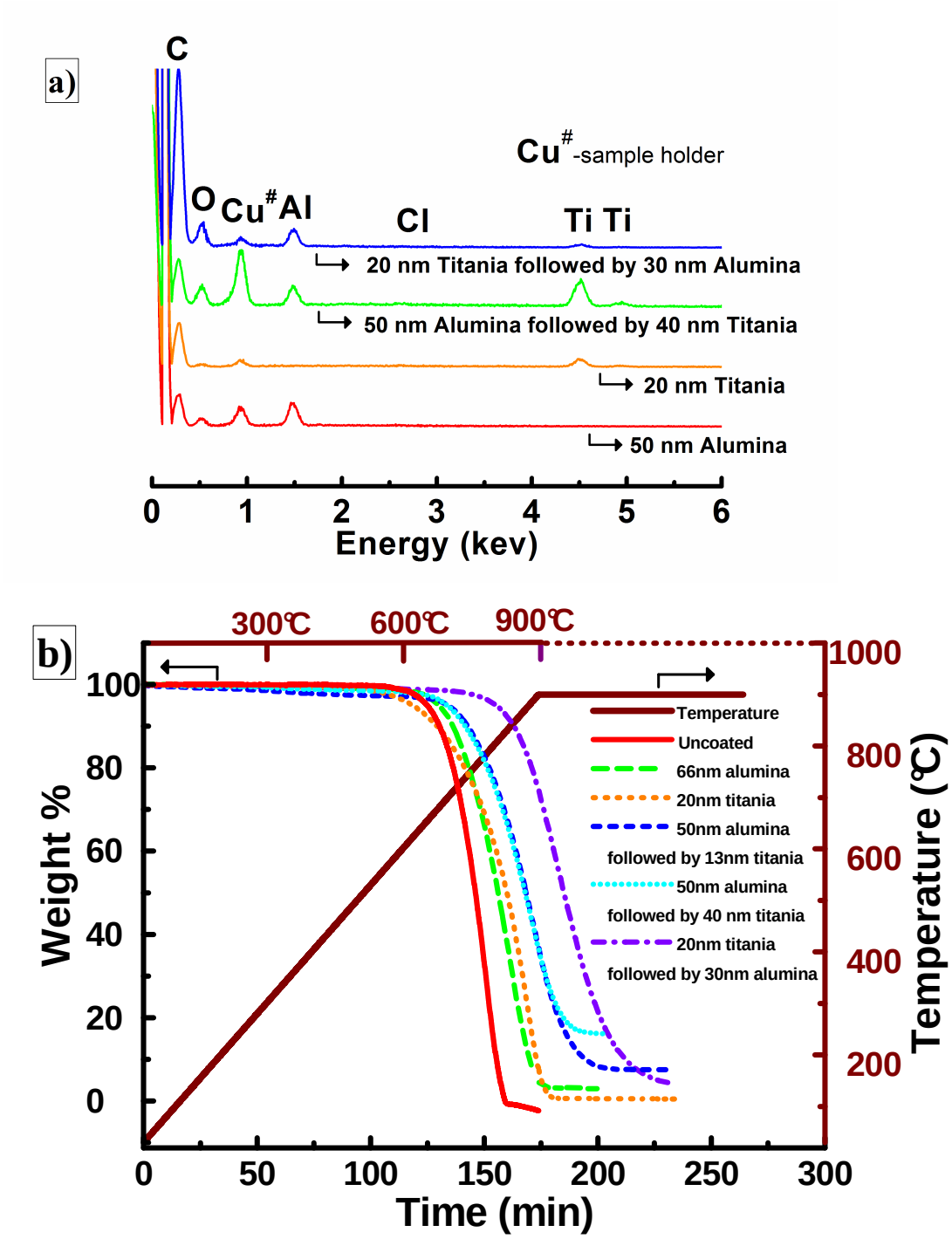


Figure 5: a) Energy dispersive X-ray spectroscopy (EDXS) of the coated fibers. b) Thermogravimetric analysis (TGA) of fibers coated by titania, alumina and double layers of these oxides. The specimens were heated from 30 °C to 900 °C with a heating rate of 5 °C/minute and subsequently held for certain time (30 minutes, or 60 minutes) at a temperature of 900 °C in synthetic air.

In Figure 3, fibers coated by 150 cycles of titania followed by 125 cycles of alumina are shown: The physical appearances of the coated fibers were similar to all the other cases described above. Transmission electron microscopy (TEM) image of the cross-section of the fiber–coating interface is shown in Figure 4. This was also prepared by the same method as explain above. This sample was not as good as another one but still one can see the two separate layers on fiber surface (indicated by arrows).

Elemental analysis of the coated fibers by energy dispersive X-ray spectroscopy (EDXS) (see Figure 5a) reveal a dominating carbon content, titanium, oxygen, and a small amount of chlorine. The dominating amount of carbon was expected because of the carbon fiber, the presence of titanium, and oxygen confirms the expected titania coating. The small amount of chlorine can be regarded as an impurity from the titanium trichloride precursor. Alumina and titania that were revealed by the EDXS agree with the proportion expected from the relative layer thicknesses.

The oxidation resistances of the coated fibers were characterized by thermogravimetric analysis (TGA): 5 mm long coated fiber specimens were heated from 30 °C to 900 °C with a heating rate of 5 °C/minute and subsequently held at 900 °C for certain time (30 minutes, or 60 minutes) in a flow of synthetic air. The results are shown in Fig. 5b. The oxidation onset temperature (3% weight loss) for the uncoated fiber was approximately 630 °C and it was burned completely at temperatures of approximately 825 °C. In case of fibers coated with a 66 nm thick layer of alumina, the oxidation starts at a temperature of approximately 630 °C and the fibers were burned completely at a temperature of approximately 900 °C. Titania coating of 20 nm thickness improves the oxidation resistance almost similar to the 66 nm thick alumina coating, the oxidation onset temperature was lower (approximately 590 °C) but the rate of oxidation was slower compared to alumina.

If the fiber was coated by alumina and subsequently by titania both effect seems to overlap. Carbon fibers coated with alumina/titania had the same oxidation onset as alumina coated fibers but the rate of oxidation was decreased compared to alumina. This feature was independent of the thickness of the titania, at least in the regime investigated (50 nm alumina followed by 13 nm and 40 nm titania). On the other hand, if the sequence of deposition was changed, i.e., depositing the titania first and alumina subsequently (20 nm titania followed by 30 nm alumina) this improved the oxidation onset temperature higher than in the previous cases of alumina/titania. The oxidation onset temperature of fibers coated with titania/alumina was approximately 750 °C. The fibers were burned completely when temperature was further increased to 900 °C and held another 60 minutes at 900 °C.

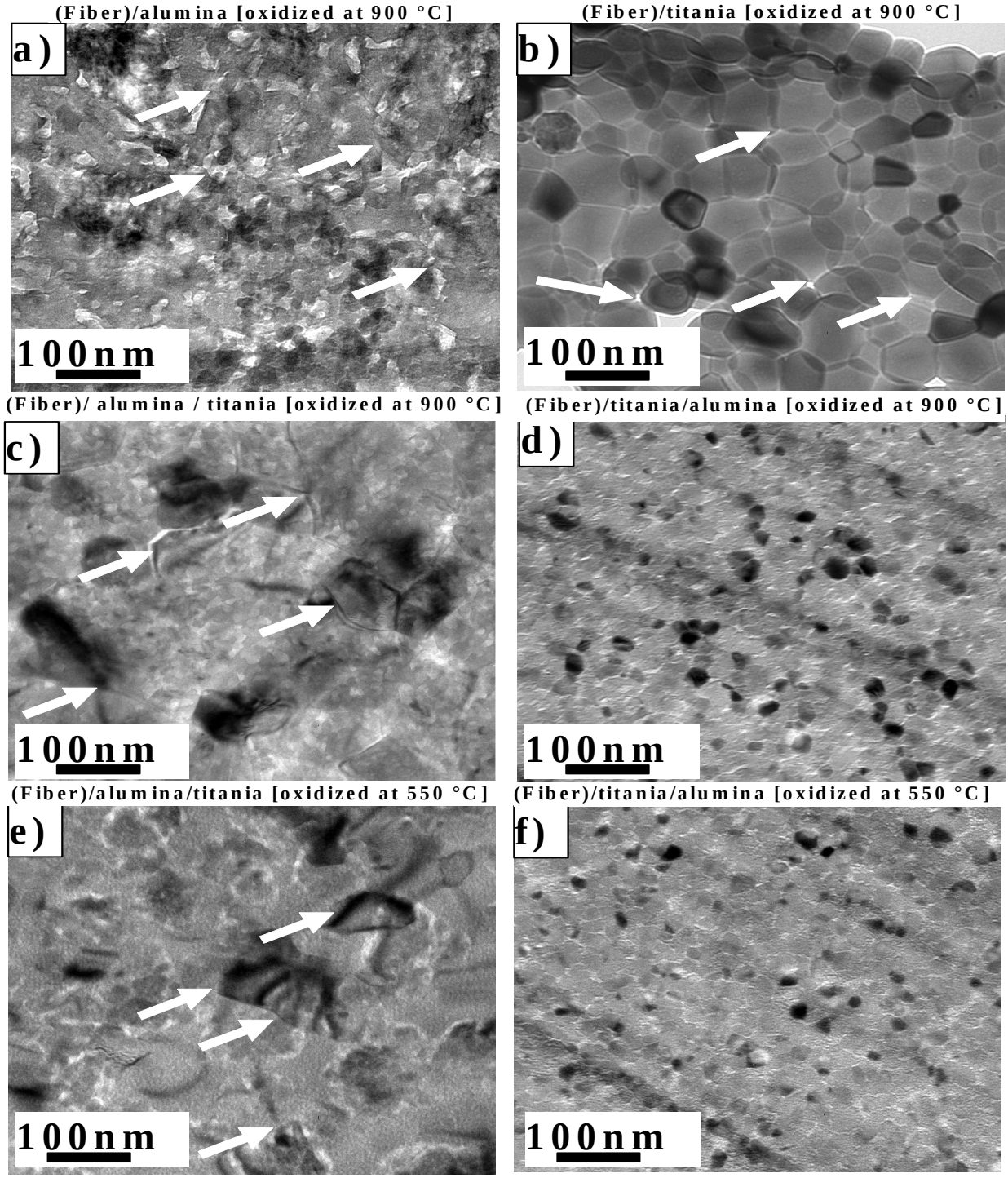


Figure 6: Transmission electron microscopic (TEM) images of the residual coatings after oxidative degradation of the fibers: Residual coatings after thermogravimetric analysis that have been exposed to 900 °C: a) 66 nm alumina, arrows indicate grain boundaries b) 20 nm titania c) 50 nm alumina followed by 40 nm titania d) 20 nm titania followed by 30 nm alumina. Residual coatings after oxidative degradation of fibers at temperatures of 550 °C in a tube furnace: e) 50 nm alumina followed by 40 nm titania, f) 20 nm titania followed by 30 nm alumina.

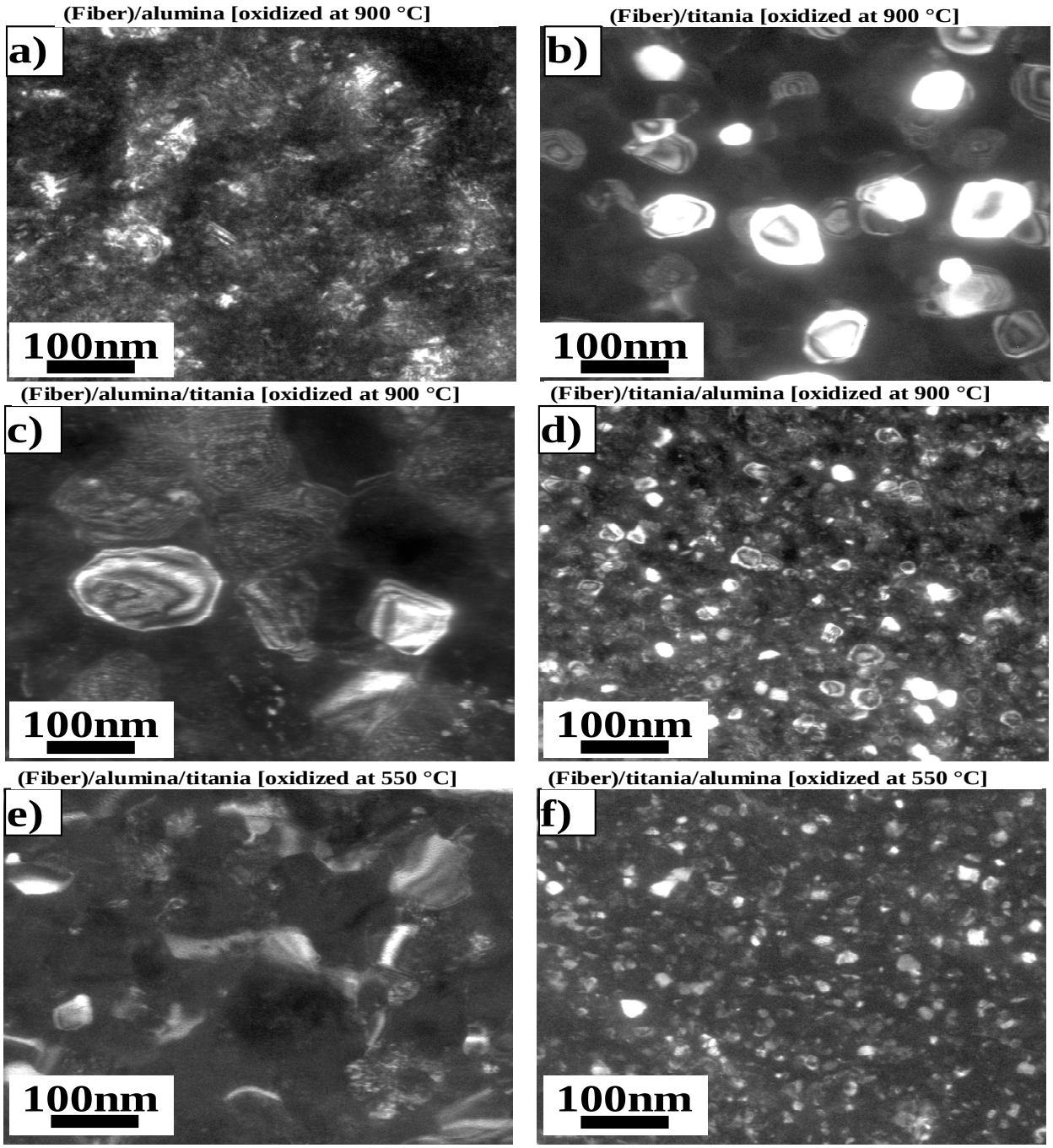


Figure 7: Dark-field transmission electron microscopic (TEM) images of the residual coatings after oxidative degradation of the fibers. Grains that appear bright are crystals orientated in favorable direction for Bragg diffraction: Residual coatings after thermogravimetric analysis have been exposed to 900 °C: a) 66 nm alumina b) 20 nm titania c) 50 nm alumina followed by 40 nm titania d) 20 nm titania followed by 30 nm alumina. Residual coatings after oxidative degradation of fibers at temperatures of 550 °C in a tube furnace: e) 50 nm alumina followed by 40 nm titania, and f) 20 nm titania followed by 30 nm alumina.

This double layer sequence improves oxidation onset temperature not only compared to single layer coatings, but even compared to another double layer coating. Thus, oxidation property of the coated fibers depends not only on the type of oxide coatings, or the thickness of layers it depends as well on the sequence of the layers.

In order to investigate the oxidation behavior at fixed temperature, these four types of coated fibers (66 nm alumina, 20 nm titania, 50 nm alumina followed by 40 nm titania, and 20 nm titania followed by 30 nm alumina) were separately heated at 550 °C in a tube furnace in open air. Since the carbon is black and the coatings are colorless, one can easily determine the point of total oxidation of the fibers by a change in color from black, a dark gray to white (for detail see Figure 1 of chapter 7). Uncoated fibers were completely oxidized within 8 hours, whereas 66 nm alumina, 20 nm titania, 50 nm alumina followed by 40 nm titania, and 20 nm titania followed by 30 nm alumina need oxidation times of 12 hours, 10 hours, 13 hours and 30 hours, respectively. Thus, oxidation at a fixed temperature of 550 °C confirms the trends observed in thermogravimetry. On the other hand, raising the temperature can speed up oxidation as well due to an Arrhenius type increase of reaction rates or due to the increase of the diffusion coefficient of the gases. Thus, carbon fiber coated with titania/alumina double layer coating not only improves oxidation onset temperature in TGA. It increases as well the life-time in long term moderate temperature oxidation.

To get more insight into the origin of this dependency, the coatings that remain after TGA were investigated via TEM. The shape of the residual coatings resemble microtubes, thus their inner surface has the same morphology as the fiber surface (for detail of such microtubes see chapter 7)[12]. It is known that alumina and titania coating deposited via ALD at moderate temperatures are predominantly amorphous[13, 14]. Amorphous alumina and titania films crystallizes upon annealing[15, 16]. Here, both the as deposited alumina and titania layers were to a certain extent crystalline, with significantly small grain size, at least one can see in TEM image of Figure 3. When these coatings were annealed during the thermogravimetry, degree of crystallization increases compared to as deposited state, especially size of the grains (see the transmission images, and the dark field images, Figure 6 and 7). These images expose details that may be interpreted as grain boundaries which open cracks (Figure 6a and c) or voids (Figure 6b) within the coatings. Thus, it is likely that the observed lowering of the oxidation stability at higher temperatures is due to crystallization. In the case of double layer coatings one shining fact is visible: If titania coating is on the outside (Figure 6c and 7c) the titania crystals are significantly more coarse than in the case of titania being in between the fiber and the alumina (see Figure 6d and 7d). Obviously, the sequence

of the layers influences the crystallization behavior. This in turn might give rise to the observed differences in oxidation stability.

Question arises, whether this difference in grain size occurs only at temperatures above the onset of oxidation, it may occur even before this temperature is reached. Thus the residues left after slow oxidation (coated fibers oxidized at 550 °C) were investigated by TEM as well (see Figure 6e-f and Figure 7e-f). TEM images revealed that the sizes of the grains in these residues are smaller (see Figure 7e-f) than in residues left after heating to 900 °C. These size differences are more prominent in cases of titania being at the outside than being covered by alumina. Thus, it might be possible that covering the titania by alumina to some extend slows down coarsening by crystallization but not supporting the titania by a layer of alumina beneath it.

5.3 Experimental Part

The reaction chamber and sample holder were identical to the one described in chapter 3. Same type of carbon fibers were used for coating after thermal desized. Fibers were coated by titania at a temperature of 200 °C and a pressure of 0.1 mbar using titanium tetrachloride ($TiCl_4$) (98% from ABCR GmbH & co. KG, Karlsruhe) and deionised water as precursors. Titanium tetrachloride was heated to 70 °C and the temperature of the water was maintained at 50 °C. A gas flow system was designed in such a way that a single inert gas (nitrogen) can act as both, purge gas and carrier gas. In purging cycles there was a flow of nitrogen of 40 standard cubic centimeters per minute. In the 1^{st} half cycle, the fiber bundle was exposed to $TiCl_4$ for 30 s followed by purging the reactor with nitrogen for 40 s. In the second half cycle, it was exposed to water vapor for 30 s followed by purging the reactor with nitrogen for 40 s. One complete cycle consisted of 140 s and was repeated for appropriate times to obtain systematically varied coating thicknesses.

Fibers were coated by alumina at a temperature of 77 °C and a pressure of 0.1 mbar using trimethylaluminum (98% from ABCR GmbH & Co. KG, Karlsruhe, Germany) and deionised water as precursors (details of this coating were reported in reference 2). In the first half cycle, the fiber bundle was exposed to trimethylaluminum for 20 s followed by purging the reactor with nitrogen for 30 s. In the second half cycle, it was exposed to water vapor for 20 s followed by purging the reactor with nitrogen for 30 s. One complete cycle consisted of 100 s and was repeated for appropriate times to obtain systematically varied coating thicknesses.

To characterize films on the fibers directly after deposition, scanning electron microscopy (SEM) and energy dispersive X-ray spectroscopy (EDXS) were recorded using a Nova NanoSEM (FEI, PHILIPS); specimens were taken from the bundles.

Thermogravimetry was performed using a TGA7 from PerkinElmer. 5 mm long coated fiber specimens (weight of 3.0 to 4.0 mg) were heated from 30 °C to 900 °C with a heating rate of 5 °C/minute and subsequently hold for 30 minutes, respectively 60 minutes at 900 °C in a flow of 20 ml per minute of synthetic air.

To characterize the residual coatings after thermal oxidation, transmission electron microscopy (TEM) was recorded using a PHILIPS CM 20 FEG. TEM images were recorded in transmission perpendicular to the natural surface of the coating.

5.4 Conclusions

Both, single layers (alumina, and titania) as well as double layers (alumina/titania, and titania/alumina), can act as an oxidation barrier coatings for carbon fibers to a certain extend. The combination of titania/alumina improves oxidation resistance better than any other coatings used here. During heat treatment crystal grains were formed, as well the grain boundaries. Oxygen might diffuse through the grain boundaries and this might limit the life-time of the coated carbon fibers at higher temperatures.

5.5 References

1. Roy, A. K.; Baumann, W.; Konig, I.; Baumann, G.; Schulze, S.; Hietschold, M.; Mader, T.; Nestler, D. J.; Wielage, B.; Goedel, W. A. Atomic layer deposition (ALD) as a coating tool for reinforcing fibers, *Analytical and Bioanalytical Chemistry* **2010,** *396* (5), 1913-1919.

2. Roy, A. K.; Baumann, W.; Schulze, S.; Hietschold, M.; Mader, T.; Nestler, D. J. Wielage, B.; Goedel, W. A. Atomic Layer Deposition of Alumina onto Carbon Fibers, *Journal of the American Ceramic Society* **2011**, DOI: 10.1111/j.1551-2916.2010.04340.x.

3. Hinke, S.; Stockel, S.; Marx, G. Characterization of BN-Films Deposited onto Carbon-Fibers by a Continuous CVD-Process. *Fresenius´ Journal of Analytical Chemistry* **1994**, *349*(1-3), 181-181.

4. Liu, Y.; Treadwell, D. R.; Kannisto, M. R.; Mueller, B. L.; Laine, R. M. Titanium nitride/carbon coatings on graphite fibers. *Journal of the American Ceramic Society* **1997**, *80*(3), 705-716.

5. Piquero, T.; Vincent, H.; Vincent, C.; Bouix, J. Influence of Carbide Coatings on the Oxidation Behavior of Carbon-Fibers. *Carbon* **1995**, *33*(4), 455-467.

6. Hackl, G.; Gerhard, H.; Popovska, N. Coating of carbon short fibers with thin ceramic layers by chemical vapor deposition. *Thin Solid Films* **2006**, *513*(1-2), 217-222.

7. Wang, Y.-Q.; Zhou, B.-L.; Wang. Z.-M.; Oxidation Protection of Carbon-Fibers by Coatings. *Carbon* **1995**, *33*(4), 427-433.

8. Baklanova, N. I.; Zima, T. M.; Titov, A. T.; Isaeva, N. V.; Grashchenkov, D. V.; Solntsev. S. S. Protective coatings for carbon fibers. *Inorganic Materials* **2006**, *42*(7), 744-749.

9. Hashishin, T.; Murashita, J.; Joyama, A.; Kaneko, Y. Oxidation-resistant coating of carbon fibers with TiO_2 by sol-gel method. *Journal of the Ceramic Society of Japan* **1998**, *106*(1), 1-5.

10. Landry, C. C.; Barron, A. R. MOCVD of Alumina-Silica Oxidation-Resistant Coatings on Carbon-Fibers. *Carbon* **1995**, *33*(4), 381-387.

11. Cho, D.; Protective behavior of thermal oxidation in oxidized PAN fibers coated with phosphoric acid. *Carbon* **1996**, *34*(9), 151-1154.

12. Roy, A. K.; Knohl, S.; Goedel. W. A. Alumina microtubes prepared via template-directed pulsed chemical vapor deposition (pulsed CVD), *Journal of Material Science* **2011**, *46 (14)*, 4812-4819.

13. Groner, M. D.; Fabreguette, F. H.; Elam, J. W.; George, S. M., Low-temperature Al_2O_3 atomic layer deposition. *Chemistry of Materials* **2004,** *16* (4), 639-645.

14. Aarik, J.; Aidla, A.; Uustare, T.; Sammelselg, V., Morphology and Structure of TiO_2 Thin-Films Grown by Atomic Layer Deposition. *Journal of Crystal Growth* **1995**, *148* (3), 268-275.

15. Oh, H. J.; Lee, J. H.; Ahn, H. J.; Jeong, Y.; Heo, C. H.; Chi, C. S. Effects of potential and heat treatment on phase transition of alumina dielectric layer. *Journal of Electroceramics* **2006**, *17*(2-4), 369-373.

16. Karunagaran, B.; Kumar, R. T. R.; Mangalaraj, D.; Narayandass, S. K.; Rao, G. M. Influence of thermal annealing on the composition and structural parameters of DC magnetron sputtered titanium dioxide thin films. *Crystal Research and Technology* **2002**, *37*(12), 1285-1292.

6. Atomic layer deposition of aluminum phosphate*

6.1 Introduction

Embedding fibers into metallic or ceramic matrices can increase their toughness through a distributed damage mechanism. The predominant reason for this effect is that cracks propagating through the matrices do not crack the fibers. Thus, finally the mechanical load that otherwise would give rise to a large stress in a small volume at the tip of the crack is distributed over a large numbers of fibers, therefore, yielding a reduced stress that is spread out over a large volume. This mechanism, however, needs a weak bonding between the fiber and the matrix.[1] This weak bonding may be achieved by weakening the matrix in proximity of the fiber, often it is achieved by covering the fiber with a "weak" coating before embedding. "Weak" coating should still transfer the applied load from matrix to fiber and at the same time it should arrest the cracks at the interface to protect the fibers. Examples of such "weak" coatings are graphitic carbon or boron nitride.[2] At the beginning graphitic carbon was used as a coating, this material having good crack deflection ability due to a layered structure[3]. However, oxidation resistance is poor at high temperatures. It is stable only up to a maximum of 400 °C. In the second generation, hexagonal boron nitride (BN) was used as a "weak" coating [4, 5]. It has a good ability to deflect cracks like graphitic carbon due to similar structure. It has much better oxidation resistance compare to graphitic carbon, however, oxidation resistance and a stability to deflect cracks depends on the structures[6], degree of crystallinity, crystallographic orientation and impurities which are all affected by synthesis and/or deposition conditions. Generally, a high deposition temperature results in an ordered structure, with decreasing basal interplanar spacing that gives more oxidation resistance. However, in presence of moisture, formations of thermodynamically stable fugitive species of boric acids (such as HBO_2, H_3BO_3) are possible and thus the oxidation of BN[7, 8] is enhanced. Thus, both coatings are prone to oxidation, especially in moisture and oxidative environments.

In previous chapters, atomic layer deposition (ALD) has been used to deposit oxidation resistant coatings such as alumina and titania onto carbon fibers. The properties typical for ALD − deep infiltration, precise thickness control and conformality – were achieved and the coatings were efficient in protecting the fibers against oxidation. However, none of these coatings can be considered "weak". Thus, the goal of the present contributions

*Most of the results of this chapter were submitted for publication in the following manuscript:

Roy, A. K.; Lungwitz, R.; Spange, S.; Mäder, T.; Nestler, D. J.; Wielage, B.; Schulze, S.; Hietschold, M.; Goedel; W. A. Non-aqueous Atomic Layer Deposition (ALD) of Aluminum Phosphate.

is to develop an atomic layer deposition process to deposit a "weak" and oxidation stable coating onto carbon fibers. Various phosphates ($AlPO_4$, $CaPO_4$, $LaPO_4$, $CePO_4$) can act as "weak" interfaces with improved oxidation resistance.[9-11] Thus, phosphate coatings may replace other coatings. To the best of my knowledge, none of these materials has been deposited by ALD. Out of the potential precursors for these materials, the precursors that may be used to deposit $AlPO_4$ are the most volatile and least expensive. In addition, aluminum orthophosphate ($AlPO_4$) is a covalent, electrically neutral, and chemically inert material. Because of these properties, it has widespread applications in additional fields like catalysis or microelectronics.[12, 13] Polycrystalline forms of $AlPO_4$ can be used for microelectronic packing. A polymorph of $AlPO_4$, berlinite, has piezoelectric properties.[14] Aluminum orthophosphates have interesting ion exchange and adsorption properties and may also be used in lithium ion batteries.[15, 16] Thus, we chose here to find parameters and precursors that may be used to deposit $AlPO_4$.

There are several reports about the synthesis of aluminum orthophosphates via sol-gel routes.[17, 18] In most of the sol-gel methods, phosphoric acid is used as a phosphate source. Sol-gel methods are limited, especially if uniform coatings onto individual filaments of fiber bundles are desired.[1] Additionally, in these method aqueous sols of the precursors is used, which may be problematic for non-oxide fibers (such as carbon and silicon carbide) because they are prone to oxidation. Thus, the sol-gel route may not be an ideal deposition tool for reinforcing fibers, especially for non-oxide fibers.

Pure phosphoric acid is not an option for CVD precursor in because phosphoric acid has a very low vapor pressure at room temperature and heating leads to decomposition (mainly into P_2O_5 and water) instead of evaporation. Thus, until now phosphate deposition is limited by lack of suitable precursors. There has been a brilliant publication about thermal chemical vapor deposition (CVD) of aluminum phosphate onto glass by using as single organometalic precursors, either $[Me_2AlO_2P(O^tBu)_2]_2$, or $[Al(O^iPr)_2O_2P(O^tBu)_2]_4$ which were synthesized prior to the deposition.[19]

6.2 Results and discussion

Atomic layer deposition of aluminum phosphate was applied onto bundles of carbon fibers using alternating pulses of commercially available trimethylaluminum ($AlMe_3$) and triethylphosphate ($OP(OEt)_3$), at reduced pressure and a temperature of 250 °C. Scanning electron microscopic (SEM) images of a part of the coated fiber bundle after this process are shown in Figure 1. Figure 1a and 1b reveal that the fibers within the bundle are still separated

from each other, no bridging has been formed, and that coatings have been deposited evenly onto fibers. In these images, carbon fibers appear darker than the coatings. This later fact is especially evident from Figure 1c and d where the coating was partially removed and the underlying carbon fiber is visible. In our previous reports about alumina on carbon fibers we observed delamination of coatings from the ends of cut fibers and the formation of clear straight steps. In the case of aluminum phosphate shown here, we often observe no clear delamination, the border between coating and underling fiber often being smeared out and forming an irregular line. Thus, it is likely that in the present case cohesion is weaker than adhesion. Thus, aluminum phosphate might count as “weak” coating at least in comparison to alumina.

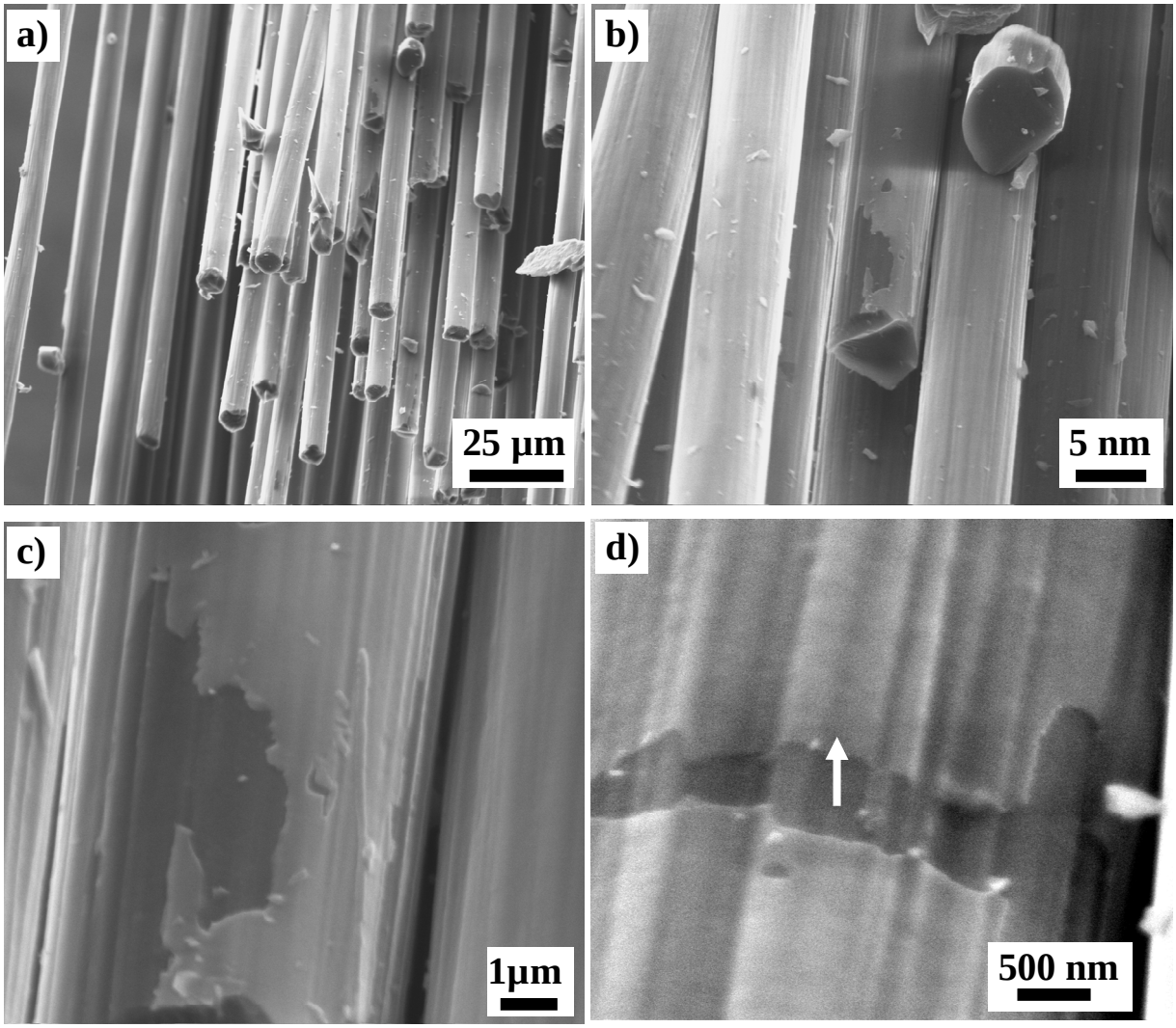


Figure 1: Scanning electron microscopic (SEM) images of coated fibers, after 200 cycles of coating deposition, coating was deposited at a temperature of 250 °C: a), and b) are part of the fiber bundle, c) and d) are single fiber, arrows indicate coating was removed.

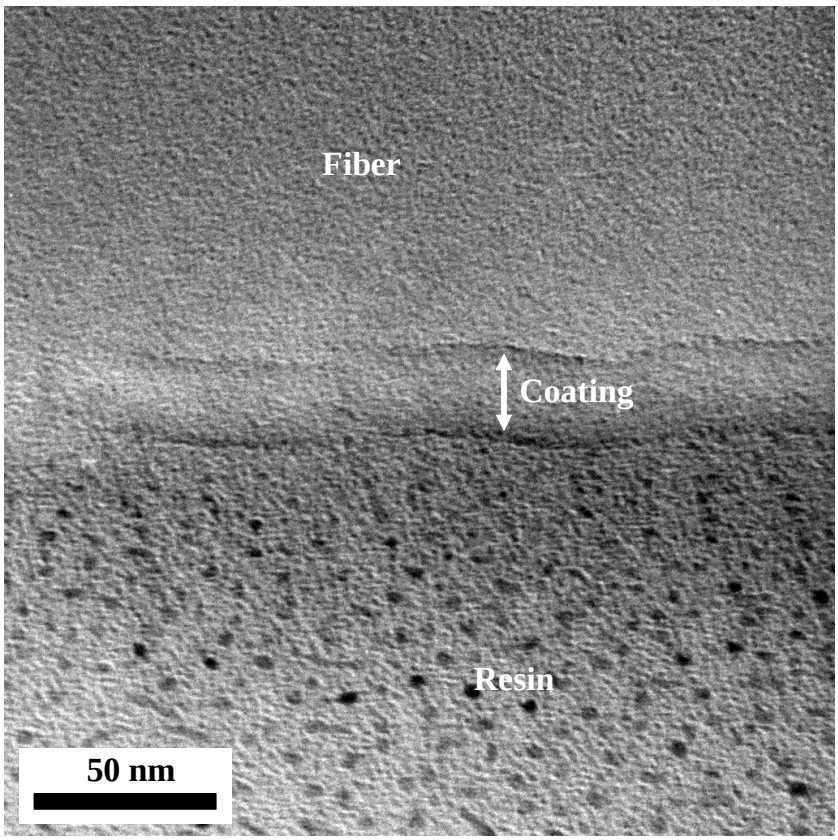


Figure 2: A cross sectional view of a single fiber in transmission electron microscopy (TEM), after 350 cycles of deposition (sample was prepared by focus ion beam).

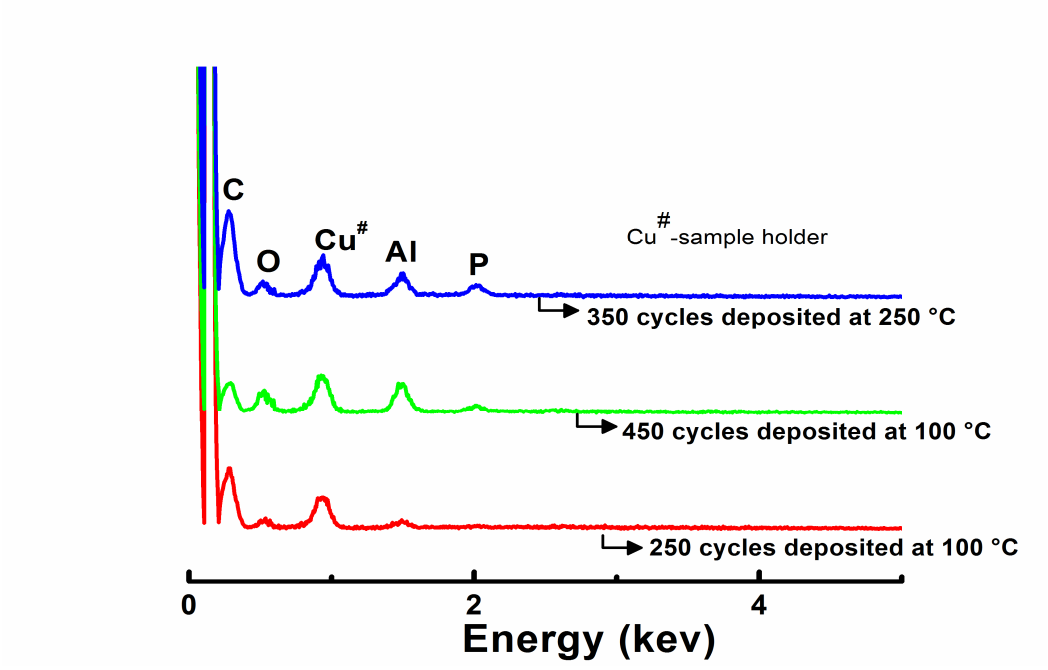


Figure 3: Energy dispersive X-ray spectroscopy (EDXS) of a selected area (4.6 x 3.8) μm^2 on a single fiber for deposition temperature of 100 °C and 250 °C. The spectrum indicate that carbon, aluminum, oxygen, and phosphorous are present in all these samples.

A TEM image of a cross section of the interface between the fiber and the coating (prepared using a focused ion beam) shows that the coating is conformal; (see Figure 2). The coating thickness was approximately 25 nm for 350 cycles. Assuming linear dependency between thickness and number of deposition cycles this translates into an average deposition rate of 0.07 nm per cycle.

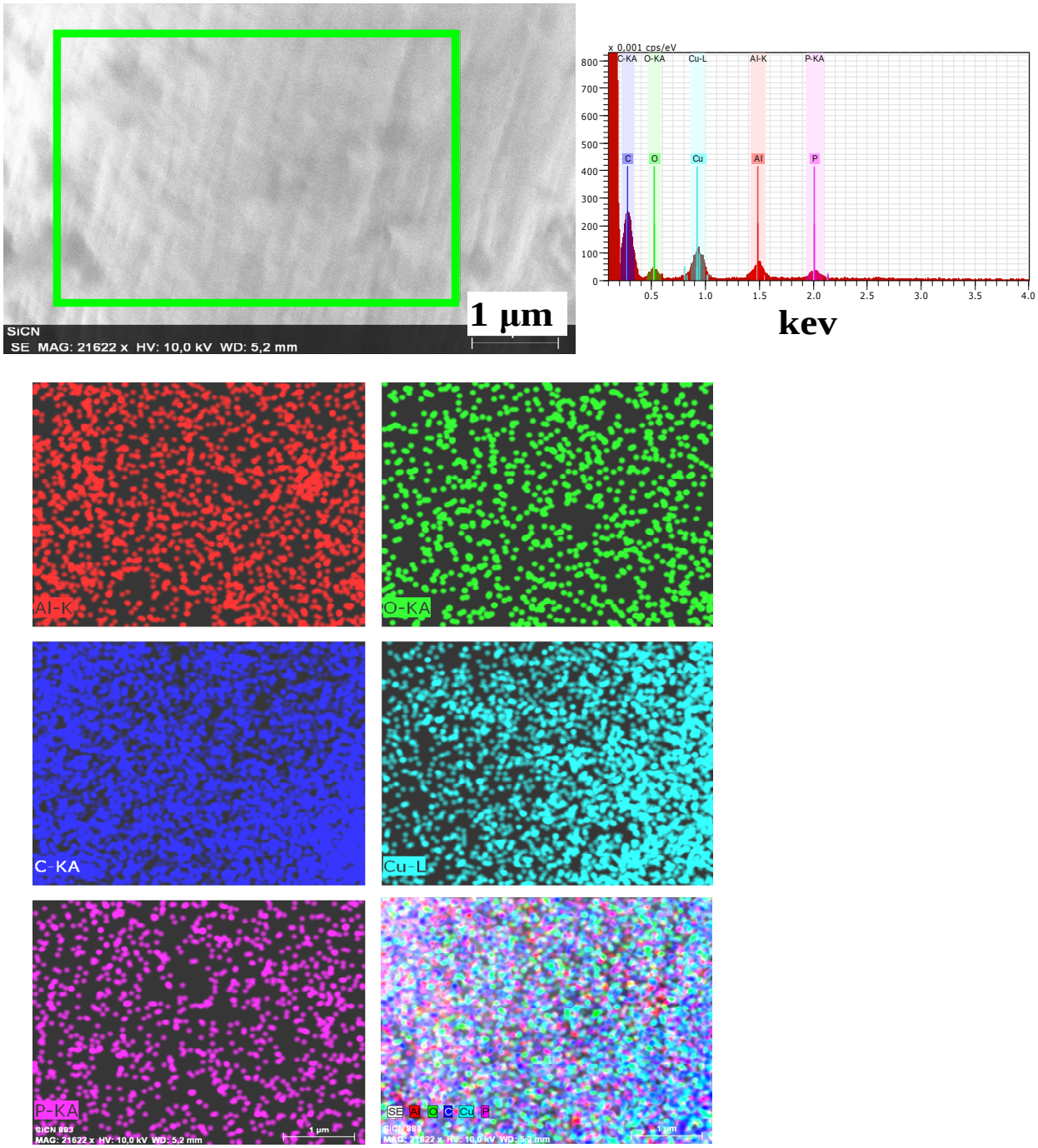


Figure 4: Elemental maps from Energy dispersive X-ray spectroscopy (EDXS) for a selected area (4.6 x 3.8) μm^2 of a single fiber for 250 °C deposition temperatures. Spectrum indicates carbon, aluminum, oxygen, and phosphorous and a uniform distribution of Aluminum and phosphorous (at least in a µm length scale).

Elemental analysis of the coated fiber by EDXS (see Figure 3 and Figure 4) revealed a dominating carbon content as well as aluminum, oxygen and phosphorous. The dominating amount of carbon was expected because of the carbon fiber, the presence of aluminum, oxygen, and phosphorous confirms the expected aluminum phosphate. Coatings deposited at a temperature of 100 °C had lower phosphorus content than those deposited at 250 °C (see Figure 3). In addition, phosphorous contained might be lower than one can aspect for pure alumium phosphate even at the deposition temperature of 250 °C.

In addition, the coating that was deposited onto the inner side of the reactor simultaneously to the one deposited onto the fibers was scrapped off and characterized by elemental flash analysis and solid state nuclear magnetic resonance (NMR). Elemental flash analysis revealed a content of carbon, hydrogen, and nitrogen of 4.06%, 1.60% and no nitrogen (if the nitrogen was there that might be less than the detection limit of the instrument, i.e.,<0.01%), respectively. Aluminim and phosphorous contain of the coating deposited onto the inner side of the reactor was investigated separately via atomic absorption spectroscopy (AAS). It was revealed that alumium and phosphorous of 26.2% and 3.6%, respectively, whereas pure alumium phosphate (ACROS ORGANICS, Geel, Belgium) contained 17.3% and 28.3% respectively. The phosphorous contained in the coating deposited onto the inner side of the reactor was lower than the pure phosphate. The coating deposited onto the inner side of the reactor was collected from the both ends of the reactor. Ends had lower deposition temperatures compare to the middle of the reactor. As one can see from EDXS results (Figure 3), when the deposition temperature is lower, specimen have less phosphorous contained. Thus, it is likely that the coating deposited at both ends had lower phosphorous contained than the coating deposited onto the fibers.

Furthermore, ^{27}Al and ^{31}P solid state NMR spectroscopy were used in order to investigate the molecular structure and the chemical composition of the coating onto the inner side of the reactor. NMR analysis of the coating deposited directly onto fibers was not possible. Thus, the coating deposited onto the inner side of the reactor was considered as a representative sample. The ^{27}Al and ^{31}P NMR spectra of a representative sample of the coating are shown in Figure 5. Both spectra exhibit pronounced spinning side bands (see inset), as well as relatively narrow and well separated signals that indicate a well-defined chemical structure. The ^{27}Al NMR spectrum shows four well resolved signals at 72, 39, 4, and –15 ppm, which are all typical for aluminum phosphates.[18-18][20] The peak at 39 ppm can be assigned to AlO_4 units with four phosphorous atoms as next nearest neighbors.

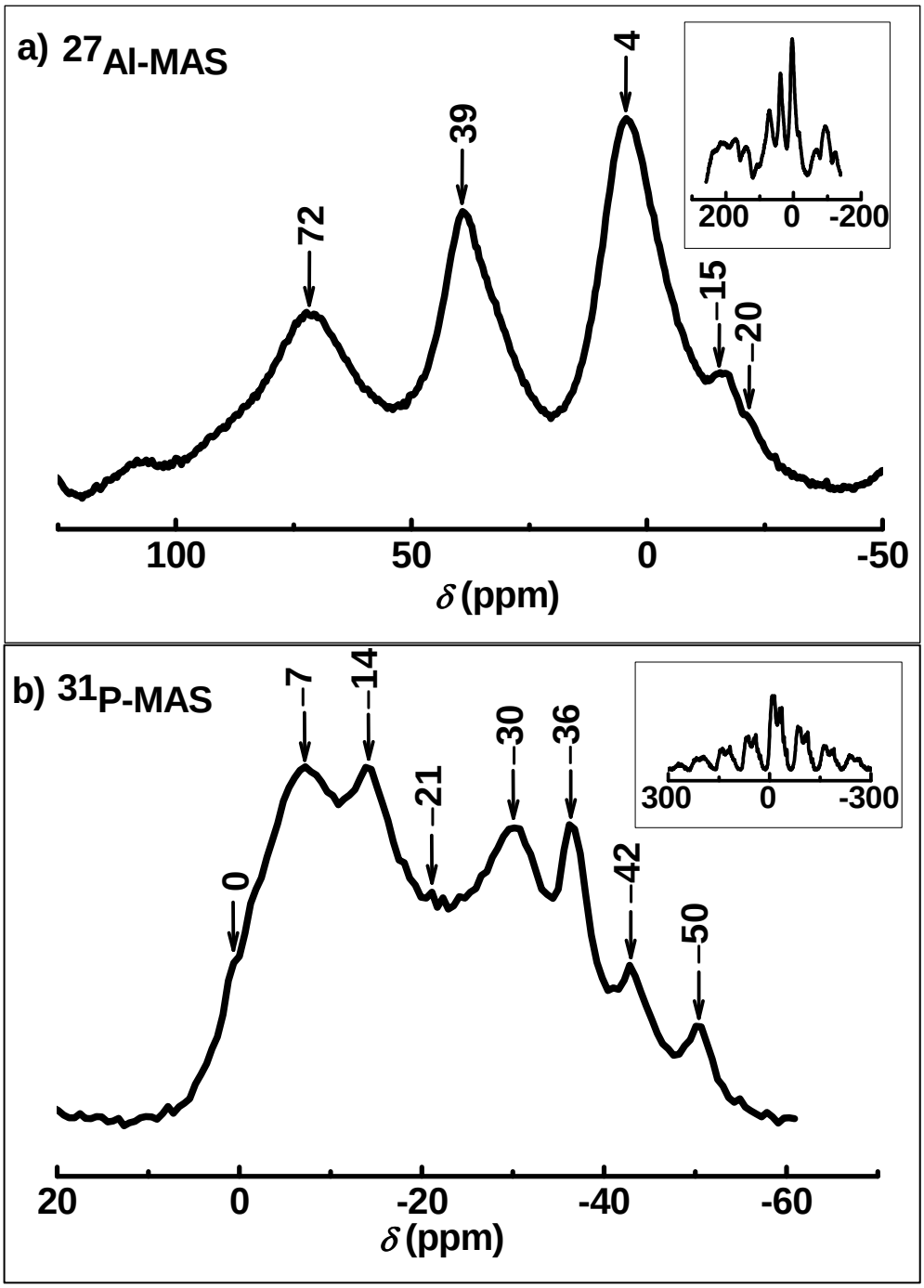


Figure 5: Solid state nuclear magnetic resonance (NMR) spectra of the coating deposited inner side the reactor: a) ^{27}Al spectra, peaks at 72 ppm, 39 ppm 4 ppm, –15 ppm can be assigned to the structural units, $Al(OAl)_4$, $Al(OP)_4$, AlO_5, AlO_6, respectively, a hump approximately between –15 ppm and –20 ppm might indicate $Al(OP_3)_3$, and b) ^{31}P spectra, peaks at 0 ppm, –7 ppm, –14 ppm, –21 ppm, –30 ppm, indicate orthophosphate species bound to zero, one, two, three and four aluminum atoms, respectively and peaks at –36 ppm, –42 ppm, –50 ppm indicate $Al(PO_3)_3$ (monoclinic), and $Al(PO_3)_3$ (cubic) polymorphs, respectively.

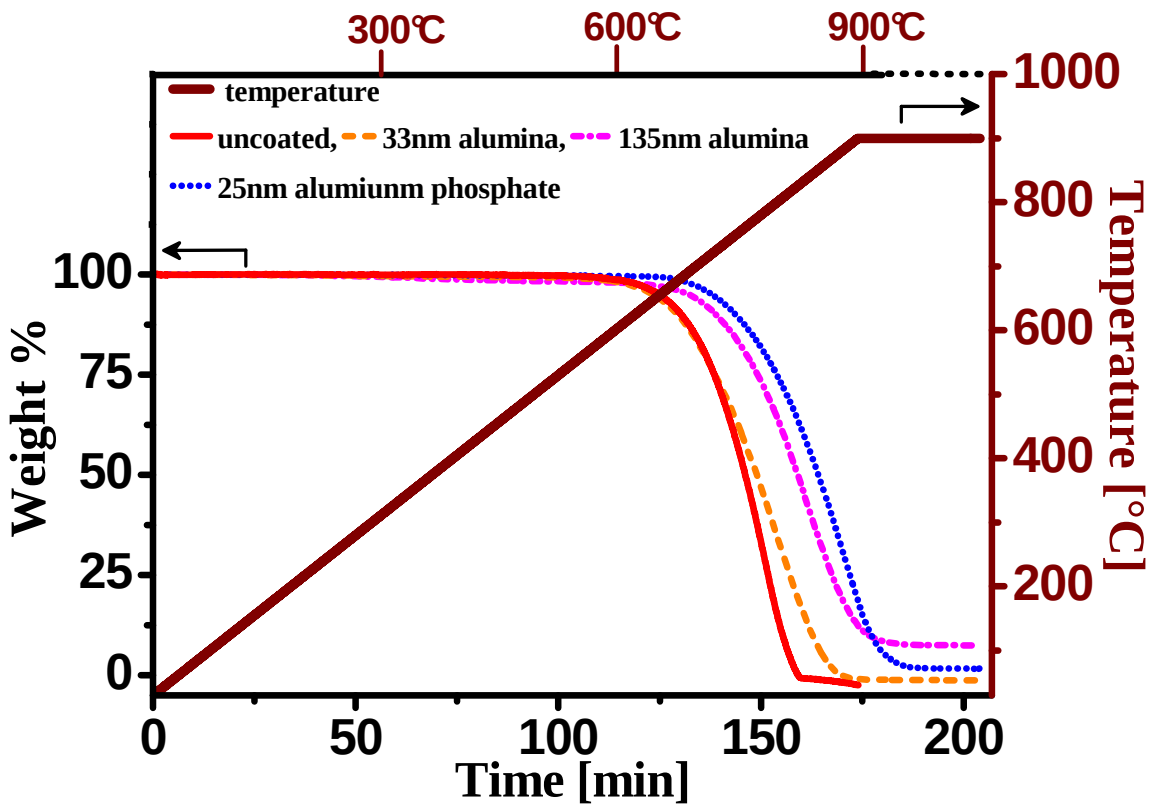


Figure 6: Thermogravimetric analysis (TGA) of carbon fibers, uncoated, and coated with alumina and aluminum phosphate, respectively. The specimens were heated from 30 °C to 900 °C with a heating rate of 5 °C/minute and subsequently held at 900 °C for 30 minutes in synthetic air.

Its position is identical to the one of pure (crystalline) aluminium orthophosphate.[18] The signals at around 4 and –15 ppm can be assigned to AlO_5 and AlO_6 species with aluminum or phosphorous atoms as next nearest neighbors and have as well been observed in aluminum orthophosphate gels[18]. Thus, peaks are in accordance with the assumptions that the layers comprise "aluminum ortho phosphate" as structural element. The peak at 72 ppm most likely indicates AlO_4 units with four alumina atoms as next nearest neighbors[20]. Thus, besides pure orthophosphates there might be regions that are locally depleted of phosphorous. In addition, monoclinic (*m*) or cubic (*c*) $Al(PO_3)_3$ might also be formed during the reaction. These species will show signals at –15 (*m*) and –21 (*c*) ppm, but – based on the ^{27}Al NMR spectra – they can neither be clearly identified nor excluded.

In the ^{31}P NMR spectra five signal components at 0 (shoulder), –7, –14, –21 to –22 (hardly visible), and –30 ppm can be distinguished. The peak at –30 ppm can be assigned to phosphorous atoms in orthophosphate surrounded by four aluminum atoms as next nearest

neighbors (in reference 17 designed as Q_4^0) and thus corresponds to the peak at 39 ppm in the ^{27}Al NMR spectrum. Furthermore the peaks in the region of 0 to –22 ppm can be assigned to phosphorous atoms with zero, one, two and three aluminum atoms as next nearest neighbors (Q_0^0, Q_1^0, Q_2^0, respectively Q_3^0). Thus, locally there might be regions depleted of aluminum atoms as well. The peaks at –36 and –42 ppm are typical for the monoclinic phase of $Al(PO_3)_3$ and the cubic aluminum metaphosphate phase is indicated by the signal at –50 ppm. In conclusion, the ^{27}Al and ^{31}P solid state NMR spectra evidence the formation of a coating that comprises oxidized aluminum and phosphorous atoms in close proximity and might be regarded as a disordered mixture of aluminum orthophosphate and $Al(PO_3)_3$.

One of our goals is to improve oxidation resistance of the carbon fibers. Thus, the oxidation resistance of the alumina coated fibers is characterized by thermogravimetric analysis (TGA): 5 mm long coated fiber specimen were used for TGA. These specimens were heated from 30 °C to 900 °C with a heating rate of 5 °C/minute and subsequently held at 900 °C for 30 minutes in a flow of synthetic air. The results are shown in Figure 3; the oxidation onset temperature (3% weight loss) for the uncoated fiber is approximately 630 °C and the fibers are completely burned at temperatures of approximately 825 °C. On the other hand, fibers coated with 33 nm and 135 nm thick layers of alumina start oxidation at approximately 630 °C and 660 °C, respectively. In case of fibers coated with a 25 nm thick layer of aluminum phosphate, the oxidation starts at a temperature of approximately 700 °C and the fibers are not completely burned when the temperature of 900 °C is reached, but need approximately 20 minutes additional time at that temperature to be completely oxidized. Thus, aluminum phosphate improves the oxidation resistance of the carbon fibers to some extend and seems to be even better than alumina coatings of a significantly higher thickness.

6.3 Exprimental Part

The reaction chamber and sample holder were identical to the one described in chapter 3. Same type of carbon fibers were used for coating after thermal desized. The reaction chamber and sample holder are identical to the one described in chapter 3. Fibers are coated with aluminium phosphate at a temperature of 250 °C using pulses of trimethylaluminum (98% from ABCR GmbH & co. KG, Karlsruhe) and of triethylphosphate, $(C_2H_5)_3PO_4$ (99% from ABCR GmbH & co. KG, Karlsruhe) as precursors in a homebuilt reactor. The supply vessel of trimethylaluminum was heated to 60 °C. The temperature of the triethylphosphate supply was maintained at 100 °C. Two streams of nitrogen were used as carrier for trimethylaluminum and triethylphosphate respectively, as well as purge gas, their

flow was controlled by two mass flow controllers each set to 20 standard cubic centimeters per minute (sccm). In the first half cycle, the fiber bundle was exposed to trimethylaluminum for 20 s followed by purging the reactor with nitrogen for 30 s. In the second half cycle it was exposed to triethylphosphate for 20 s followed by purging the reactor with nitrogen for 30 s. In both exposures the valve in front of the pump was closed, it was opened fully during the purge time.

Scanning electron microscopy (SEM) was recorded using a Nova NanoSEM (FEI, PHILIPS), directly taking the specimens from the bundles after deposition. The same instrument was used to perform energy dispersive X-ray spectroscopy (EDXS). Samples for imaging with transmission electron microscopy (Figure 2) were prepared using a focused ion beam (FIB). The details of this method were reported elsewhere.[21]

Thermogravimetry was performed using a TGA7 from PerkinElmer. 5 mm long coated fiber specimens (weight varying between 1.0 mg to 1.4 mg) were heated from 30 °C to 900 °C with a heating rate of 5 °C/minute and subsequently hold for 30 minutes at 900 °C in 20 ml per minute synthetic air flow.

AAS was carried out by an analytical company (BERGHOF Aalytik + umweltengineering GmbH & Co. KG, Chemnitz, Germany) using the method of DIN EN ISO 11885 (E22).

NMR measurements were carried out at ambient temperature on a Bruker Avance 400 spectrometer, using a double tuned 4 mm MAS (magic angle spinning) probe. At the field strength of 9.4 T, the resonance frequencies were 104.26 MHz for ^{27}Al and 161.97 MHz for ^{31}P. All spectra were recorded at a MAS rotation frequency of 12.5 kHz using zirconium oxide rotors. Typical acquisition parameters were puls length 4.1 μs (90°) for ^{27}Al and 4 μs (40°) for ^{31}P, recycle delay 5 s (^{31}P) and 8 s (^{27}Al), respectively. The ^{27}Al and ^{31}P NMR Chemical shifts were referenced to 1M $Al(NO_3)_3$ aqueous solution (0 ppm) and 85% H_3PO_4 (0 ppm), respectively.

6.4 Conclusions

Aluminum phosphate (comprising structural elements of $AlPO_4$ as well as $Al(PO_3)_3$) was successfully deposited onto carbon fibers by atomic layer deposition. These layers were smooth, uniform and conformal and provided protection against oxidation. Further optimization will be needed if pure aluminum orthophosphate coatings are desired.

6.5 References

1. Kerans, R. J.; Hay, R. S.; Parthasarathy, T. A.; Cinibulk, M. K., Interface design for oxidation-resistant ceramic composites. *Journal of the American Ceramic Society* **2002,** *85* (11), 2599-2632.

2. Naslain, R.; Dugne, O.; Guette, A.; Sevely, J.; Brosse, C. R.; Rocher, J. P.; Cotteret, J., Boron Nitride Interphase in Ceramic-Matrix Composites. *Journal of the American Ceramic Society* **1991,** *74* (10), 2482-2488.

3. Helmer, T.; Peterlik, H.; Kromp, K., Coating of Carbon-Fibers - the Strength of the Fibers. *Journal of the American Ceramic Society* **1995**, *78* (1), 133-136.

4. Hinke, S.; Stockel, S.; Marx, G. Characterization of BN-Films Deposited onto Carbon-Fibers by a Continuous CVD-Process. *Fresenius´ Journal of Analytical Chemistry* **1994**, *349*(1-3), 181-181.

5. Dietrich, D.; Martin, P. W.; Nestler, K.; Stockel, S.; Weise, K.; Marx, G., Transmission electron microscopic investigations on SiC- and BN-coated carbon fibres. *Journal of Materials Science* **1996,** *31* (22), 5979-5984.

6. Jacobson, N.; Farmer, S.; Moore, A.; Sayir, H., High-temperature oxidation of boron nitride: I, monolithic boron nitride. *Journal of the American Ceramic Society* **1999,** *82* (2), 393-398.

7. Sheldon, B. W.; Sun, E. Y.; Nutt, S. R.; Brennan, J. J., Oxidation of BN-coated SiC fibers in ceramic matrix composites. *Journal of the American Ceramic Society* **1996,** *79* (2), 539-543.

8. More, K. L.; Ailey, K. S.; Lowden, R. A.; Lin, H. T., Evaluating the effect of oxygen content in BN interfacial coatings on the stability of SiC/BN/SiC composites. *Composites Part A* **1999,** *30* (4), 463-470.

9. Bao, Y. H.; Nicholson, P. S., $AlPO_4$ coating on alumina/mullite fibers as a weak interface in fiber-reinforced oxide composites. *Journal of the American Ceramic Society* **2006,** *89* (2), 465-470.

10. Mucalo, M. R.; Wielage, B.; Mucha, H., Deposition of calcium phosphate on carbon fibers using sol-gel-based reactions: The consequences of using predominantly organic solvents on the ultimate phase of calcium phosphate formed. *Journal of Materials Science* **2005,** *40* (9-10), 2671-2673.

11. (a) Boakye, E.; Hay, R. S.; Petry, M. D., Continuous coating of oxide fiber tows using liquid precursors: Monazite coatings on Nextel 720 (TM). *Journal of the American Ceramic Society* **1999,** *82* (9), 2321-2331. (b) Parthasarathy, T. A.; Boakye, E.; Cinibulk, M. K.; Perry,

M. D., Fabrication and testing of oxide/oxide microcomposites with monazite and hibonite as interlayers. *Journal of the American Ceramic Society* **1999,** *82* (12), 3575-3583.

12. Parida, K.; Mishra, T., Transition Metal Promoted Amorphous $AlPO_4$ Catalysts 1. Acid–Base and Textural Properties. *Journal of Colloid and Interface Science* **1996,** *179* (1), 233-240.

13. Roy, D. M., New Strong Cement Materials - Chemically Bonded Ceramics. *Science* **1987,** *235* (4789), 651-658.

14. Wang, H.; Xu, B.; Liu, X. L.; Han, J. R.; Shan, S. X.; Li, H., The Piezoelectric and Elastic Properties of Berlinite and the Effect of Defects on the Physical-Properties. *Journal of Crystal Growth* **1986,** *79* (1-3), 227-231.

15. Kandori, K.; Ikeguchi, N.; Yasukawa, A.; Ishikawa, T., Control of size and adsorptive properties of spherical aluminum phosphate particles. *Journal of Colloid and Interface Science* **1996,** *182* (2), 425-430.

16. Lee, S. E.; Kim, E.; Cho, J. P., Improvement of electrochemical properties of natural graphite anode materials with an ovoid morphology by $AlPO_4$ coating. *Electrochemical and Solid State Letters* **2007,** *10* (1), A1-A4.

17. Zhang, L.; Eckert, H., Sol-gel synthesis of Al_2O_3-P_2O_5 glasses: mechanistic studies by solution and solid state NMR. *Journal of Materials Chemistry* **2004,** *14* (10), 1605-1615.

18. Zhang, L.; Bogershausen, A.; Eckert, H., Mesoporous $AlPO_4$ glass from a simple aqueous sol-gel route. *Journal of the American Ceramic Society* **2005,** *88* (4), 897-902.

19. Lugmair, C. G.; Tilley, T. D.; Rheingold, A. L., Di(tert-butyl)phosphate complexes of aluminum: Precursors to aluminum phosphate xerogels and thin films. *Chemistry of Materials* **1999,** *11* (6), 1615-1620.

20. Engelhardt, G.; Michel, D. High-Resolution Solid-State NMR of Silicalites and Zeolite. Wiley, New York, **1987**.

21. Mucha, H.; Kato, T.; Arai, S.; Saka, H.; Kuroda, K.; Wielage, B., Focused ion beam preparation techniques dedicated for the fabrication of TEM lamellae of fibre-reinforced composites. *Journal of Electron Microscopy* **2005,** *54* (1), 43-49.

7. Alumina microtubes*

7.1 Introduction

Oxide microtubes and nanotubes are of interest because of their potential applications in solar energy conversion devices[1, 2], gas sensors[3, 4], single-DNA sensing[5], molecular separations[6], and drug delivery systems[7]. Microtubes and nanotubes can be synthesized by (i) self organization[8, 9], (ii) deposition from spherical catalysts[10, 11], (iii) by rolling up thin solid films[12], (iv) covering the walls of cylindrical pores or (v) covering cylindrical fibers[13]. The last two methods are known as 'template directed' synthesis. Templates should have such a property that they can withstand the deposition conditions and can easily be removed after deposition without affecting the tubes. Various materials already have been used as templates such as nanorods, carbon nanotubes, electrospun fiber and porous media etc[13].. Compared to other methods, the template directed route is of advantage because one can control the size and shape of the tubes easily. Several methods already have been applied to a template directed synthesis of metal oxide microtubes, such as: sol-gel deposition[14], atmospheric chemical vapor deposition (Atmospheric CVD)[15] and atomic layer deposition (ALD)[16]. Sol-gel deposition and Atmospheric CVD often generate inhomogeneous films and the thickness of the walls varied from one tube to another. Microtubes are often bridged in these two methods. On the other hand, ALD and pulsed CVD have the advantage that one can produce microtubes of uniform wall thickness with smooth and homogeneous surfaces. However, the coating deposition rate of ALD is quite slow, e.g., the average deposition rate of alumina onto electrospun poly(vinyl alcohol) fibers using trimethyaluminum and water is 0.08 nm/cycle[16], and 0.03 nm/cycle onto graphitic carbon fibers using aluminum trichloride and water[17].

There is one very carefully done publication on the preparation of microtubes by ALD onto polymeric fibers and selective removable of the fibers using thermal

* Most of the results of this chapter were published in the following article:

Roy, A. K.; Knohl, S.; Goedel, W. A., Alumina microtubes prepared via template-directed pulsed chemical vapor deposition (pulsed CVD), *Journal of Material Science*, **2011,** *46* (14), 4812-4819.

oxidation[16]. In this work it was shown that one can obtain tubes with controlled wall thickness. On the other hand, the template used was a felt of fibers, thus the tubes were limited in length, non-aligned and not accessible as individuals. Pulsed chemical vapor deposition can be used to coat 'endless' fibers (see chapter 4). Here, it has been shown that one can produce 'endless' microtubes of several centimeters in length, that are well aligned in bundles and in principle might be handled as individuals further applications.

7.2 Results and discussions

Bundles of alumina microtubes were prepared by depositing alumina onto bundles of 'endless' carbon fibers via pulsed chemical vapor deposition and subsequent removal of the fibers.

7.2.1 Fibers before coating deposition

Before coating deposition, the fibers have a black appearance and are aligned parallel to each other in bundles (see in Figure 1a and 1b). For SEM images of the fibers see chapter 3, Figure 1. Individual fibers have a corrugated surface bearing grooves parallel to the fiber axis and irregular protuberances; this morphology varies from fiber to fiber. According to the literature, the fibers are composed of amorphous and crystalline regions, the crystalline regions having to some extend preferential orientations with respect to the fiber axis[18]. Thus, the fiber exposes various functionalities to the surface enabling the physisorbtion or chemisorption of either TMA[19, 20] or water.

7.2.2 Coatings on the carbon fibers

Alumina deposited onto these carbon fibers using trimethylaluminum and water as precursors at a temperature of 77 °C in a flow type reactor via pulsed chemical vapor deposition (pulsed CVD). In the 1st half cycle, the fiber bundle was exposed to trimethylaluminum for 20 s followed by purging the reactor with nitrogen for 30 s. In the second half cycle it was exposed to water vapor for 20 s followed by another purging of the reactor with nitrogen for 30 s.

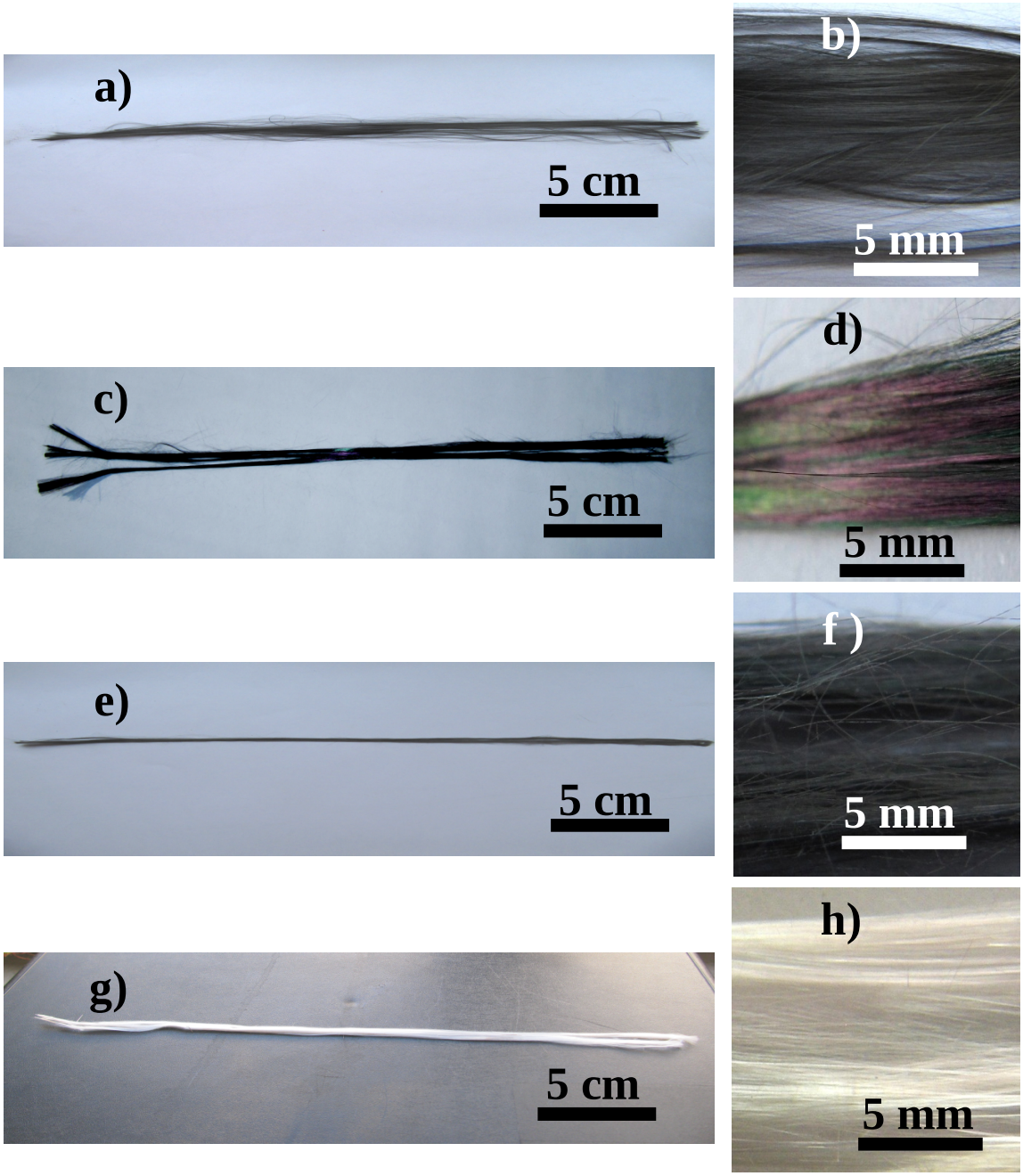


Figure 1: Photographic images of a), and b) carbon fibers before film deposition c), and d) carbon fibers after film deposition e), and f) at an intermediate stage of oxidation g), and h) microtubes.

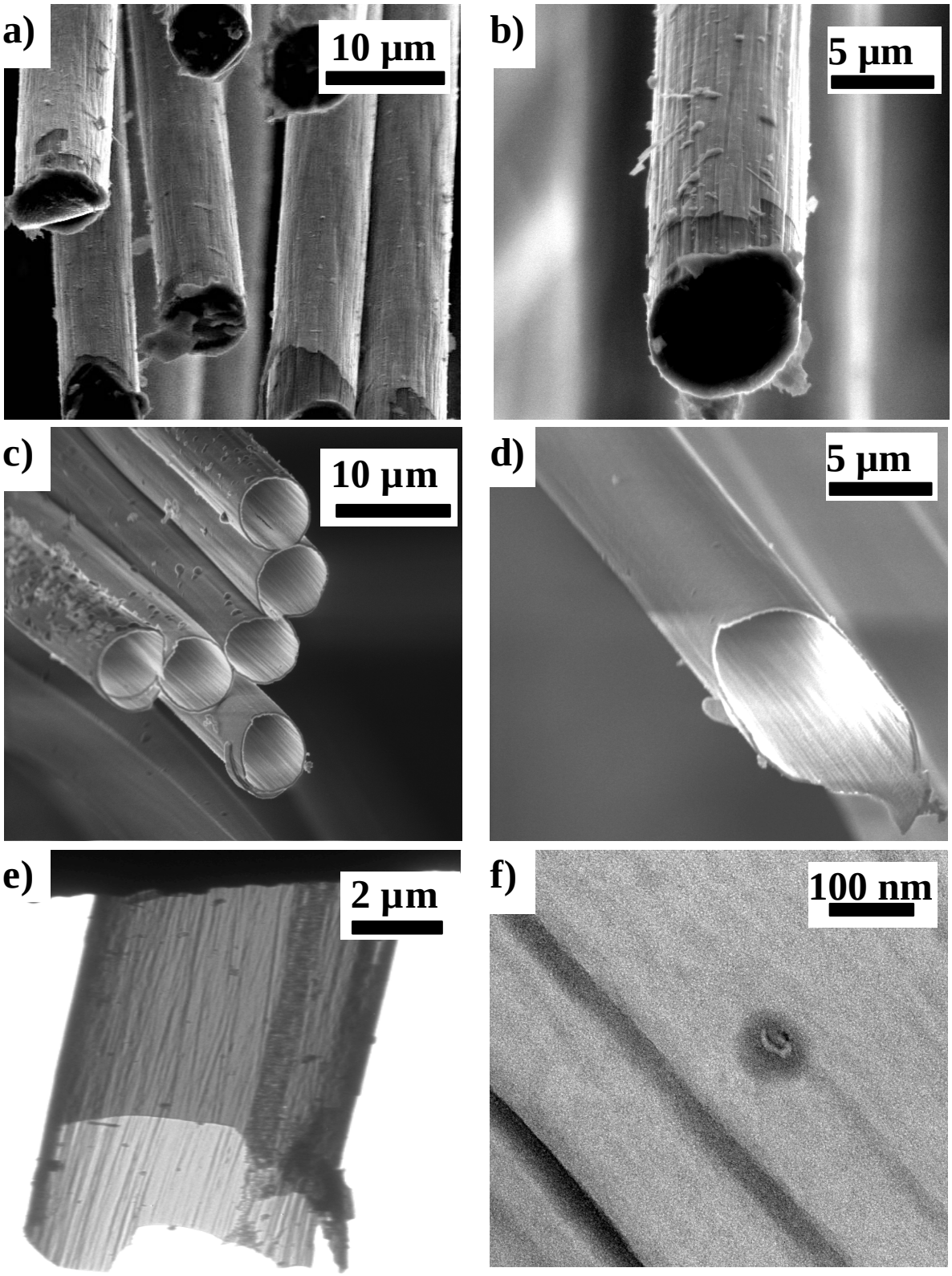


Figure 2: Scanning electron microscopic images (SEM) of a), b) carbon fibers after thin film deposition c), d) microtubes, and e), f) transmission electron microscopic (TEM) image of a microtube: e) a single microtube f) a part of the microtube.

After coating, the bundles of fibers have essentially the same morphology but are colored, see Figure 1c and 1d, indicating interference of light reflected at the outer and inner interface of the films.

Various segments of fiber bundles were observed under scanning electron microscope (SEM) after exposing certain numbers of deposition cycles. The fibers within the bundle are separated from each other, no bridging has been observed and the films were deposited evenly onto each individual fiber (see for example Figure 2a). Figure 2b shows a single fiber cut after coating deposition; there is a slight contrast between a part of the fiber adjacent to the front and the part further up. Obviously, close to the front, a part of the coating was damaged and removed by the cutting process, exposing the carbon inside; further up the slightly more bright appearance indicates undamaged coating. Close up images of this part reveals a clear step in the surface profile. Elemental analysis of the thin films deposited onto fibers by energy dispersive X-ray spectroscopy (EDXS) revealed a dominating carbon content as well as aluminum and oxygen (see Figure 3a). The dominating amount of carbon was expected because of the carbon fiber, the presence of aluminum and oxygen confirms the expected alumina coating. The average thicknesses of the coating were estimated from various fibers, and presented in Figure 3b as a function of the number of deposition cycles. There is a linear relationship between the coating thickness and the number of cycles with an average deposition rate of (0.34 ± 0.03) nm per cycle. The deposition rate is higher than the value that can be estimated theoretically for a monomolecular layer of alumina[21]. Thus the process used here is a pulsed chemical vapor deposition (pulsed CVD) rather than the strict atomic layer deposition (ALD) used in reference[16]. For the detail of (pulsed CVD), see chapter 4.

7.2.3 Microtubes

Microtubes were synthesized by removing the carbon fibers via thermal oxidation in air at temperatures exceeding 550 °C using a tube furnace. To remove the fibers, time spans between 3 to 12 hours were needed, depending on coating thickness (50 nm to 200 nm) and the process temperature (550 °C to 900 °C). At 550 °C, it was needed between 10 to 12 hours, and 3 to 4 hours at 900 °C.

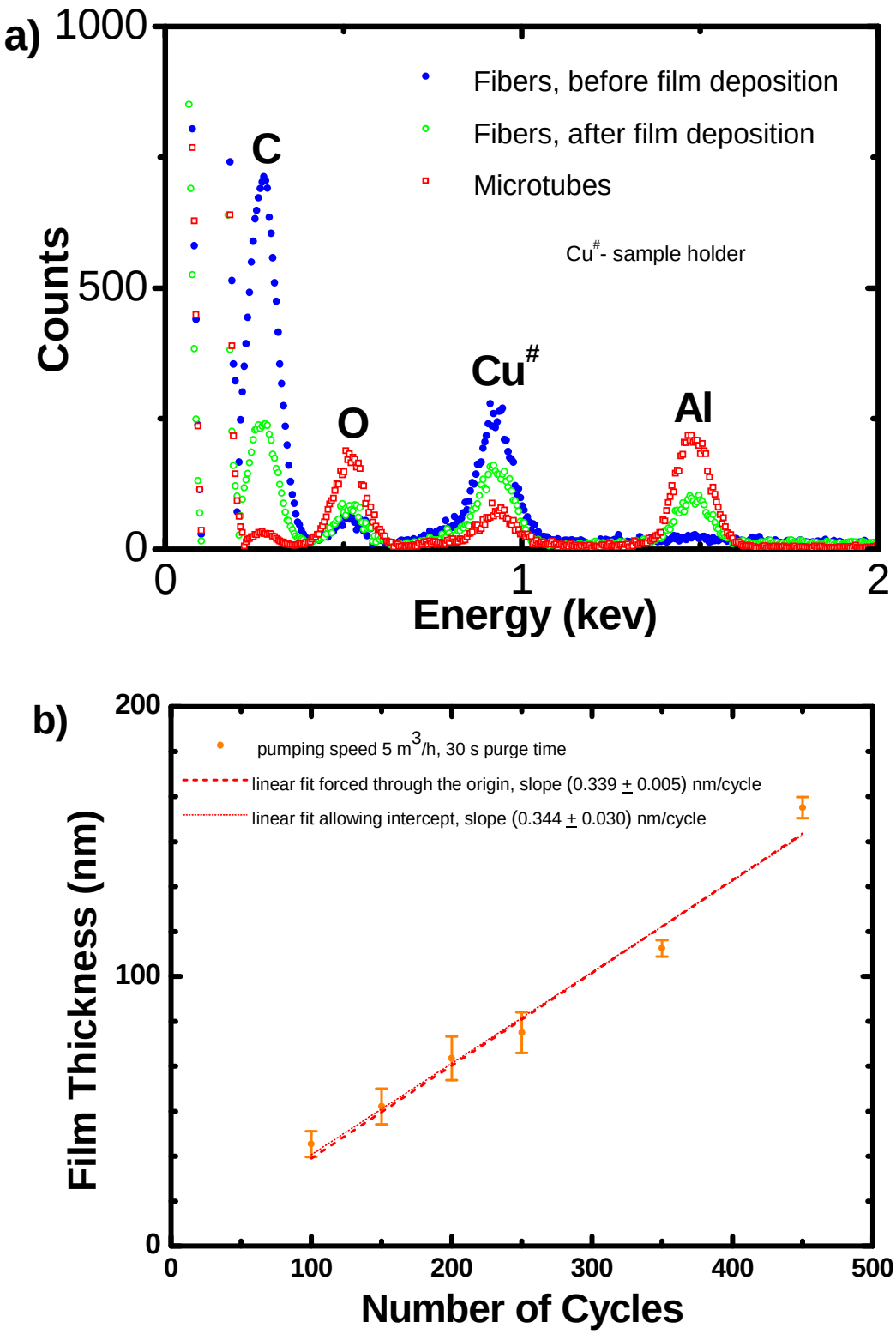


Figure 3: a) Energy dispersive X-ray spectrums (EDXS) of fibers before film deposition, fibers after film deposition, and microtubes. b) Film thickness with respect to number of deposition cycles.

This thermal treatment was accompanied by a change in color from dark to white, the overall shape and arrangement of the bundles being unaffected (see Figure 1g and 1h). The change of color occurred evenly along the bundles. SEM and TEM images after thermal oxidation revealed that the desired microtubes indeed were obtained (see Figure 2 c—e). The tubes are still separated from each other as were the fibers after coating deposition and the inner diameters are equivalent to the diameter of the fibers. The tubes have the same inner morphology as the surface of the carbon fibers, i.e., a corrugated surface bearing grooves parallel to the fiber axis and irregular protuberances that were present on the fibers already before the coating process. In addition, the fibers bear a few fragments of tubes that were shattered and displaced when the tubes were cut. The maximum length of the tubes thus prepared was 30 cm, however, it was primarily limited by the dimension of the used furnace, and thus it will be possible to synthesize tubes longer than 30 cm.

The elemental composition of the microtubes was analyzed by EDXS which revealed aluminum and oxygen and a small amount of carbon (see Figure 3a). The small amount of carbon might be because of residual fragments of the carbon fiber template, the presence of aluminum and oxygen confirms the expected alumina film. EDXS does not always yield accurate quantitative chemical compositions, especially, for lower atomic weight elements; thus the carbon, nitrogen and hydrogen content of the microtubes were measured via elemental flash analysis. Results of this analysis indicate that the amount of carbon, hydrogen, and nitrogen within the residue of thermal oxidation were 1.61%, 0.06% and no nitrogen was detected (if nitrogen was present, that might be less than the detection limit of the instrument, i.e., <0.01%), respectively. Possibly, this small amount of hydrogen and a part of the carbon can be attributed to a decomposition product of the trimethylaluminum, and the rest of the carbon as an irremovable part of the fiber. Overall, the amount of impurities in the microtubes is low.

Compared to the previously mentioned publication[16], we obtained here centimeter long microtubes and took advantage of higher coating deposition rate per cycle. One can manipulate the tubes which are presented here. The authors of the previous paper are of the opinion that the coating is impermeable to gases. We observe the contrary in our case: If the coating is impermeable to oxygen, oxidation of the fibers has to proceed

starting from both open ends. However, in our case the coated fibers gradually turn gray at intermediate stages of oxidation, they do not turn white from the end only (see Figure 1e and 1f). Furthermore, SEM images reveal that the diameter of the fibers along the whole length decreases gradually with time—See for example Figure 4. Already at early stages of oxidation, one can observe a slight decrease of diameter of the fibers and a clear and uniform gap between the tube and the remaining fiber. In addition in this early stage of oxidation one observes the formation of 'pits' in the surface of the fibers.

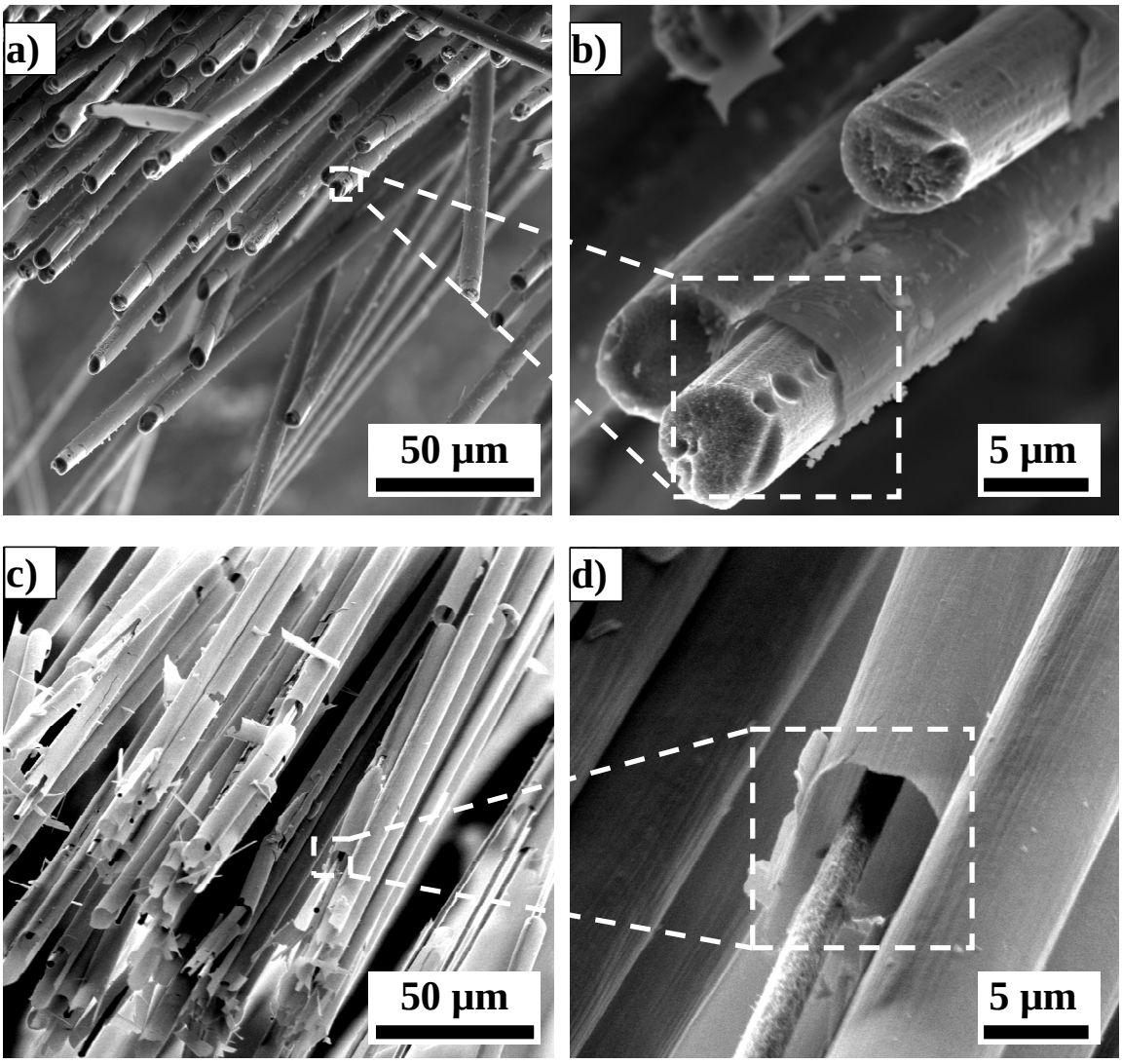


Figure 4: Scanning electron microscopic (SEM) images of bundle of coated fiber after incomplete thermal oxidation: a) within the TGA heating to 700 °C with a rate of 5 °C/min and subsequent annealing for 30 minutes, c) in tube furnace at a temperature of 650 °C for 3 hours. b) & d) are close up views of a) and c), respectively.

However these pits form as well if uncoated fibers are oxidized (see Figure 5). Thus they are characteristics of the fiber and not of the coating, probably indicating inhomogeneities within the fiber[16]. The decomposition of the coated fibers by annealing in air was repeated in a thermogravimetric analyzer, heating the fibers with a constant heating rate to a desired temperature (700 °C or 900 °C) and annealing them further at that temperature (see Figure 6). The uncoated fibers start to lose weight at approximately 630 °C and completely burned at approximately 825 °C, whereas the coated fibers start to lose weight at approximately 660 °C and completely burned at approximately 900 °C. This indicates that the coating slows down the decomposition to a little extent by acting as a barrier between the air and the fiber and that the decomposition of the fiber is due to oxidation into gaseous carbon oxides. Thus, in our case there has to be some permeability for oxygen and combustion products at least at elevated temperatures.

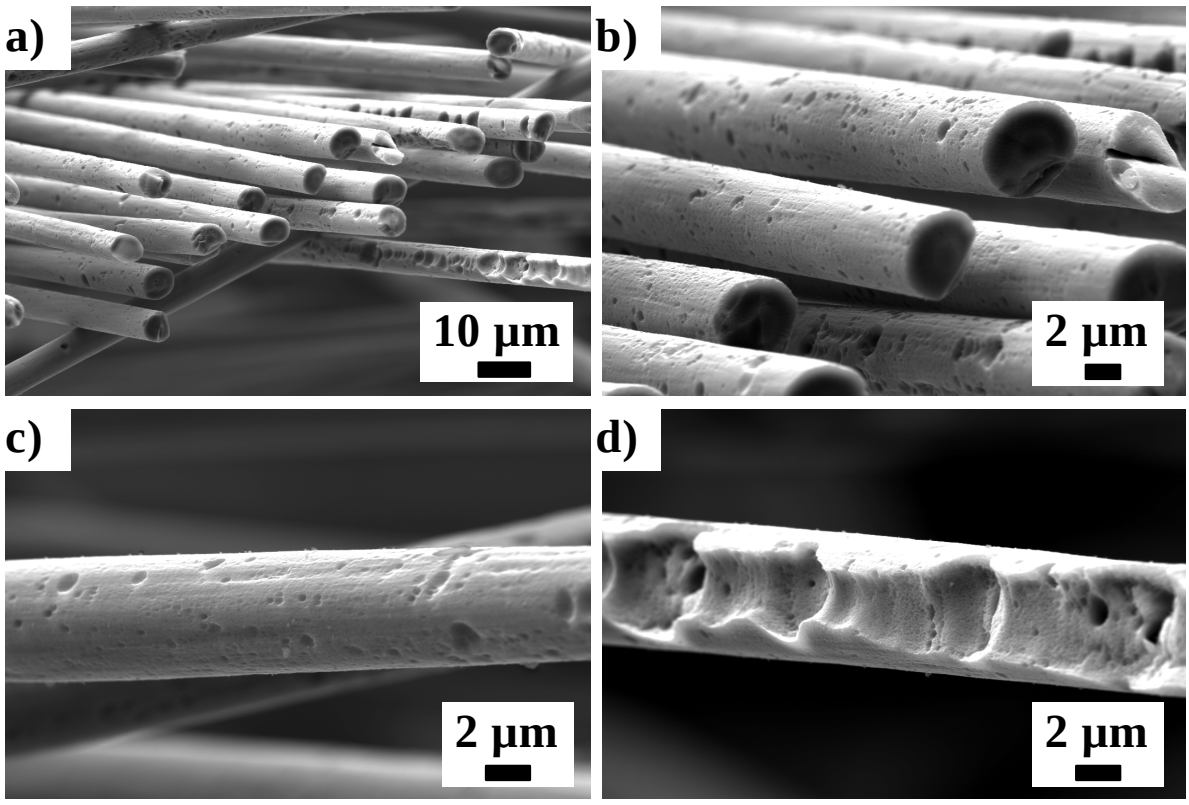


Figure 5: Scanning electron microscopic (SEM) image of a bundle of uncoated fibers after incomplete thermal oxidation within the TGA heating from 30 °C to 700 °C with a rate of 5 °C/min and held at 700 °C until 20% weight loss: a) and b) bundle of fibers c) a single fibers, pits are visible all around the surface d) a single fiber severely oxidized. All these images indicate an inhomogenous oxidation patterns which varied from fiber to fiber.

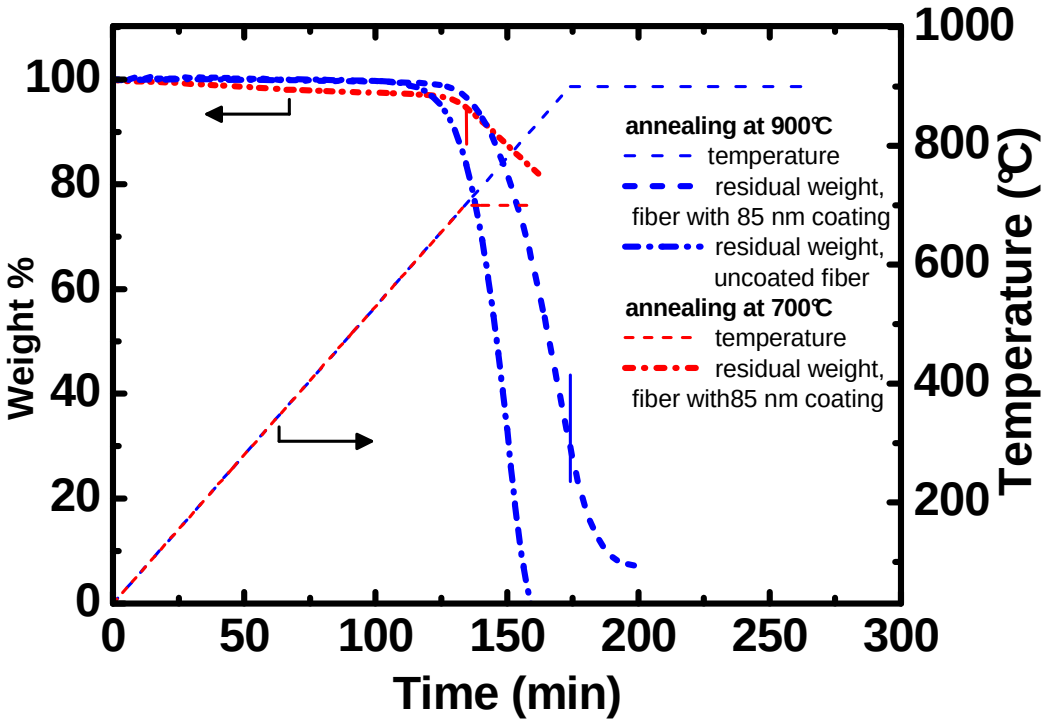


Figure 6: Thermogravimetric analysis (TGA) of uncoated and coated fibers in synthetic air. The specimens were heated to the desired temperature (700 °C or 900 °C, indicated by thin vertical lines) with a constant heating rate of 5 °C/min and subsequently held at that temperature.

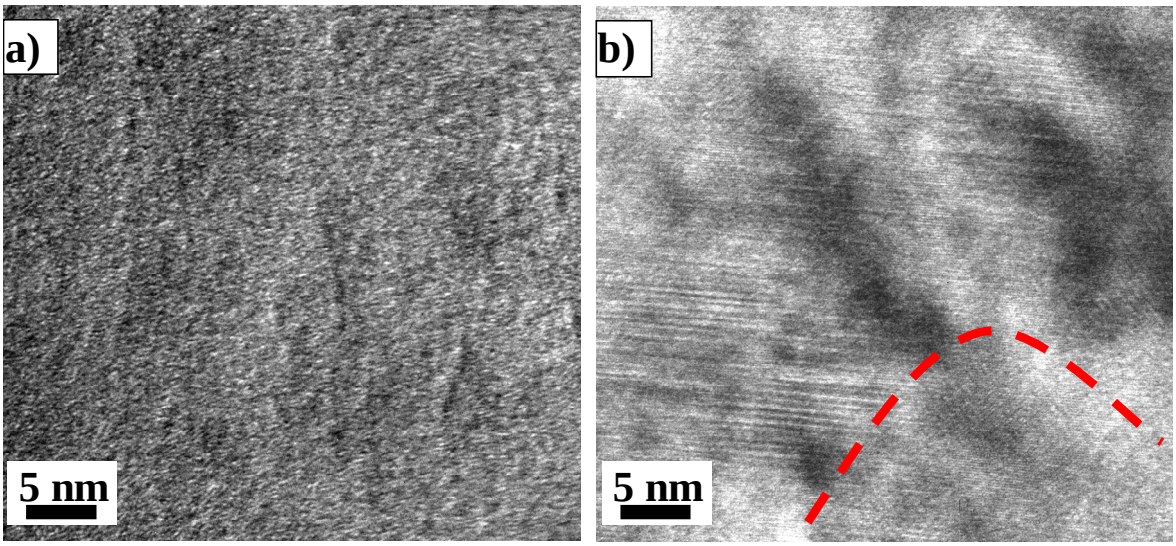


Figure 7: High resolution transmission electron microscopic (HRTEM) images of the walls of alumina microtubes a) prepared at 550 °C b) at 900 °C.

This assumption of permeability of the coating for gases is in agreement with the results presented in reference[16]. The layers prepared in this reference[16] via strict ALD enable removal of the fiber templates via annealing and thus need to be permeable for gaseous products as well. Layers prepared via strict ALD usually are less permeable than those prepared via pulsed CVD. Thus, one can expect that removal of gaseous products in our case is even more facile than the result presented in reference[16], however, we have seen similar oxidation behaviour in case of ALD layer, at least via thermogravimetic analysis (see Figure 5 of chapter 3).

High resolution transmission electron microscopic (HRTEM) images reveal that Tubes obtained via oxidation at 550 °C have low degree of crystallinity (Figure 7a) whereas the tubes obtained via oxidation at 900 °C (Figure 7b) showed a significant degree of crystallinity, even exposing details that may be interpreted as grain boundaries. This change in structure might influence the barrier properties of the layer.

7.3 Experimental part

The reaction chamber and sample holder were identical to the one described in chapter 3. Same type of carbon fibers were used for coating after thermal desized. Fibers are coated with alumina at a temperature of 77 °C using pulses of trimethylaluminum (98% from ABCR GmbH & co. KG, Karlsruhe) and of deionized water. The supply vessel of trimethylaluminum was heated to 60 °C. The temperature of the water supply was maintained at 50 °C. Two streams of nitrogen were used as carrier for trimethylaluminum and water, respectively as well as purge gas; their flow was controlled by two mass flow controllers each set to 20 standard cubic centimeters per minute (sccm). In the first half cycle, the fiber bundle was exposed to trimethylaluminum for 20 s followed by purging the reactor with nitrogen for 30 s. In the second half cycle it was exposed to water vapor for 20 s followed by purging the reactor with nitrogen for 30 s. Nominal pumping speed (as specified by the manufacturer) during the purging cycle was 5 m^3/h (PFEIFFER VACUUM, Duo 5, Mod. Nr.: PK D61 705 AA) in all the experiments. From the vapor pressure of TMA(106 hPa[22]) respectively Water (123 hPa[23]) in the reservoirs and flow of carrier gas one can calculate a total exposure per cycle of 16×10^8 Langmuir of TMA and 18.5×10^8 Langmuir of water (1Langmuir = 10^{-6} Torr s). In

both exposures the valve in front of the pump was closed, it was opened fully during the purge time.

Carbon fibers were removed selectively after coating deposition via thermal oxidation at temperatures exceeding 550 °C in air using a tube furnace.

To characterize films onto the fibers directly after deposition, scanning electron microscopy (SEM) and energy dispersive X-ray spectroscopy (EDXS) were recorded using a Nova NanoSEM (FEI, PHILIPS), specimens were taken from the bundles. To characterize tubes after thermal oxidation, transmission electron microscopy (TEM) was recorded using a PHILIPS CM 20 FEG taking directly the microtubes. TEM images were recorded in transmission perpendicular to the natural surface of the coating.

Elemental flash analysis was performed via flash pyrolysis/oxidation of the sample, coupled to a chromatographic separation and detection of the gaseous oxidation products using a FLASHAE 1112 from (Thermo Fischer Scientific, Waltham, Massachusetts, USA).

7.4 Conclusions

Pulsed chemical vapor deposition (pulsed CVD) is a convenient technique which applied successfully for coatings deposition onto carbon fibers at a low temperature with uniform and conformal films and gives rise to a deposition rate of (0.34 ± 0.03) nm per cycle. Thermal-oxidation is a useful method to remove the carbon without affecting much the alumina layers and thus allows to prepare tubes with morphologies similar as to the fibers. Microtubes of titania and double layer coatings are also obtained from respective coated fibers.

7.5 References

1. Uchida, S.; Chiba, R.; Tomiha, M.; Masaki, N.; Shirai, M., Application of titania nanotubes to a dye-sensitized solar cell. *Electrochemistry* **2002**, *70* (6), 418-420.

2. Ohsaki, Y.; Masaki, N.; Kitamura, T.; Wada, Y.; Okamoto, T.; Sekino, T.; Niihara, K.; Yanagida, S., Dye-sensitized TiO_2 nanotube solar cells: fabrication and electronic characterization. *Physical Chemistry Chemical Physics* **2005**, *7* (24), 4157-4163.

3. Varghese, O. K.; Gong, D. W.; Paulose, M.; Ong, K. G.; Grimes, C. A., Hydrogen sensing using titania nanotubes. *Sensor Actuators B* **2003**, *93* (1-3), 338-344.

4. Varghese, O. K.; Gong, D. W.; Paulose, M.; Ong, K. G.; Dickey, E. C.; Grimes, C. A., Extreme changes in the electrical resistance of titania nanotubes with hydrogen exposure. *Advanced Materials* **2003**, *15* (7-8), 624-627.

5. Fan, R.; Karnik, R.; Yue, M.; Li, D. Y.;Majumdar, A.; Yang, P. D., DNA translocation in inorganic nanotubes. *Nano Letters* **2005**, *5* (9), 1633-1637.

6. Lee, S. B.; Mitchell, D. T.; Trofin, L.; Nevanen, T. K.; Soderlund, H.; Martin, C. R., Antibody-based bio-nanotube membranes for enantiomeric drug separations. *Science* **2002,** *296* (5576), 2198-2200.

7. Martin, C. R.; Kohli, P., The emerging field of nanotube biotechnology. *Nature Reviews Drug Discovery* **2003,** *2* (1), 29-37.

8. Spahr, M. E.; Bitterli, P.; Nesper, R.; Muller, M.; Krumeich, F.; Nissen, H. U., Redox-active nanotubes of vanadium oxide. *Angewandte Chemie-International Edition* **1998,** *37* (9), 1263-1265.

9. Niederberger, M.; Muhr, H. J.; Krumeich, F.; Bieri, F.; Gunther, D.; Nesper, R., Low-cost synthesis of vanadium oxide nanotubes via two novel non-alkoxide routes. *Chemistry Materials* **2000,** *12* (7), 1995-2000.

10. Iijima, S.; Ichihashi, T., Single-Shell Carbon Nanotubes of 1-nm Diameter. *Nature* **1993,** *363* (6430), 603-605.

11. Bethune, D. S.; Kiang, C. H.; Devries, M. S.; Gorman, G.; Savoy, R.; Vazquez, J.; Beyers, R., Cobalt-Catalyzed Growth of Carbon Nanotubes with Single-Atomic-Layer walls. *Nature* **1993,** *363* (6430), 605-607.

12. Schmidt, O. G.; Eberl, K., Nanotechnology - Thin solid films roll up into nanotubes. *Nature* **2001,** *410* (6825), 168-168.

13. Bae, C.; Yoo, H.; Kim, S.; Lee, K.; Kim, J.; Sung, M. A.; Shin, H., Template-directed synthesis of oxide nanotubes: Fabrication, characterization, and applications. *Chemistry of Materials* **2008,** *20* (3), 756-767.

14. Caruso, R. A.; Schattka, J. H.; Greiner, A., Titanium dioxide tubes from sol-gel coating of electrospun polymer fibers. *Advance Materials* **2001,** *13* (20), 1577-1579.

15. Bognitzki, M.; Hou, H. Q.; Ishaque, M.; Frese, T.; Hellwig, M.; Schwarte, C.; Schaper, A.; Wendorff, J. H.; Greiner, A., Polymer, metal, and hybrid nano- and mesotubes by coating degradable polymer template fibers (TUFT process). *Advance Materials* **2000,** *12* (9), 637-640.

16. Peng, Q.; Sun, X. Y.; Spagnola, J. C.; Hyde, G. K.; Spontak, R. J.; Parsons, G. N., Atomic layer deposition on electrospun polymer fibers as a direct route to Al_2O_3 microtubes with precise wall thickness control. *Nano Letteers* **2007,** *7* (3), 719-722.

17. Roy, A. K.; Baumann, W.; Konig, I.; Baumann, G.; Schulze, S.; Hietschold, M.; Mader, T.; Nestler, D. J.; Wielage, B.; Goedel, W. A., Atomic layer deposition (ALD) as a coating tool for reinforcing fibers. *Analytical and Bioanalytical Chemistry* **2010,** *396* (5), 1913-1919.

18. Bai, Y. J.; Wang, C. G.; Lun, N.; Wang, Y. X.; Yu, M. J.; Zhu, B., HRTEM microstructures of PAN precursor fibers. *Carbon* **2006,** *44* (9), 1773-1778.

19. Kisker, D. W.; Stevenson, D. A.; Miller, J. N.; Stringfellow, G. B., The Vapor-Phase Interaction of Trimethylaluminum with Graphite during OMVPE. *Journal De Physique* **1982,** *43* (NC-5), 221-227.

20. Kisker, D. W.; Stevenson, D. A., Mechanism of Graphite Baffle Gettering in Organometallic Vapor-Phase Epitaxy; Adsorption of Trimethylaluminum on Graphite. *Journal of Electronic Materials* **1983,** *12* (2), 459-482.

21. a) Puurunen, R. L., Growth per cycle in atomic layer deposition: A theoretical model. *Chemical Vapor Deposition* **2003,** *9* (5), 249-257. b) Puurunen, R. L., Growth per cycle in atomic layer deposition: Real application examples of a theoretical model. *Chemical Vapor Deposition* **2003,** *9* (6), 327-332.

22. Bamford, C. H.; Levi, D. L.; Newitt, D. M., Physical and Chemical Properties of Organo-Metallic Compounds .1. The Vapour Pressurs and Freezing Points of Simple Metal Alkyls of Group-II, Group-III, and Group-V. *Journal of Chemical Society* **1946,** (May), 468-471.

23. Landolt, H.; Börnstein, R; Eucken, A, Zahlenwerte und Funktionen aus Physik, Chemie, Astronomie, Geophysik und Technik 6th ed, vol 2. Springer, Berlin, p 61, **1960**.

8. Conclusions

There was no commercial reactor which can be used for atomic layer deposition (ALD) onto "endless" fibers. There might be one possibility to manipulate one of the commercially available reactors for ALD onto fibers but they are expensive. (150, 000 to 200, 000 euro). Thus, a reactor has been designed for ALD onto bundle of fibers. Total expenditure of the home-built reactor was about 30, 000 euro. Aluminum oxide (alumina), titanium oxide (titania), double layer coatings made out of alumina and titania have been successfully deposited onto carbon fibers. The deposition of these coatings via ALD in principle was already known, the main aspect here is the deposition onto reinforcing fibers. Furthermore, a process to deposit aluminum phosphate was developed. To the best of my knowledge, aluminum phosphate has not been reported via ALD regardless of substrate.

In general, all these coatings were uniform and conformal on the fiber surfaces. Thickness and the morphology of the coatings depend on the purge time; which have been discussed in detail for alumina deposition in chapter 4. Coated fibers have been used successfully to prepare alumina, titania, and alumina followed by titania, and titania followed by alumina microtubes synthesis (alumina microtubes characterized thoroughly in chapter 7).

Alumina has been deposited onto carbon fibers at a deposition temperature of 500 °C using non-flammable precursors, aluminum trichloride ($AlCl_3$) and water. This process was quite successful; there were few problems, at these conditions carbon fibers partially damaged during deposition. When deposition temperature was decreased down to 300 °C, carbon fibers were intact as revealed in scanning electron microscopic (SEM) images. At 500 °C average coating deposition rate was 0.06 nm per cycle whereas it was 0.033 nm per cycle at 300 °C. Controlling the aluminum trichloride dose was another problem. At room temperature aluminum trichloride is a solid but ALD is a gas-phase method. To obtained sufficient vapor pressure thermal evaporation is one of the ways. Sufficient vapor pressure was achieved by heating the aluminum trichloride to a temperature of 150 °C. However, these vapors are often deposited inside the carrier tube. Additionally, aluminum trichloride reacts rapidly with oxygen and/or moisture, and forms aluminum oxide. Aluminum oxide and chloride mixtures formed very hard, high temperature stable solid material. This solid material often blocked the carrier tube of aluminum trichloride. As a result the deposition process often had to be terminated midway, although there

was still enough aluminum trichloride inside the precursor chamber. In this process hydrochloric acid is formed as a byproduct which is a corrosive substance and thus can affect the reactor. As for example, the valve responsible for delivering the aluminum trichloride precursor was damaged within six months, which is not possible to repair according to the manufacturer. After first alumina deposition, it has been proven that the ALD can be applied for reinforcing fibers and also proven that the home-built reactor was functioning properly.

Alumina deposition was continued by replacing the aluminum trichloride with trimethylaluminum ($Al(CH_3)_3$) at a lower temperature (77 °C) than the previous cases. After deposition, there was a weight loss of carbon fibers of about 1%. One can conclude that the carbon fibers are almost intact even though there was water involved in the process. This preservation of the fiber might be due to low process temperature of 77 °C. A qualitative adhesion test has been conducted by bending alumina coated fibers around cylinders of radii. Results indicated that the coatings were well adhesion to the fiber surfaces. Adhesion is a function of residual mechanical stress and of defects within the material. Residual stress might arise from mismatch of thermal expansion coefficients, if deposition is done at an elevated temperature and the fibers are subsequently cooled down. Defects might arise from thermally induced recrystallisation after deposition that causes faulty lines and grain borders within the material. The process depicted here is conducted at a comparatively low temperature (77 °C), thus it is likely that there is a low amount of residual stress and defects, which favors the adhesion of the coatings to the fibers. An average deposition rate was (0.25 ± 0.02) nm per cycle at 77 °C which was comparatively higher than reported in literature, when the deposition temperature raised to 150 °C, growth per cycle decreased to (0.17 ± 0.03) nm/cycle. One of the reasons for higher growth rate at lower temperature (77 °C) might be because of physically adsorbed water molecules. Physically adsorbed water molecules facilitate additional growth on ALD layer during the next pulse of trimethylaluminum.

By varying the duration of the purge time, one can tune the morphology of the deposited coatings from a gas phase precipitation reaction to deposition controlled by surface saturation. A purge time of 15 s leads to non-uniform and non-conformal coatings. Thicker coatings have been deposited onto the fibers at the perimeter of the bundle compared to the fibers inside the bundle. Coating deposition rate inside the bundle was about 0.83 nm/cycle, which is much higher than a single alumina monolayer per cycle. This indicates a significant precipitation of alumina from gas phase reactions onto the carbon fibers. With increasing purge time,

homogeneity and conformality of the coatings improved and the variation of thickness from perimeter to inside the bundle decreased significantly. At 30 s purge time, the coatings were already smooth and conformal, as expected for a deposition controlled by surface saturation, and the deposition rate was 0.34 nm/cycle. Further increase of purge time up to 100 s, did not change the morphology significantly, and lead to a deposition rate of 0.27 nm/cycle which is less than expected for a monolayer. Experiments conducted at increased pumping speed gave essentially the same results.

Coating deposition by using trimethylaluminum and water as precursors was successful. One important message regarding the safety of laboratory is that trimethyalumium is a pyrophoric liquid; it has to be handled with extreme care. Trimethylaluminum is an expensive chemical in comparison to aluminum trichloride. Thus, if one can overcome the above mention difficulties of aluminum trichloride, it can also be a good precursor for alumina deposition.

Titanium oxide (titania) was deposited using titanium tetrachloride ($TiCl_4$) and water. Average deposition was approximately 0.13 nm per cycle. Titanium tetrachloride is a liquid at room temperature; it was easy to control compared to aluminum trichloride. Double layer coatings of alumina and titania, i.e., alumina followed by titania (alumina/titania) and titania followed by alumina (alumina/titania) were deposited successfully. In the case of double layer coatings, alumina was deposited using trimethylaluminum and water, whereas, titania was deposited using titanium tetrachloride and water. Alumina and titania seem to be partially crystalline as revealed from the transmission electron microscopic images but it is difficult to predict the degree of crytallinity.

Aluminum phosphate has been deposited using trimethylalumium and triethylphosphate ($(C_2H_5)_3PO_4$) at a temperature of 250 °C. To the best of my knowledge aluminum phosphate is a new ALD material. Coating deposition rate was approximately 0.07 nm per cycle. Aluminum phosphate seems to be a “weak” coating at least compared to other coatings used here. This deposition process is a non-aqueous process, from the insitu oxidation point of view; it might be more suitable for carbon fibers than other routes that use water as precursor. Deposited layers comprise structural elements of $AlPO_4$ as well as $Al(PO_3)_3$. Further optimization will be needed if pure aluminum orthophosphate is desired.

Alumina coatings improved oxidation resistance of the carbon fibers slightly (from about 630 °C to 660 °C) after alumina coating deposition. The resistance was linearly increased with the coating thickness (up to 660 °C) and getting saturated over a thickness of 120 nm.

Oxidation onset temperature of the titania coated carbon fibers (590 °C) was lower to the uncoated fibers (630 °C) but the rate of oxidation was slower, especially at high temperatures. Aluminum phosphate coating improved oxidation resistance to a certain extent. In case of fibers coated with a 25 nm thick layer of aluminum phosphate, the oxidation starts at a temperature of approximately 700 °C and the fibers are burned completely at a temperature of approximately 900 °C during 20 minutes holding time. If the fiber is coated by alumina and subsequently by titania both effect seems to overlap. This coating has the same oxidation onset as alumina but the rate of oxidation delayed significantly compared to uncoated and alumina coated fibers. This feature is independent of the thickness of the titania, at least in the regime investigated (50 nm alumina followed by 13 nm and 40 nm titania). On the other hand, if the sequence of deposition is changed, i.e., depositing the titania first and alumina subsequently (20 nm titania followed by 30 nm alumina) this improves the oxidation onset temperature higher than any of the previous cases. Oxidation starts at a temperature of approximately 750 °C and the fibers are burned completely at a temperature of approximately 900 °C after 60 min holding time. Obviously, the sequence of the layers influences the crystallization behavior. Thus, oxidation protection of the carbon fiber coated with titania followed by alumina was better than any other coating used here.

During removable of sample holder, coating that deposited inside the reactor, often plugged out and formed flakes on fibers (because sample holder was designed in such a way which can just fits into the reactor). They were also forming during the SEM sample preparation, coating that removed from the front parts of the fibers during the segregation of samples can also formed flakes. Often process had to be terminated, because it was needed to collect intermediate specimens and there was no possibility to run the process overnight. After specimen collection, depositions were resumed. Flakes which are formed because of the above two reasons might be embedded into coating and revealed as rough coatings.

Thus, there were flakes of coatings on the fiber surfaces Flakes which are formed by the first two ways were removed to a certain extent by using a soft brash or by blowing air. Flakes which were embedded to the coatings were not possible to remove.

Alumina microtubes have been synthesized using alumina coated carbon fibers. The carbon fibers were selectively removed using thermal oxidation in air at temperatures exceeding 550 °C. The length of the tubes was primarily limited by the dimension of the used furnace. The longest tubes thus had a length of 30 cm. Scanning electron microscopic (SEM) images of the microtubes revealed that individual tubes were separated from its neighbors and that they had an

almost uniform wall thicknesses. SEM and transmission electron microscopic (TEM) images indicate that the inner side of the wall has the same morphology as the fiber template. Similarly microtubes of titania, and both the double layers can be obtained from respective coated fibers. As deposited alumina and titania coatings are partially crystalline with small grain size. During thermal annealing, degree of crystallization increased and the grains are coarse. Transmission electron microscopic images of the microtubes indicate features that may be interpreted as grain boundaries which open cracks or voids within the coatings. It is likely that the observed lowering of the oxidation stability at higher temperatures is due to crystallization. In the case of double layer coatings one shining fact is visible: If titania coating is on the outside the titania crystals are significantly coarse than in the case of titania being in between the fiber and the alumina. This in turn might give rise to the observed differences in oxidation stability.

Thus, atomic layer deposition has been successfully applied for coating deposition. In the field of composite science and technology, sol-gel and chemical vapor deposition have been used for coating deposition onto bundle of reinforcing fibers. In future ALD may be used for uniform and conformal coating deposition onto bundle of fibers.

Acknowledgements

First of all, I would like to thank my supervisor, Prof. Werner. A. Goedel, for his scientific ideas, encouragements, and his kind helps in all situations. His attitude towards science and great patience during discussions and guidance to a completely unknown scientific field I will remember throughout my life.

I would like to thank Dr. W. Baumann, Mrs. S. Stöckel, and Mr. I. König for valuable discussion and suggestions regarding the construction of ALD reactor. Dr. Baumann was deeply involved in this project, unfortunately he is no more with us, and did not witness completion of the project. I am grateful to Mr. H. Rose, for designing the control software of the ALD reactor, Mr. F. Diener and Mr. F. Sternkopf for building components of ALD reactor. Without their deep involvement in designing control software and building components would not have gone through with success.

It was great pleasure for me to work with Mr. Stefan Knohl during his advance lab course. Without his deep involvement in experiments, especially, alumina depositions and microtube preparations would not have gone through with success.

My sincere thank goes to Prof. M. Hietschold, Dr. S. Schulze, Mrs. G. Baumann for guidance and valuable discussion during TEM, SEM and EDXS measurements.

My sincere thank goes to Prof. B. Wielage, Dr. D. J. Nestler, Mr. T. Mäder for valuable discussion and TEM sample preparations using focus ion beam (FIB).

I am grateful to Prof. S. Spange, Dr. A. Seifert, Mr. R. Lungwitz for Solid state NMR measurements and for valuable discussions.

I am grateful to Deutscher Akademischer Austauschdienst by a fellowship within the STIBET program for financial support.

I am grateful to Prof. H. Lang, Mrs. U. Stöß, and Mrs. J. Fritzsch for elemental flash analysis.

I would like to thank my parents and grant parents for their constant encouragement and support from my childhood till today. Without their support and love, it would not have been possible. My parents made lot of sacrifice for me and I am grateful for them and privileged to have them as my parents. I also would like to thank my brother, who always encouraged and supported me.

I am grateful to all my colleagues. I spent wonderful time with former members of physical chemistry, David, Joanna, Mahendra, as well with present group members, Cornell, Robert, Ina, Susann, Sabine, Annemarie, Yana, Doreen, Lutz, Arnd, Andreas, Kerstin, and Sigrun. I am thankful to Dr. S. Hemeltjen for valuable suggestions. I am grateful to Petra for her assistance during TGA measurement. I am thankful to Mrs. S. Uhlmann, Mrs. G. Goldmann for their kind helps.

I am thankful to my friends with whom I spend wonderful time in Chemnitz: Kausik, Achanta Gopa, Guhan, Sukumar, Deepak, Joydeep, Paritosh, Masud, Millind, Biswajit, Pradeep. I am thankful to my friends Mithun, Anup, Anobic, especial thanks goes to Anupam, Debjit, and Sayak for providing several literature most of them are sited in the reference sections of this dissertation.

I wish to thank all those who directly and indirectly helped me during my thesis.

Last but not the least; I would like to thank my wife, Sumita for her support, and encouragement in every moment of my life.

Curriculum Vitae

Personal Information

Name:	Amit Kumar Roy
Date of Birth:	6th January 1981
Nationality:	Indian
Address (private):	Vetterstrasse 52, Room 32, 09126 Chemnitz, Germany.
Address (office):	Chemnitz University of Technology, Institute of Chemistry, Physical Chemistry, Strasse der Nationen 62, 09111 Chemnitz.
Family Status:	Single

Educational Backgrounds

- (From October 2006) PhD student at the institute of chemistry in **Chemnitz University of Technology, Germany.**
- (2005-2006) One year post M. Sc. diploma in biophysical science, from **Saha Institute of Nuclear Physics (SINP), India.**
- (2003-2005) Master of Science in Chemistry with full scholarship from **Indian Institute of Technology (IIT) KGP, India**, Grade: 7.79 (CGPA) out of 10 Grade**.**
- (1999-2003) Bachelor of Science in Chemistry, from Gushkara Mahavidylaya under the University of Burdwan, Gushkara, India.
- (1997-1999) Higher Secondary (High school, 12th level), from Gushkara Purnananda Public Institution, Gushkara, India.
- (1992-1997) Secondary (School, 10th level), from Orgram High School, Orgram, India.

Publications

Patent Application

- A. K. Roy, W. A. Goedel, "Fiber coating by atomic layer deposition," *UK patent application* GB 2467928 A.

Peer Review Journals

- A. K. Roy, W. Baumann, I. König, G. Baumann, S. Schulze, M. Hietschold, T. Mäder, D. J. Nestler, B. Wielage, W. A. Goedel, "Atomic layer deposition (ALD) as a coating tool for reinforcing fibers," *Analytical and Bioanalytical Chemistry* **2010**, *396* (5), 1913-1919 /Erratum at: Anal Bioanal Chem 2011;401:1455.

- A. K. Roy, W. Baumann, S. Schulze, M. Hietschold, T. Mäder, D. J. Nestler, B. Wielage, W. A. Goedel, "Atomic layer deposition of alumina onto Carbon fibers" *Journal of American Ceramic Society* **2011**, *94,* 2014-2022. /Erratum at: J Am Ceram Soc 2011;94:3604.

- A. K. Roy, S. Knohl, W. A. Goedel "Alumina Microtubes Prepared via Template Directed Pulsed Chemical Vapor Deposition" *Journal of Material Science* **2011**, *46* (14), 4812-4819 / Erratum at : http://dx.doi.org/10.1007/s10853-011-6069-4.

- A. K. Roy, W. A. Goedel "Control of Thickness and Morphology of Thin Alumina Films Deposited via Pulsed Chemical Vapor Deposition (Pulsed-CVD) through Variation of Purge Times" resubmitted after minor revision in *Surface and Coating Technology* **2011**, *205* (17-18) 4177-4182.

- A. K. Roy, S. Schulze, M. Hietschold, W. A. Goedel, "Oxidation protection of carbon fibers with alumina and/or titania using atomic layer deposition" *Carbon* **2012**, *50,* 761-770.

Submitted Articles

- A. K. Roy, R. Lungwitz, S. Spange, T. Mäder, D. J. Nestler, B. Wielage, S. Schulze, Michael Hietschold, W. A. Goedel "Non-aqueous Atomic Layer Deposition (ALD) of Aluminum Phosphate".

Conference Proceedings

- A. K. Roy, S. Schulze, M. Hietschold, T. Mäder, D. J. Nestler, B. Wielage, W. A. Goedel, "Atomic Layer Deposition (ALD) of Nanoscaled Alumina onto Carbon Fibers**"** conference proceeding in *8th International Nanofair Conference,* **6-7 July 2010**, Dresden.
- A. K. Roy, W. Baumann, I. König, S. Schulze, M. Hietschold, T. Mäder, D. J. Nestler, B. Wielage, W. A. Goedel, "Atomic Layer Deposition (ALD) of Alumina onto Carbon Fibers: Oxidation Barrier Coating," conference proceeding, ISBN 978-3-00-032049-1, page 78-83 in *7th International HT-CMC7 Conference,* **September 20-22, 2010**, Bayreuth, Bavaria, Germany.
- A. K. Roy, W. A. Goedel, "Atomic Layer Deposition of Double Layer Coating of Alumina and Titania onto Carbon Fibers: Oxidation Barrier Coating" conference proceeding submitted in *Verbundwerkstofftagung: 18. symphosym, Verbundwerkstofftag ung und Werkstoffverbunde*, 30 March - April 1, 2011, Chemnitz, Germany.

Scholarships

- **DAAD scholarship as an international student** from Chemnitz University of Technology during PhD.
- Full scholarship for **'1st International DAAD-Summer-Academy'**, held in Chemnitz from 13th to 26th of September.
- **Qualified for NET-UGC** for both Lectureship in college and scholarship for PhD.
- **One year (2005-2006) scholarship** during post M. Sc. diploma in biophysical science from Saha Institute of Nuclear Physics (SINP).
- **Two years (2003-2005) full MCM scholarship** during Master of Science from Indian Institute of Technology (IIT **KGP**).

Presentation at conferences

Talk

- 15th Tagung Festkörperanalytik, Chemnitz, Germany 12-16, July 2009. "Atomic Layer Deposition (ALD) of Alumina onto Carbon Fibers".

- 6th Zigmondy colloquium, Chemnitz, Germany 22-24, September 2010. “Atomic Layer Deposition (ALD) of Nanoscaled Alumina onto Carbon fibers”.
- 7th International HT-CMC7 Conference, September 20-22, 2010, Bayreuth, Bavaria, Germany. “Atomic Layer Deposition (ALD) of Alumina onto Carbon Fibers: Oxidation Barrier Coating”.

Poster

- 6th Zigmondy colloquium, Chemnitz, 22-24, September 2010. “Atomic Layer Deposition (ALD) of Al_2O_3 onto Carbon fibers: A Template Directed Route to Alumina Microtubes”.
- 8th International Nanofair Conference, Dresden 6-7 July 2010. “Atomic Layer Deposition (ALD) of Nanoscaled Al_2O_3 onto Carbon fibers”.

Selbständigkeitserklärung

Hiermit erkläre ich an Eides statt, die vorliegende Arbeit selbständig und ohne unerlaubte Hilfsmittel durchgeführt zu haben.

Amit Kumar Roy

Chemnitz, den 23.05.2011